VISION-BASED NAVIGATION AND MAPPING USING NON-CENTRAL CATADIOPTRIC OMNIDIRECTIONAL CAMERA

Manas Khurana

A Thesis submitted to the Faculty of Graduate Studies in Partial Fulfillment of the Requirements for the Degree of Master of Science

Graduate Program in Earth and Space Science

York University, Toronto, Ontario

November 2016

Abstract

This thesis details the development of an indoor navigation and mapping system using a catadioptric omnidirectional camera. Omnidirectional catadioptric cameras find their use in navigation and mapping, owing to their wide field of view. Having a wider field of view, or rather a potential 360^0 field of view, allows the user to see and move more freely in the navigation space.

A catadioptric camera system is a low cost system which consists of a mirror and a camera. Any perspective camera can be used. A platform was constructed in order to combine the mirror and a camera to build a catadioptric system. A calibration method was developed in order to obtain the relative position and orientation between the two components so that they can be considered as one monolithic system. The position of the system was determined, for an environment using the conditions obtained from the reflective properties of the mirror. Object control points were used for initialization. These were set up and experiments were performed at different sites to test the mathematical models and the achieved location and mapping accuracy of the system. The obtained positions were then used to map the environment using epipolar geometry. The mapping of an indoor environment while navigating the mobile platform is an iterative process of positioning and mapping. Several experiments were performed utilizing these processes. The positioning results and 3D coordinates of mapped points along with the accuracies (average 17 cm) were obtained. These were compared to manually measured results and the errors were analyzed to determine the efficiency of the

system.

Finally, recommendations to future works are provided with the potential of improving the accuracy and efficiency of the system. Some modifications are also suggested which aim towards increasing the potential applications of the system.

Acknowledgments

I am very grateful for my supervisor Dr. Costas Armenakis, for the encouragement and motivation he has provided me with in the course of this degree and for his patience in his dealings with me. I am truly indebted for his guidance and support.

I would like to thank my examination committee members, Dr. Baoxin Hu, Dr. Regina Lee and Dr. Burton Ma for their valuable time spent in assessing my work.

I thank the Natural Sciences and Engineering Research Council (NSERC) of Canada for financially supporting this research.

I would also like to thank CrossWing for providing the mobile platform (affectionately known as Jughead).

Last but not least, I would like to thank God and my family: my parents, Rajeev and Sangeeta and my sister Apoorva, for their love and support.

Contents

List of Tables

List of Figures

Chapter 1

Introduction

Indoor navigation and mapping, especially using mobile robots, is in ever increasing demand owing to its multiple applications. Many different sensors can be used for indoor navigation and mapping, including laser scanners, odometers, and different vision-based systems. The simplest and the lowest cost components are cameras. The light weight of cameras, as compared to some other sensors such as 3D laser scanner, is another beneficial characteristic. However, camera based navigation and mapping usually entails high processing and complex mathematical models.

Camera systems that can be used for this purpose are also of a wide variety. They can vary from a single camera to stereo camera to more complex systems such as dioptric and catadioptric systems. A single and a stereo camera system is shown in Figure 1.1((a) single and (b) stereo). Dioptric (example shown in Figure 1.2) and catadioptric (example shown in Figure 1.3, where the image on the left shows the system and the image on the right, a camera image) systems are gaining popularity due to their high field of view.

Figure 1.1: (a) Single Camera System (Super droid robots, 2013) and (b) Stereo Camera System (Stereo vision camera, 2011)

Dioptric cameras are lens based systems. A commonly used dioptric camera is the fish-eye lens camera. Catadioptric cameras are a combination of a conventional camera with mirror. Most commonly used catadioptric cameras aim to combine mirrors and lenses in such a way as to achieve a 360^0 horizontal view (Daniilidis and Geyer, 2003, Ohte et al., 2005, Gaspar and Victor, 1999). Such a catadioptric camera system is explored in this research. Although several configurations of catadioptric cameras are possible, the configuration most useful for this application, is a mirror in shape of a quadratic surface, for example a hemisphere, a paraboloid or a hyperboloid, symmetric about the line of the optical axis of the camera. The camera and mirror facing each other thus form an omnidirectional sensor (Figure 1.4).

Figure 1.2: Fish-eye lens (Nikon Fisheye lens, 2011)

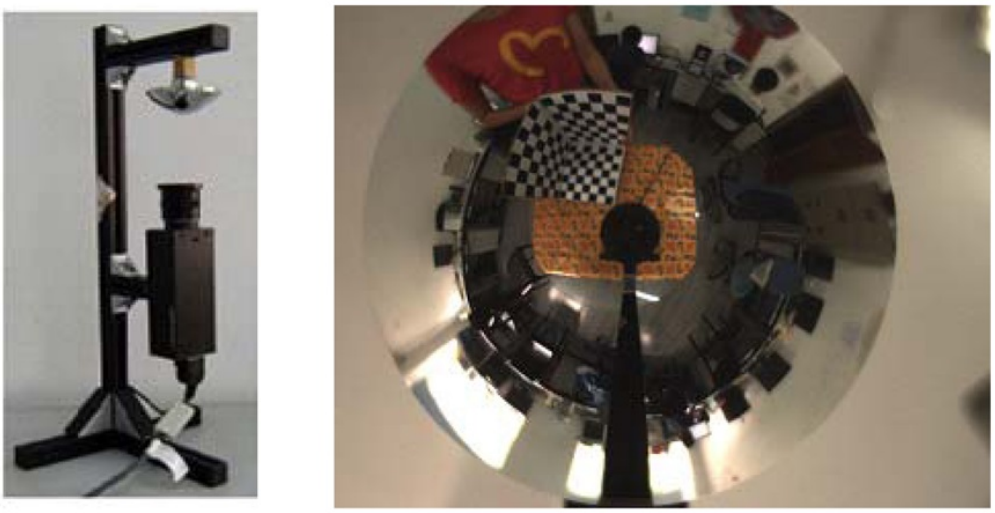

Figure 1.3: An example of Catadioptric Camera (Xiang et al., 2012)

Besides its wide field of view, there are further benefits of using a catadioptric camera for the purpose of navigation and mapping such as less processing due to the reduced number of images for the same amount of data, and thus resulting in the use of less storage space and higher processing speeds. Another advantage of catadioptric cameras as compared to a single perspective camera or a stereo camera system is that the 360^0 view allows for navigation in all directions without having to turn to view the whole environment or the direction of movement

if it is not visible, i.e. a higher spatial awareness. This will be further explored in detail in the later chapters of the thesis.

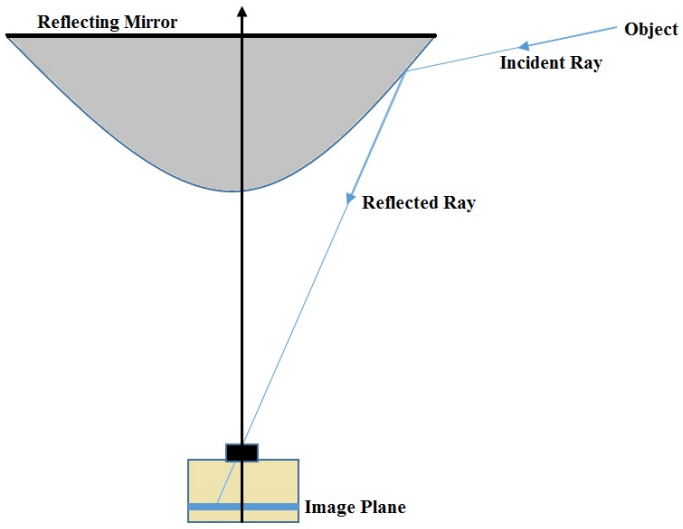

Figure 1.4: Working concept of a catadioptric camera.

1.1 Types of Catadioptric Cameras

Catadioptric cameras can be further divided into two types: central and non central (Baker and Nayar, 1999, Baker and Nayar, 2001, Swaminathan et al., 2006).

i) Central catadioptric cameras: A vision system is said to be central when the optical rays to the viewed objects intersect at a single point in 3D called single effective viewpoint (Figure 1.5a).

ii) Non-central catadioptric cameras: Non central catadioptric cameras do not have a single effective viewpoint (Figure 1.5b).

The existence of a single effective viewpoint depends on the type of mirror, type of camera and the relative position of the mirror and the camera. Central catadioptric camera systems

have an advantage over non-central catadioptric systems because of their geometry. Having a single effective viewpoint makes calculations simpler due to additional constraints in geometry. Therefore, developing a mathematical model for navigation and mapping using a central catadioptric camera system is relatively easier. On the other hand, the construction of a central catadioptric camera is very difficult to achieve.

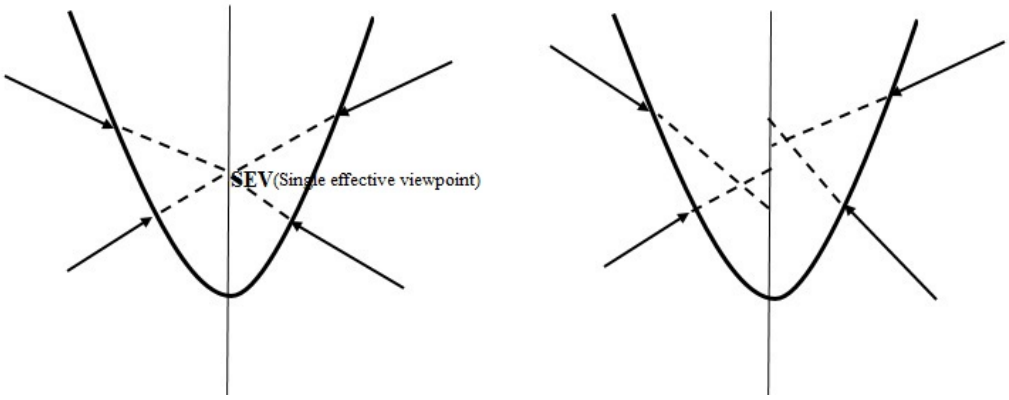

Figure 1.5: (a) Central and (b) Non-central Catadioptric Camera.

A central catadioptric camera consists of a hyperbolic or an elliptical mirror with a perspective camera or a telecentric lens with a parabolic mirror. Telecentric (or orthographic) lenses are lenses designed so that objects viewed through them do not show any magnification based on their distance. In all the aforementioned configurations, the axis of the mirror is to be perfectly aligned with the axis of the camera to obtain a single effective viewpoint. Another condition for construction of central catadioptric cameras in the case when elliptical or hyperbolic mirrors are used, is the placement of perspective camera at one of the focal points of the mirror. Therefore central catadioptric cameras have very specific configurations. Other configurations such as a spherical mirror with a perspective camera is a non central camera or even a hyperbolic mirror with a perspective camera and a misaligned optical axis do not have a single effective viewpoint. In solving for a non central catadioptric camera, not only is

there a requirement to overcome the lack of a single effective viewpoint but also to overcome a misalignment of the optical axis with the mirror. Therefore an additional calibration step is required in the mathematical model.

Even though the mathematical models provided in this thesis were developed for non-central catadioptric cameras, they can be implemented for both central and non-central systems since only the common reflection properties of the two are utilized.

1.2 Advantages and Applications

A summary of the advantages of the catadioptric system over other imaging systems systems follows:

1. Wide Field of View - The catadioptric camera systems provide 360^0 horizontal field of view, which is greater than any other single camera system or even a stereo camera system.

2. Low Cost - The catadioptric system is a relatively low cost system which can produce maps. Other mapping systems such as 3D laser range scanners are much more expensive.

3. Light weight - Both camera and mirrors are very light. Since a very high quality camera is not required, there aren't many restrictions and a light weight camera such as a USB camera can be used.

4. Flexibility - Several configurations can be used, i.e. options of different mirrors and cameras, of varying size and quality.

5. Mobility - Can be easily mounted on a mobile platform.

There are, however, certain limitations to the system as well.

1. The primary limitation of the catadioptric system is the sensitivity of positioning results. Small calibration errors or construction errors in the system can lead to large positioning and mapping errors. This is further described in Section 5.3.4. This exists due to the shape of the mirror and the overall geometry of the catadioptric system.

2. Another disadvantage of using catadioptric system arises due to the difficulty in designing or availability of the mirror. Mirrors with precise shapes are required for which a mathematical model can be developed.

3. Another limitation arises because of the distortions in the image. For automation of the procedure, a feature matching algorithm is required and the distortions of the objects in the catadioptric or unwrapped image, make it harder for them to be detected. This limits the number of points being mapped.

Vision based navigation and mapping using catadioptric camera systems, mounted on a mobile platform, are gaining popularity due to their potential applications (Thibault, 2008, Ilizirov and Filin, 2016). They have applications in the fields of:

1. Medicine: A mobile robot mounted with an imaging system can be used in hospitals to communicate with doctors, patients and nurses. It is expected to have additional tools such as a tablet so that doctors can communicate with their patients. They can also be used in nursing homes, again for primarily communication purposes (Bauer, 2007).

2. Inspection and Maintenance: Robotic catadioptric systems can be used to inspect environments by mapping the potentially harmful environments (such as mines) and relaying the map so as to test whether they are suitable for humans to enter or not. They can also be used to inspect environments which might be in need of maintenance (such as

tunnels) and relay the map. Other sensors which may help detect such risks, like video cameras or lasers, can be mounted on the mobile platform for such an application.

3. Security - Recently, robots are finding use in the security and defense sectors. They can be used with additional sensors for identification of toxic industrial (nuclear, radiological, chemical and biological) agents in an environment.

4. Agriculture - Robotic mapping and navigation can be useful especially during the fertilization stage in the agricultural process. This can be done mounting the fertilization tools on the robot. However, its application in the agricultural field requires mapping and navigation to be performed in an outdoor environment in contrast to other applications where mapping and navigation is performed indoors. (Singh et al., 2015, Pedersen et al., 2008)

5. Logistic Systems: They can be used in offices for cost optimization and task time reduction. A common example of a task which they can be used for is transporting objects such as files from one location to another. A further developed model with voice control could potentially be very useful in such an environment for other such purposes as well.

1.3 Research Objectives

The goal of this research is to design and construct a low-cost catadioptric camera system and use it for navigation of a mobile platform and mapping of an indoor environment. The aim is to make use of the advantages of a catadioptric system over other vision systems. For this purpose a portable system was constructed and experiments performed in a controlled environment in order to obtain an estimate of accuracy of mapping and navigation using a

catadioptric camera. Very few few restrictions were imposed on the constructed system in order to make it usable for a variety of cameras and mirror combinations. The experiments were performed using a parabolic mirror with a phone camera directly beneath it.

The mathematical models to solve for this system were designed keeping the flexibility of cameras and mirror in mind such that a changes in input parameters would account for the hardware changes. The overall approach and requirements of the system are described below:

Calibration - The most significant contribution of this research is the flexibility in terms of cameras and mirrors used and the unified solution provided for non-central and central catadioptric camera. A calibration process was an essential step required to achieve this. This process uses the targets set up on the system to obtain relative orientation and translation between mirror and camera. These can be accounted for in further calculations, allowing the mirror and camera to be considered a single monolithic system and thus allowing for flexibility.

Positioning and Navigation - The aim was to position the system in a known environment using the known ground control points in that environment. Reflection equations of the mirror were used for this purpose. A math model was designed so that the position of the system could be obtained using at least three known control points. More were used to obtain better accuracy. For navigation purposes, position of the system was determined using tie-points which were calculated by mapping.

Mapping - Mapping was performed using at least two known positions from where catadioptric images were obtained. Tie points, which were common points viewed in the catadioptric images from different locations, were obtained using two or more images and were used to determine the position of the system once it had moved further.

Accuracy - Since extensive work has not been done in this field, one of the goals of the

research was to find out the accuracy of a system with such a design. Accuracy of the order of decimeters (10-35 cm) was obtained for both positioning and mapping of the system. It is also to be noted that there can be a significant improvement in accuracy based on the mirrors and cameras used.

1.4 Thesis Outline

This thesis details the development of an indoor navigation and mapping system using a non-central catadioptric omnidirectional camera. Chapter 2 details the previous work done and development in the field of navigation and mapping using catadioptric cameras along with some of the unique contributions of this research. Chapter 3 describes the constructed mobile platform in order to test the proposed solutions. The specifications of the system are given along with its advantages. Calibration steps for the system are also provided. Chapter 4 describes, in detail, the methodology and the mathematical models involved in order to successfully perform navigation and mapping using the mobile platform. Chapter 5 describes the experimentation process. Images of experimentation sites are also provided along with the obtained result. Finally an error and efficiency analysis of the results is provided. This is followed by Chapter 7 which contains the conclusions from this research and provides suggestion for future development and research on the subject using the provided model.

Chapter 2

Background and Related Work

Several researchers from around the world have contributed to this field with most of the work focusing on calibration of omnidirectional cameras in order to obtain perspective-view images (panoramic images viewed as a mosaic of perspective images) from the system (Daniilidis and Geyer, 2000, Scaramuzza et al., 2006, Puig et al., 2001, Aliaga, 2001, Mei and Rives, 2007). Some of that research (Tahri and Araujo, 2012, Lhuillier, 2008) explored trajectory determination using common detected features and even 3D mapping using incremental bundle adjustment. However the initial and the main step in those studies focused on removing the image distortion caused by the shape of the mirror. The solutions for navigation and mapping using catadioptric cameras can be broadly divided into two categories: a) solutions based on ray-optics geometry (Daniilidis and Geyer, 2000, Aliakbarpour et al., 2014, Micusik and Pajdla, 2004) and b) solutions based on image unwrapping based on geometric conditions (Aliaga, 2001, Daniilidis and Geyer, 1999). Some of the solutions are discussed below, as they apply to this research.

2.1 Solution based on ray-optics geometry

These methods make use of the physical geometry of the catadioptric system, the mirror shape and reflection equations to obtain the respective image coordinates of a physical point

(in the object space) observed in the image. This is done in two steps involving the following coordinate transformations (Figure 2.1):

- Transformation of object coordinates (X_o, Y_o, Z_o) to mirror dome coordinates (X_d, Y_d, Z_d)
- Transformation of mirror dome coordinates (X_d, Y_d, Z_d) to camera (image) coordinates (x_c, y_c, f_c)

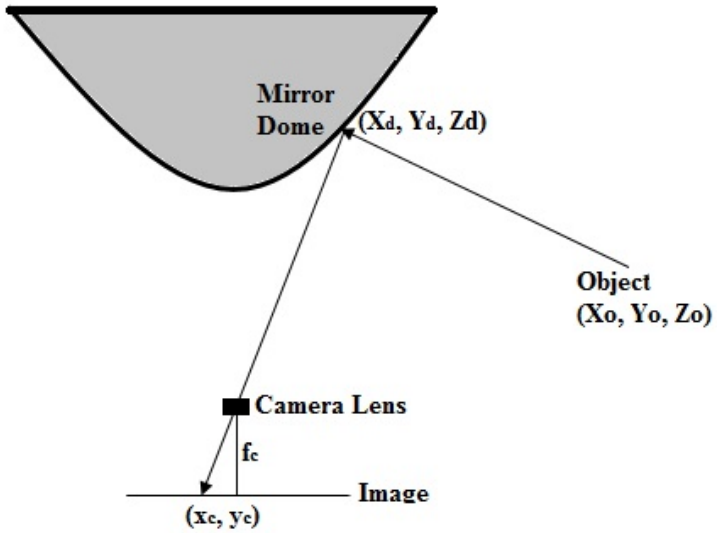

Figure 2.1: Solution based on ray-optics geometry

The mathematical models describe the relationship between the object point, its mirror surface reflection and the image of the physical point as captured by the camera lens. Once these mathematical models are known, the coordinates of the 3D points in the object space can be determined from their image coordinates using the mirror surface as an intermediate step.

An example of such a method is a widely used unified model proposed by Daniilidis and Geyer (2000) which has been implemented in several solutions with appropriate modifications (Daniilidis and Geyer, 2003, Aliaga, 2001, Mei and Rives, 2007). The objective of the solution is to project the 3D object coordinates on to a camera image plane by using a

unit sphere projection. A four step process of the approach was summarized by Scaramuzza (2014) and is described below (Figure 2.2):

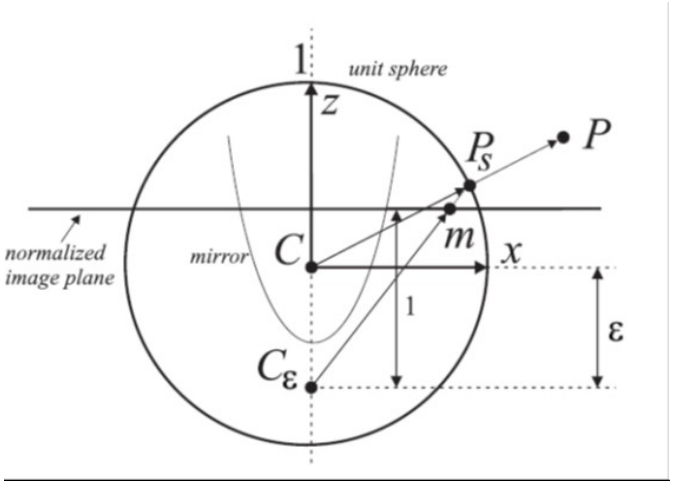

Figure 2.2: Unified model proposed by Geyer and Daniilidis (2000)

1. Projection of object point P on to a unit sphere: $P_S = \dfrac{P}{||P||} = (x_S, y_S, z_S)$.

2. Centering the coordinate reference frame at projection center: $P_\varepsilon = (x_S, y_S, z_S + \varepsilon)$, where $\varepsilon = C - C_\varepsilon$, where $C_\varepsilon$is $(0,0,-\varepsilon)$. The value of ε ranges between 0 (for planar mirror) and 1 (for parabolic mirror). The correct value of ε can be obtained knowing the distance between the foci of the conic and the latus rectum. The latus rectum of a conic section is the chord through a focus parallel to the conic section directrix.

3. P_ε is the n projected on to the normalized image plane $\widetilde{m}(x_m, y_m, 1)$, distant 1 from C_ε: $\widetilde{m} = (x_m, y_m, 1) = (\dfrac{x_S}{z_S + \varepsilon}, \dfrac{y_S}{z_S + \varepsilon}, 1) = g^{-1}(P_S)$.

4. $\widetilde{m}(x_m, y_m, 1)$ is then mapped on to camera image point $\tilde{p} = (u, v, 1)$ using intrinsic parameter matrix: $\tilde{p} = K\widetilde{m}$, where K is the intrinsic parameter matrix.

From this approach a direct relationship between object coordinate P and its image coordinate $\tilde{p}$ is established as shown in equation 2.1:

$$\tilde{p} = K.g^{-1}(\frac{P}{||P||}) \tag{2.1}$$

The uniqueness of this projection point is equivalent to a purely rotating planar camera with the helpful property that the rotated image is collineation of the original one (Daniilidis and Geyer, 2000). This solution is applicable only to catadioptric systems that have a single viewpoint geometry. In addition to applying the above solution to a system, certain other errors and distortions, such as lens distortion, need be accounted for in order to provide a more accurate solution (Mei and Rives, 2007).

Most other solutions also use central catadioptric systems (Barreto and Araujo, 2001). A couple of studies, however, do use non-central catadioptric cameras (Aliakbarpour et al., 2014, Micusik and Pajdla, 2004). Micusik and Pajdla (2004) use image feature matching to observe motion as discussed in next section.

Aliakbarpour et al. (2014) provide a model to allow for effective image-based visual servoing (IBVS) of a mobile robot using non-central catadioptric system symmetric with its mirror on an axis coinciding with the optical axis. The approach is very similar to the one described in this work. However the catadioptric system used in this research is fixed and the camera and the mirror are connected to each other. The mobile robot used along with the catadioptric camera is shown in Figure 2.3.

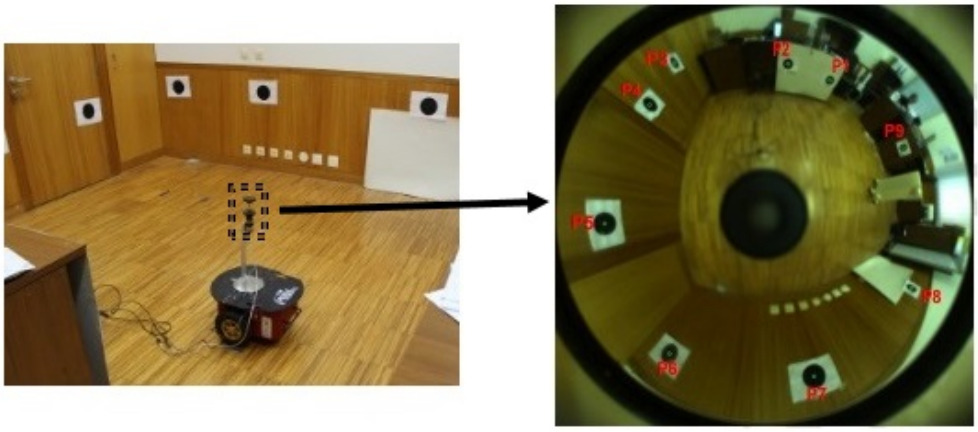

Figure 2.3: Mobile Robot and catadioptric images used in Aliakbarpour et al., 2014

2.2 Solutions based on object geometric condition and image unwrapping

This process makes use of geometric conditions of object features (e.g. vanishing points geometry) in order to obtain the parameters of distortion in the image and with the aim of rectifying it (image unwrapping, Figure 2.4). The rectified image can then be used to obtain object 3D coordinates by performing feature matching between two or more images taken using a catadioptric camera in motion. Image unwrapping is not necessary for feature matching, but if not done can result in a number of mismatches. An alternative would be rigorous post processing involving the removal of outliers (Micusik and Pajdla, 2004). Therefore image unwrapping is very useful. The functions used for image unwrapping are not simple collinearity models since conic sections are perceived as straight lines in the image. Therefore, due to the mirrors used in catadioptric cameras e.g. parabolic, hyperbolic, spherical, etc. complex mathematical models are required.

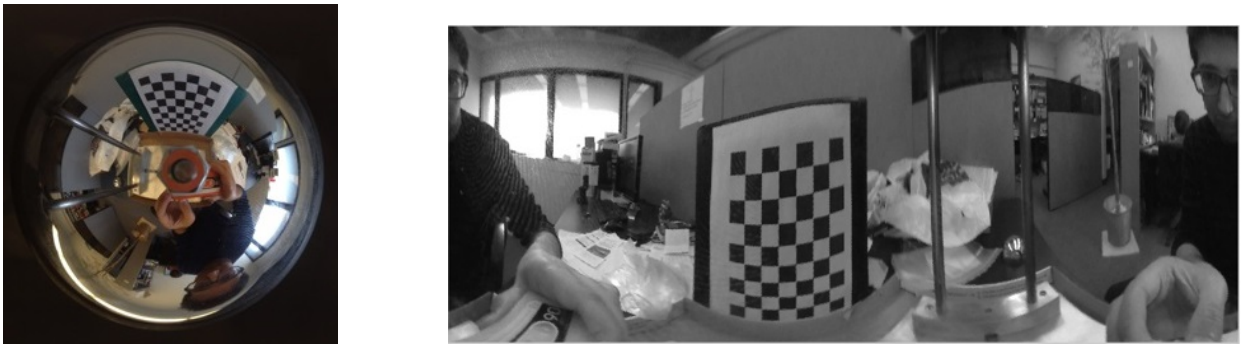

Figure 2.4: Image unwrapping

Daniilidis and Geyer (1999) extract spherical lines with the assumption that vanishing points of lines with coplanar directions lie on a circles. These are then used to obtain geometrical information, in order to rectify the image (Figure 2.5). Another approach which makes use of the mathematical projection of the image geometry is the Direct Linear Transformation (DLT) like approach as proposed by Puig et al. (2001). In the DLT approach a calibration technique for single viewpoint catadioptric systems was presented. It utilized a 6 x 10 projection matrix which was estimated using 3D-2D correspondences from a 3D calibration pattern and was decomposed to obtain interior and exterior orientation of the camera.

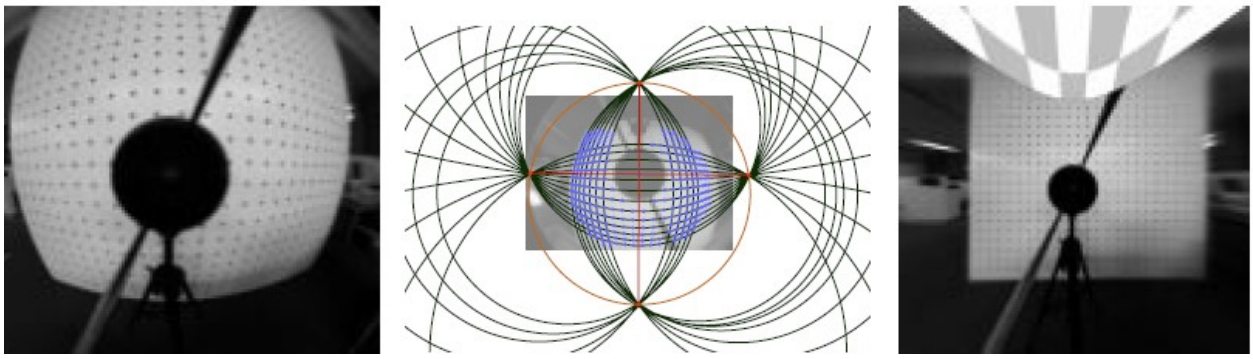

Figure 2.5: Using spherical lines to rectify images (Daniilidis and Geyer, 1999)

Other researches focus on unwrapping the catadioptric images, for example Bourgeois et al. (2011). However, they derive the mathematical model for unwrapping using the ray-optics geometry of the catadioptric system.

An example is a method by Svoboda et al. (1998). The main contribution of the paper is the derivation of the epipolar geometry between a pair of panoramic cameras. They decompose the mathematical model of a central panoramic camera into two central projections and therefore allow for an epipolar geometry formulation. However, despite its flexibility in these areas it is designed for central catadioptric cameras and as has been discussed before, those are hard to obtain in practice due to their precise construction.

Another approach proposed by Mabius and Tang (2008) uses an unwrapping transformation along with the nearest neighbor interpolation approach. Their unwrapping transformation consists of overcoming the curvilinear distortions present in the omnidirectional image by unwrapping it from a polar space to a cartesian one. However, the obtained results still have distortions and are not flexible for different mirrors. Therefore, using the resulting images for an application such as navigation and mapping would lead to considerably high errors.

Micusik and Pajdla (2004) using a non-central catadioptric camera, aimed to reconstruct the 3D environment from automatically established point correspondences between two images taken using a catadioptric camera in motion. But since the results were contaminated by mismatches, the focus of their research was to incorporate the auto calibration procedure into a robust estimation technique like Random Sample Consensus (RANSAC) (Fischler and Bolles, 1981). They proposed to solve the problem by constructing a hierarchy of camera models which includes a simplified central catadioptric model. The simplified model allows for the automatic recovery of inliers. Further, an accurate and complex non-central model is fitted to the point correspondences validated in the first step. The non-central model allows for the accurate reconstruction of scene geometry. However, in their case the mirror-camera

axis is horizontal. It was also observed that sparse 3D points are obtained. Based on the results it can be noted that this system is much more suited for crowded environments (with a lot of objects as common features) and not for navigation in open spaces, such as hallways.

2.2.1 Comparison of the two solutions

Both solutions (ray optics geometry and image unwrapping), besides having their own advantages and disadvantages are closely related. For example, if using ray optics geometry a relationship between object coordinates and respective image coordinates is obtained, then a mathematical model can be developed to obtain an unwrapped image at certain distance. Therefore, an unwrapped image can be obtained using the shape of the mirror and geometry of the catadioptric system.

However, this approach is not taken by any of the aforementioned researches. Using object geometric conditions such as spherical lines and vanishing points might not provide an exact solution for image unwrapping but do result in a much more simplified mathematical model. This results in the unwrapped image still having distortions. There is therefore a strong correspondence between the two solution and unwrapped image can be obtained from ray optics geometry, however, in many researches a simplified mathematical model is used. The reason for taking this approach might depend on the application. The solution using an wrapped image (based on object geometric conditions) might provide a denser point cloud with reduced accuracy.

2.3 Other Systems

Some of the other recent researches make use of alternative systems such as range finders. Range finders measure distance in a single plane but have recently been used with rotating platforms for 3D mapping. One such research by Chou and Liu (2013) makes use of a rotating laser range finder on a mobile platform. Several scans are performed and then co-registered using simultaneous localization and mapping. This process is performed iteratively to obtain a dense map of the environment. Another research done by Wang et al (2014) uses data obtained simultaneously from two range finders arranged perpendicularly to each other. One of the range finders is arranged normal to the plane of motion and another parallel to plane of motion. Pose fusion algorithms are used to obtain a dense 3D map in real time. In both the aforementioned researches the main limitation is the range of the range finder and they find their application mainly in areas such as corridors. The advantage of using a range finder is the density of the point cloud obtained, however another disadvantage besides the limited range might be the noise especially on certain surfaces such as glass. It should be noted that both these limitations depend on the range finders used and their cost.

Many current researches focus on combining data from multiple sensors. For example Gerstweiler et al (2016) makes use of inertial sensors and RGB camera built into a smartphone for localization and mapping. The developed system has the capacity of delivering a continuous position and orientation of the device. Castañón–Puga et al (2015) uses Wi-fi signals from selected access points for localization. This research also focuses on smart phones. The above mentioned researches and many other making use of multiple sensors are focused around building applications for cell phones involving localization, however, researches in the are of robotics, also make use of multiple sensors. An example would be the use of odometers along with a vision system. The added information from an odometer can provide a dynamic model for mapping and navigation and improve the accuracy. Ultrasonic sensors can also be used

along with camera systems for applications involving collision avoidance during navigation. Dioptric cameras, having a wider field of view as compared to a perspective camera, are also being explored for indoor mapping and navigation. However, they still have a limited field of view as compared to an omnidirectional catadioptric camera. A combination of perspective or dioptric cameras can also be used for similar applications with an added complexity of co-registering the data.

2.4 Issues

The following are some of the common issues observed in methods discussed above.

- Mirror Specific – A lot of the solutions can be implemented for only a certain type of mirror and are not universal. For example the catadioptric calibration method proposed by Puig et al. (2001) applies only for parabolic mirrors. An exception to this, however, is the unifying theory proposed by Geyer and Daniilidis (2000).

- Single viewpoint geometry – Most solutions only deal with systems with single effective viewpoint geometry. The ones which deal with non-central system are mathematically very complex (Aliakbarpour et al., 2014, Micusik and Pajdla, 2004).

- The results obtained from many of the above listed solutions rely heavily on manual training which involves accurately selecting several target points on the image in order to perform a 3D-2D correspondence (Scaramuzza et al., 2006).

- Several proposed methods require very specific designs and might suffer from calibration/design issues (Ohte, et al., 2006) for example imperfections in mirror shape and size and failure to align camera-mirror axis perfectly during construction .

2.5 Specific Contributions

The contributions of this research are described in detail in the following chapters. A portable catadioptric camera system was built and tested and mathematical models were developed

- To determine relative orientation of the mirror and camera and combine them into a single monolithic system.
- To form a one to one relationship between image coordinates and respective mirror coordinates using collinearity equations.
- To localize the catadioptric system in an indoor environment using control points. The model was based on reflection properties of the mirror and only a single image was required for this purpose.
- To calculate the coordinates of objects in the local environment using stereo system of catadioptric cameras.

Some of the most significant improvements, advancements and modifications from the aforementioned researches include:

- Applicable to non-central catadioptric cameras - As seen before, most researches described before are aimed at catadioptric cameras with single effective viewpoint. This is a limitation since central catadioptric cameras are very hard to construct and allow for only certain mirror shapes to be used. However, this research provides a mathematical model which can be applied to both non-central and central catadioptric cameras for mapping and navigation. This is because only common reflection properties of the two types of catadioptric cameras are made use of. Therefore, a wide range of catadioptric cameras can be used.

- Flexibility in mirror shape - This research also allows for flexibility in mirror shape. The mathematical model provided can be easily applied to mirrors of many shapes such as hyperbolic, parabolic, spherical and ellipsoid. The change of mirror, therefore, can be easily done and is allowed for in the calculation by a simple change of input parameters.

- Additional Design flexibility: Additional design flexibility is provided in the constructed system which is explained in the next section. A part of the research includes a calibration process which provides additional design flexibility and accounts for any imperfections in the construction process. Some of the additional design elements for which flexibility is allowed are:

    1. Mirror size - The mirror size in the constructed system can vary from 7 cm to 25 cm.

    2. Camera - The constructed system is very flexible. For the experiments performed an iPhone camera was used. This can be replaced by a digital camera or a USB camera for suitable purposes.

    3. Mirror to Camera Distance - The mirror-camera distance can be adjusted based on the lens and the size of the mirror so that the maximum possible environment is viewed in the catadioptric image with highest resolution possible.

- Automation and feature matching - In addition to providing a model based on ray-optics geometry, an image unwrapping technique is briefly described in section 4.4. The image unwrapping can assist in feature matching by restoring the attributes of the object (such as shape) in the image. Therefore, a combination of the two approaches can help with automatic mapping and navigation for future work on the research.

Chapter 3

Catadioptric Camera System

A platform was constructed for the implementation of a catadioptric camera for the purposes of navigation and mapping. The characteristics and specific design parameters of the platform are discussed below followed by the different coordinate systems used in the calibration and positioning of the system. Next, the mathematical model for the calibration of the mirror and camera is described.

3.1 System Description

The catadioptric camera used for the purposes of navigation and mapping consists of a quadratic surface shaped mirror facing towards the camera lens (Figure 3.1a). The aim is to have the mirror symmetric the optical axis of the camera. In this case a paraboloid mirror fixed facing down to a plate is used. This is attached to a base with the camera on it, facing up. The mirror as viewed from the camera is shown in Figure 3.1b. The paraboloid mirror can be replaced by hyperbolic, spherical, conical, or elliptical mirrors of varying sizes. The system was constructed to allow for flexibility in selecting:

1. Camera – The system can handle several different cameras. In the configuration used in experiments, the mirror is placed approximately 12 cm distance from the camera. However a flexibility of up to 35 cm is permitted. Since the different cameras use different lenses with different focal lengths and depths of field, this flexibility in positioning of the mirror allows for a wide range of cameras that can be used in this system.

2. Mirror shapes – hyperbolic, paraboloid, spherical or ellipsoidal mirrors can be used.

3. Mirror size –The aim was to have flexibility in platform so that it could be used with larger mirrors. The system was constructed to allow mirrors of different sizes (going up to 25cm in diameter)

and offering portability and significant visibility based on the mirror shape.

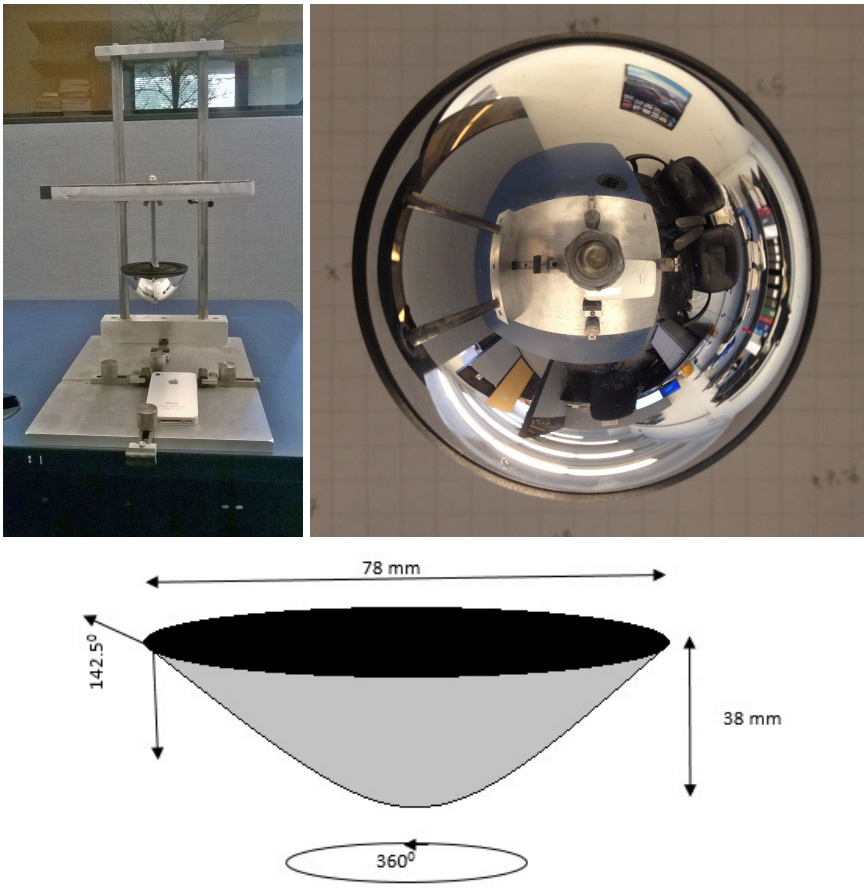

Figure 3.1: (a, top left) Constructed system, (b, top right) Corresponding Camera Image and (c, bottom) Mirror Dimensions

The mirror used is approximately 78 mm in diameter and 38 mm in height (Figure 3.1c). The mirror has a high vertical field of view of 142.5^0 (upwards from the nadir of the mirror) and

is non-central. The mirror is attached to the top plate using a ball screw in such a way that the mirror axis is perpendicular to the plate. The bottom plate, on which the camera is fixed is not assumed to be parallel to the top plate or mirror base even though attached to the top plate. This flexibility is allowed and the initial calibration process shown in the next section can be used to account for this. However, if such an assumption was made to reduce the number of calculations, it would be a safe one owing to the construction of the system. The distance between the base of the mirror and the top plate is kept fixed. The calibration method is used to calculate the distance between camera lens and the top plate and since the distance between top plate and mirror base can be measured, the distance between camera lens and mirror base, which is the one required for further calculations, can easily be calculated. The top plate can also be moved up and down to allow for the camera to capture the mirror image as best as possible. Therefore, if a mirror with a larger radius is used, a bigger gap between the top plate and bottom plate would be required. Basically, this feature exists in the system to allow for flexibility in the mirror size.

3.1.1 Platform - Mobile Robot

The final objective is to implement this system on a mobile robot (Figure 3.2). The robot shown was provided by CrossWing. The mirror on the mobile robot is approximately 4cm in radius and the distance between the camera and the mirror is measured to be approximately 12cm. Therefore, the specifications used are similar to that of the mobile robot, allowing more flexibility. The robot can have other sensors on it as well, enhancing the accuracy and increasing the applications of the system. Even though the robot shown was available, a decision was made to use the constructed system. This is because the constructed system allows much more flexibility in prototyping, not only in terms of size but also in terms of mirrors and cameras used. Several mirrors were initially tested, including convex mirrors,

mirrors of different sizes and a decision was made to use the current mirror based on the field of view, portability and the quality of the images. Another very important physical attribute which favors the use of constructed system rather than the robot for experimentation is the vertical distance between the camera and the mirror. Even though this distance is supposed to be fixed as in the case of the robot, the flexibility in the constructed system allows it to be fixed at the most suitable length, which allows the mirror to be fully viewed in the camera image as shown in the Figure 3.1b. Once experiments are performed and a suitable mirror and camera are selected, the same configurations can be implemented on a mobile robot. The use of camera and mirror located on the mobile robot would have limited the experimental process, therefore a flexible prototype system was used.

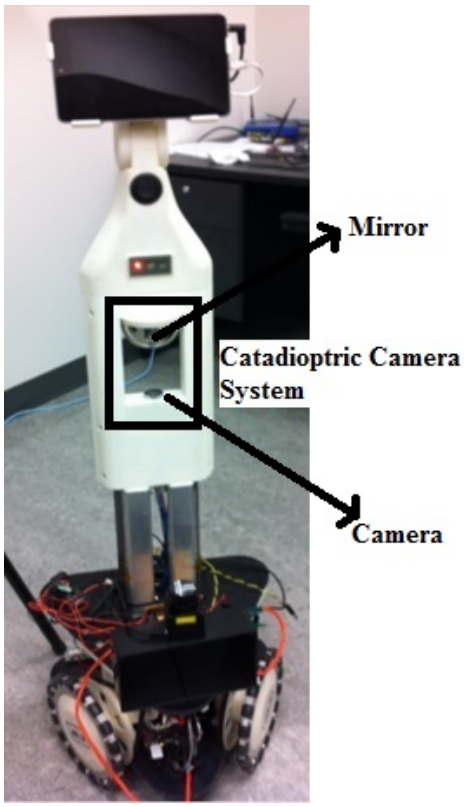

Figure 3.2: Mobile Robot

3.2 Coordinate Systems

For the purpose of developing and implementing the mathematical models for navigation and mapping, four different coordinate systems are used.

- Camera Coordinate system (X_c, Y_c, Z_c): This has the principal point as the origin, the Z axis is along the optical axis of the camera pointing to the mounting plate of the mirror, the X and Y axes form a right handed system as shown in Figure 3.3b. The X and Y axes of the camera coordinate system correspond to the X and Y axes of the image. The image coordinates exist in this coordinate system.

- Mirror Coordinate system (X_m, Y_m, Z_m): This system has the vertex of the mirror (V) as origin with the axis of symmetry as the Z axis pointing to the mounting plate of the mirror in a right handed system. The X and Y axes are parallel to the sides and front-end (respectively) of the top-plate. This is shown on the right in Figure 3.3a.

- Catadioptric coordinate system (X_{mc}, Y_{mc}, Z_{mc}): This is used for the catadioptric camera as a whole (mirror and camera). It is the same as the mirror coordinate system but a distinction is made to explain the terminology during calibration. This is because the objective of calibration is to describe the camera lens and image coordinate in the mirror coordinate system and is done by finding the relative orientation and position between the two. This coordinate system is shown in Figure 3.4.

- World Coordinate system (X, Y, Z): This is the reference system of the object space. A local coordinate system can be used, for example of a room or of a floor in a building, or a geodetic coordinate system such as NAD83 (horizontal) and NAVD88 (elevation) can be used. For the purpose of this research local coordinate system was used for the object space. Control points, which are used for the positioning of the catadioptric

camera are referred to in this system. 3D mapping will also be done in this coordinate system. This is shown in Figure 3.5.

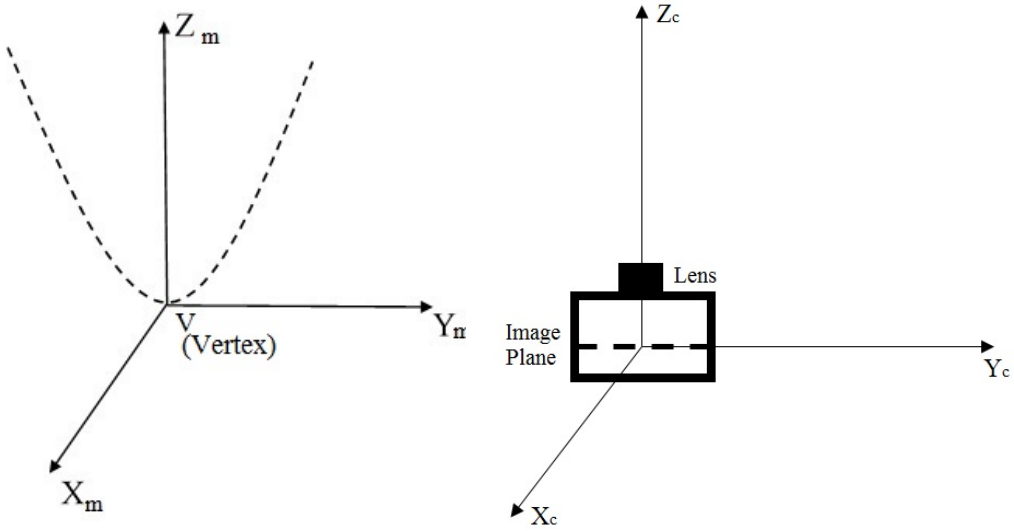

Figure 3.3: (a) Mirror and (b) Camera Coordinate System

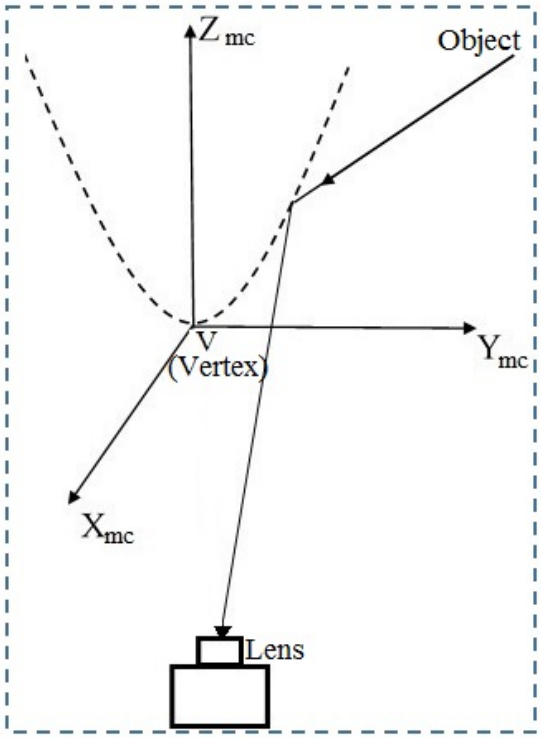

Figure 3.4: Catadioptric Coordinate System

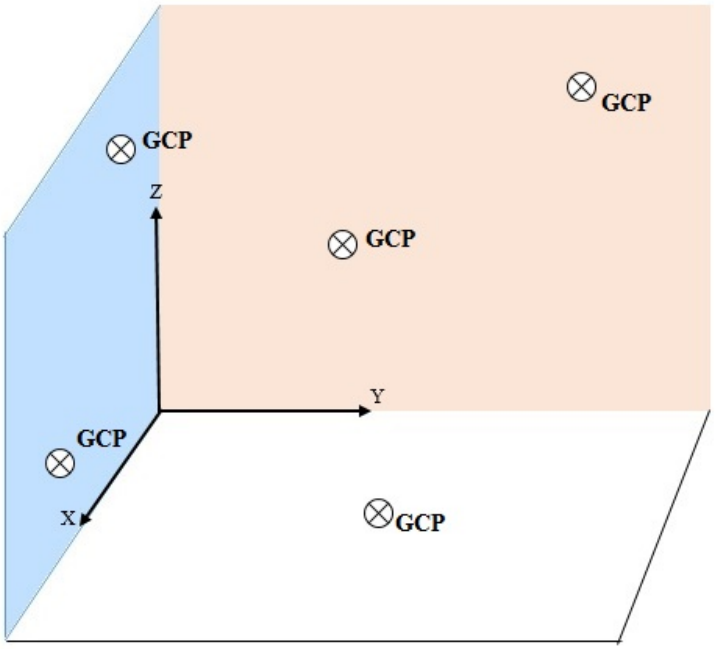

Figure 3.5: World Coordinate System

These coordinate systems are shown together in Figure 3.6. The coordinate systems are not only used to explain the mathematical model implemented, but also for the testing and assessment of models. Initially, the camera and the mirror coordinate systems are considered as separate systems, in order to obtain their relative orientation and translation. The position of the catadioptric camera is then obtained in the world coordinate system using control points. Finally the navigation and mapping results are obtained in the world coordinate system. This will be explored further in the rest of Chapter 3 and Chapter 4.

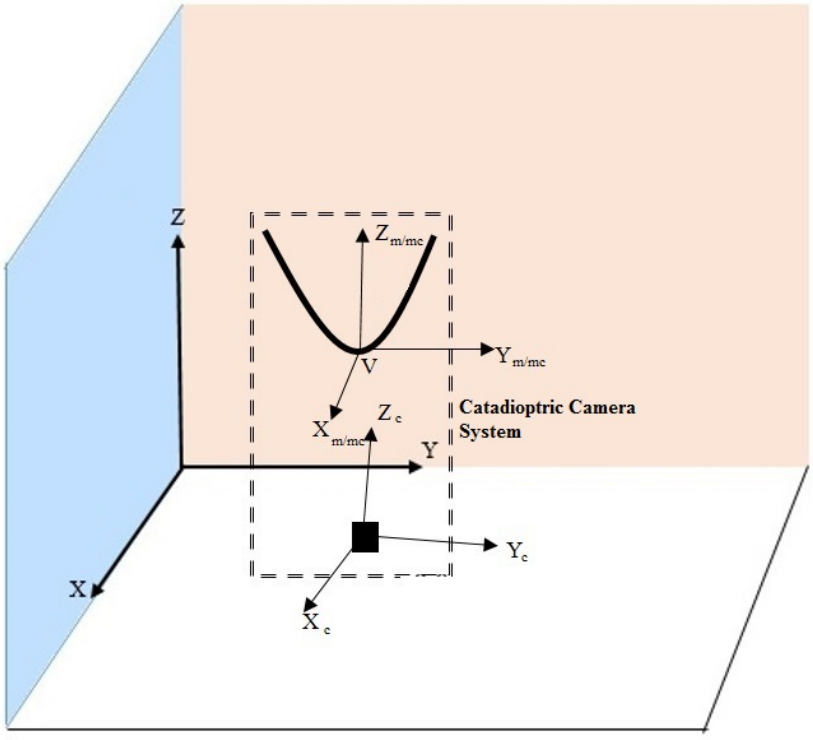

Figure 3.6: Catadioptric camera system and the relevant coordinate systems

3.3 Calibration of Mirror-Camera System

Two complexities will be examined in this section, namely:

1. Radial Distortion in camera image of the camera used in the catadioptric system (lens distortion): Radial distortion exists in the camera due to lens imperfections and cause an increase or decrease in the image magnification with an increasing distance from the optical axis. Correction parameters were found out by comparing measured pixel values and estimated ideal pixel values.

2. Relative Orientation and translation between mirror and camera in the catadioptric system: The catadioptric system consists of a camera and mirror and, as described before,

measurements from each were made in different coordinate systems. Therefore in order to consider the catadioptric system as a single monolithic system, it is essential to obtain their relative orientation and translation. Once these parameters the camera is described in the mirror coordinate system for further calculation. It is necessary for the catadioptric system to be considered as a monolithic system for calculations involving its positioning and navigation in the world coordinate system.

3.3.1 Corrections due to Radial Lens Distortion

In this subsection the radial distortion in the perspective camera used in the catadioptric system is examined. The results of camera calibration are provided in next section. The properties of radial distortion are described and a mathematical model is defined which helps in correcting the systematic errors caused due to radial distortion.

Radial distortion refers to deviation of the image points from a rectilinear projection (Figure 3.7), usually radially symmetric. It is caused due to an imperfection in the lens. Radial distortion can be of two types:

1. Negative Radial distortion: where image magnification decreases with the distance from the optical axis. This is also known as barrel distortion (Figure 3.8b).

2. Positive Radial Distortion: where image magnification increases with the distance from the optical axis. This is also known as pincushion distortion (Figure 3.8a).

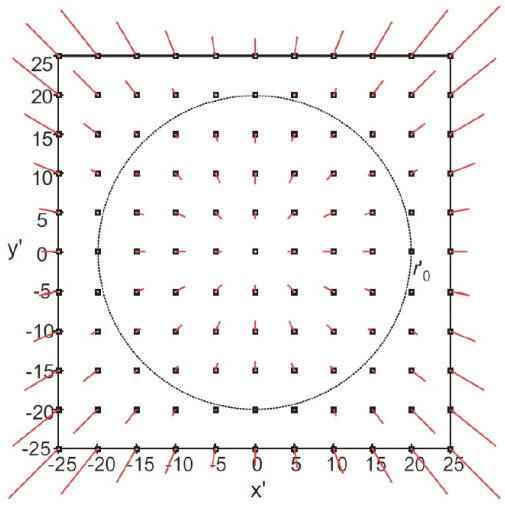

Figure 3.7: Radial Distortion

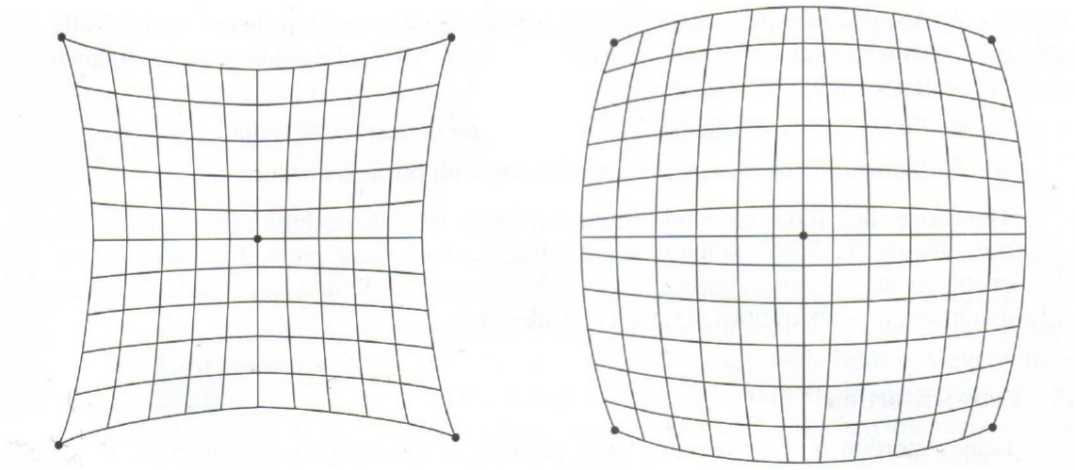

Figure 3.8: (a) Pincushion and (b) Barrel Distortion (Wikipedia, 2012)

Radial distortion can be calculated as follows:

Let p_x and p_y represent pixel values along x and y axis, and let r_{pp} represent the radial distance of that pixel from the principal point given by equation 3.1

$$r_{pp} = \sqrt{p_x^2 + p_y^2} \tag{3.1}$$

For each pixel, a new/corrected x and y pixel value, p'_x and p'_y may be obtained as shown in equation 3.2 and 3.3 (Brown, 1966, Zhang, 1998)

$$p'_x = (1 + k_1 r_{pp}^2 + k_2 r_{pp}^4) p_x \tag{3.2}$$

$$p'_y = (1 + k_1 r_{pp}^2 + k_2 r_{pp}^4) p_y \tag{3.3}$$

where k_1 and k_2 are radial distortion parameters which can be calculated by calibrating the camera.

During the calibration, the actual pixel value of points in the image is compared to the calculated ideal pixel value (where no distortion would exists) to obtain the radial distortion parameters using equations 3.2 and 3.3 and then these equations with calculated parameters can be applied to every pixel to obtain a rectified image.

Taking two known pixel values (p_{x1}, p_{y1}) and (p_{x2}, p_{y2}) and comparing them to corresponding ideal (calculated) pixel values (p'_{x1}, p'_{y1}) and (p'_{x2}, p'_{y2}), a pair of equations shown in 3.4 and 3.5 are obtained.

$$\begin{aligned} p'_{x1} &= (1 + k_1 r_{pp1}^2 + k_2 r_{pp1}^4) p_{x1} \\ p'_{y1} &= (1 + k_1 r_{pp1}^2 + k_2 r_{pp1}^4) p_{y1} \end{aligned} \tag{3.4}$$

$$\begin{aligned} p'_{x2} &= (1 + k_1 r_{pp2}^2 + k_2 r_{pp2}^4) p_{x2} \\ p'_{y2} &= (1 + k_1 r_{pp2}^2 + k_2 r_{pp2}^4) p_{y2} \end{aligned} \tag{3.5}$$

Since there are only two unknowns, theoretically only one pixel value (x and y each) is required for solution. However, to obtain an accurate solution several points are required.

This is because the ideal pixel values are manually selected and can have error in them. The over-determined system can then be solved using least squares adjustment (Levenberg, 1944, Marquardt, 1963, Ghilani, 2011).

The above equations 3.4 and 3.5 for several points can be written in matrix form as equation 3.6

$$\begin{bmatrix} r_{pp1}^2 & r_{pp1}^4 \\ r_{pp1}^2 & r_{pp1}^4 \\ r_{pp2}^2 & r_{pp2}^4 \\ r_{pp2}^2 & r_{pp2}^4 \\ \cdots & \cdots \\ \cdots & \cdots \end{bmatrix} \begin{bmatrix} k_1 \\ k_2 \end{bmatrix} = \begin{bmatrix} p'_{x1}/p_{x1} - 1 \\ p'_{y1}/p_{y1} - 1 \\ p'_{x2}/p_{x2} - 1 \\ p'_{y2}/p_{y2} - 1 \\ \cdots \\ \cdots \end{bmatrix} \tag{3.6}$$

Equation 3.6 can be re-written as equation 3.7

$$R_p \hat{k} = P_o \tag{3.7}$$

where R_p represents the design matrix, P_o represents the observation matrix shown on the right hand side in equation 3.6 and $\hat{k}$ represents the estimated radial distortion parameters and is calculated using least squares adjustment as shown in equation 3.8.

$$\hat{k} = (R_p^T R_p)^{-1} R_p^T P_o \tag{3.8}$$

3.3.2 Camera and Mirror Intrinsic Calibration

Before a calibration was performed to combine the mirror and camera into one monolithic system, an intrinsic calibration was performed for each of them. The specifications provided by the manufacturer were tested in each of these. For mirror, the shape and size was to be determined and for the camera, intrinsic parameters including focal length, principal points and radial distortion.

In order to calibrate the camera, MATLAB calibration toolbox (Bouguet, J.Y., 2015) was used. Several images of a grid were taken from varying angles. The focal length obtained for the camera was 4.5 mm. The principal points obtained were very close to the center of the image The toolbox also calculates the distortion coefficients and outputs an undistorted image.

The distortion coefficients vector was obtained as shown in Table 3.1:

Distortion Coefficients	
k_1	-0.00413
k_2	-0.01365
k_3	0.00124
k_4	0.00154

Table 3.1: Distortion Coefficients

The effect of these on the image was found to be negligible.

The principal points obtained are shown in table 3.2. The image size was determined to be 3264 x 2448 pixels.

Axes	Principal Point (Pixels)	Uncertainty (Pixels)
X	1641.76	26.79
Y	1228.02	15.75

Table 3.2: Distortion Coefficients

For mirror calibration, a couple of methods were explored. The first one involved using a profile image of the mirror against the grid, in order to obtain points along the mirror and plot it's shape along two axes. The mirror was found to be symmetrical about two of the axes with a diameter of 78 mm and height of 38 mm (along the third axes). The shape of the mirror was determined to be a paraboloid. The other method involved using range finder to obtain points on the mirror and using those to obtain it's shape. However, the results from this approach were not used due to the excessive noise caused by the surface of the mirror.

3.3.3 Collinearity Equations

The next step in calibration makes use of collinearity equations, the basics of which are described in this subsection. Collinearity equations can be used along with previously determined intrinsic matrix to determine the extrinsic parameters, i.e. relative orientation and spatial location of exposure station of the camera. Collinearity equations mathematically represent the relationship between the image and object coordinates. The collinearity equations involved along with other mechanics can be seen in Figure 3.9.

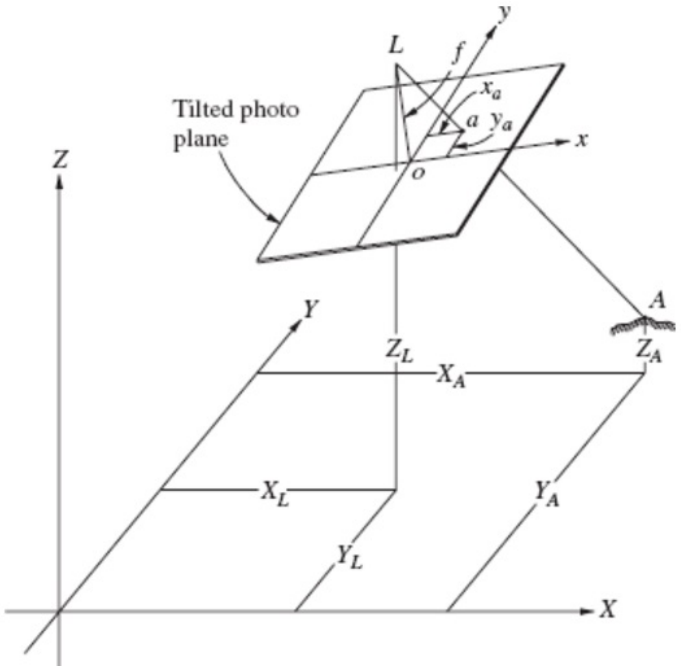

Figure 3.9: Collinearity Condition

From the Figure 3.9, two vectors $\overrightarrow{d}$ and $\overrightarrow{A}$ are defined as shown in equations 3.9 and 3.11.

$$\overrightarrow{d} = \overrightarrow{La} \tag{3.9}$$

so,

$$\overrightarrow{d} = \begin{bmatrix} x_a - x_L \\ y_a - y_L \\ -f \end{bmatrix} \tag{3.10}$$

and

$$\overrightarrow{A} = \overrightarrow{LA} \tag{3.11}$$

so,

$$\overrightarrow{A} = \begin{bmatrix} X_A - X_L \\ Y_A - Y_L \\ Z_A - Z_L \end{bmatrix} \tag{3.12}$$

Also from figure 3.9, equation 3.13 is obtained.

$$\overrightarrow{a} = kM\overrightarrow{A} \tag{3.13}$$

where k is the scale factor and M is the rotation matrix.

Using equations 3.10 and 3.12 equation 3.13 is re-written as $\begin{bmatrix} x_a - x_L \\ y_a - y_L \\ -f \end{bmatrix} = kM \begin{bmatrix} X_A - X_L \\ Y_A - Y_L \\ Z_A - Z_L \end{bmatrix}$.

Therefore for each each pair of a and A, two equations are obtained after eliminating scale factor. Therefore at least 3 pairs of a and A are required for the solution of the six unknowns (translation and rotation parameters), .

If the perspective camera is replaced by a catadioptric camera, certain complexities are added to this model.

3.3.4 Calibration of Mirror-Camera Systems

The intrinsic calibration of both camera and mirror was described earlier but since, the catadioptric camera system consists of two subsystems, the camera and the mirror (Figure 3.10), the relative linear and angular displacements between camera and mirror reference frames

are needed in order to consider the catadioptric camera as one monolithic system. These are calculated using another calibration process, which is performed between two rigid bodies with six degrees of freedom: rotation $(\omega_{mc}, \phi_{mc}, \kappa_{mc})$ and translation (X_{mc}, Y_{mc}, Z_{mc}) expressing the relative position and orientation of the two systems. A local 2D coordinate system, centered at the mirror vertex, is set up on the plate to which the mirror is attached. Four to eight points are marked as targets in this coordinate system on the top plate as shown in Figure 3.11b. The image of the targets captured by the camera (Figure 3.11a) is used to obtain relative orientation of the camera and the mirror. A 2D projective transformation is used to determine the angular and linear displacements. The 2D projective matrix has 8 unknown parameters. The eight unknown parameters exist due to the 6 degrees of freedom (rotation and translation) and 2 intrinsic parameters (x_p, y_p). The projection matrix, consisting of the 8 unknown parameters, can be compared to a homogeneous coordinate representation of collinearity equations. This representation includes a scale and intrinsic camera matrix. Since the camera has already been calibrated and its intrinsic parameters (principal points and focal length) are known, the 8 elements of projection matrix (once obtained) can be used to obtain the 6 linear and angular displacement parameters. This process is described in detail below.

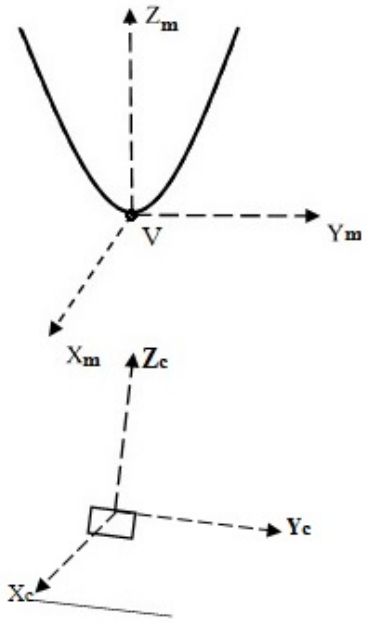

Figure 3.10: Mirror-Camera Calibration

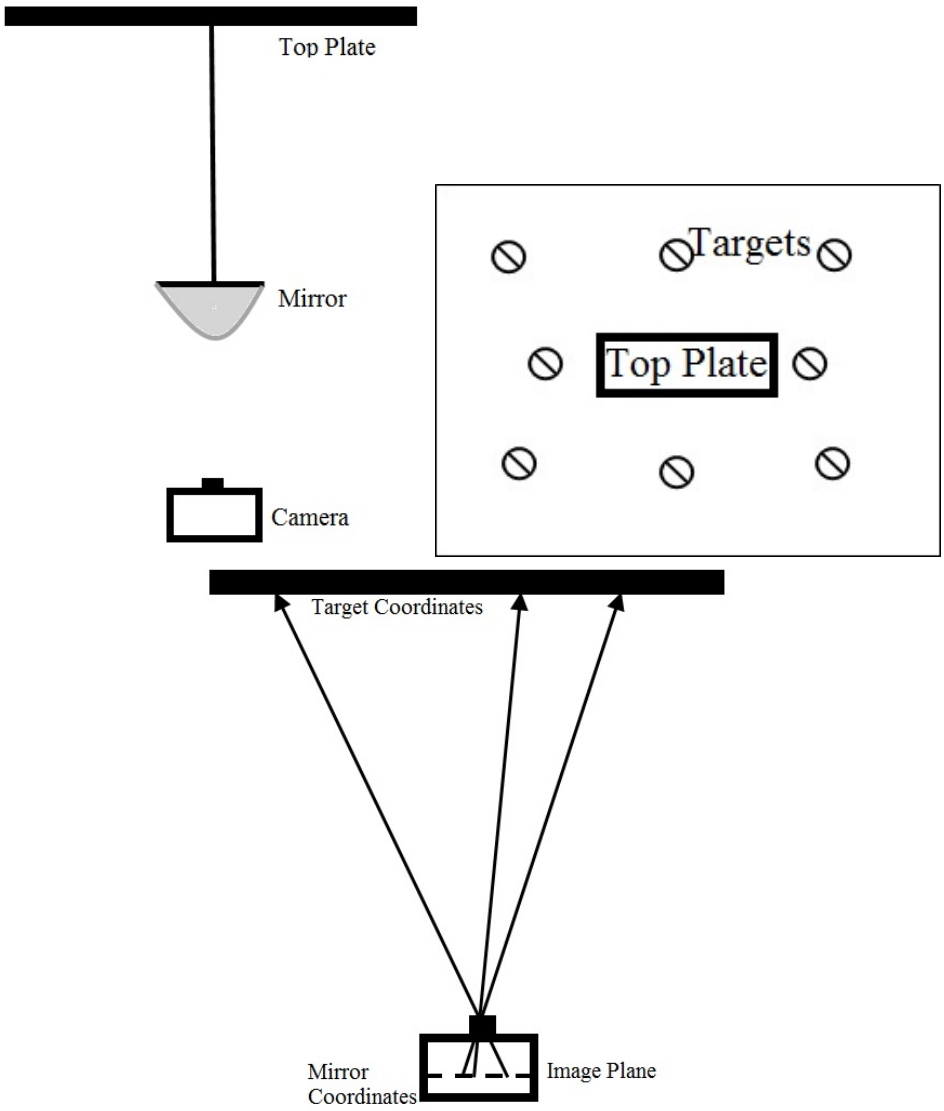

Figure 3.11: (a, left) Front and (b, right) Top view of calibration targets

The projective relationship between the plane of target coordinates and the plane image coordinates is given in equation 3.14 (Seedahmed and Habib, 2002)

$$\begin{bmatrix} x_m \\ y_m \\ 1 \end{bmatrix} = \begin{bmatrix} L_1 & L_2 & L_3 \\ L_4 & L_5 & L_6 \\ L_7 & L_8 & 1 \end{bmatrix} \begin{bmatrix} X_{tar} \\ Y_{tar} \\ 1 \end{bmatrix} \tag{3.14}$$

where X_{tar} and Y_{tar} represent the 2D coordinates of the targets on the top plate and x_m and y_m represent the image coordinates of the respective targets.

L_1.....L_8 are projection matrix elements.

The projection parameters L_i(i = 1 to 8) are calculated by mapping multiple targets from the top plate to the image. Each target gives two equations (equations 3.15 and 3.16), therefore, a minimum of four targets are required. Usually more points are used to obtain an over-determined result. The elements of the projection matrix are then used to obtain the rotation angles and translation (physical parameters) between the two planes.

Equation 3.14 can be written for the euclidean space as equation 3.15

$$\begin{aligned} x_m &= \frac{L_1 X_{tar} + L_2 Y_{tar} + L_3}{L_7 X_{tar} + L_8 Y_{tar} + 1} \\ y_m &= \frac{L_4 X_{tar} + L_5 Y_{tar} + L_6}{L_7 X_{tar} + L_8 Y_{tar} + 1} \end{aligned} \tag{3.15}$$

The image coordinates and their counterparts in the object space are treated as error free observations.

Equation 3.15 can be rewritten for more than four points in the form of equation 3.16

$$Ax = L + v \tag{3.16}$$

where x represents the unknown projection parameters shown in equation 3.17

$$x = \begin{bmatrix} L_1 & L_2 & L_3 & L_4 & L_5 & L_6 & L_7 & L_8 \end{bmatrix}^T \tag{3.17}$$

A represents the design matrix shown in equation 3.18

$$A = \begin{bmatrix} \frac{\partial x_{m_1}}{\partial L_1} & \frac{\partial x_{m_1}}{L_2} & \frac{\partial x_{m_1}}{L_3} & 0 & 0 & 0 & \frac{\partial x_{m_1}}{L_7} & \frac{\partial x_{m_1}}{L_8} \\ 0 & 0 & 0 & \frac{\partial y_{m_1}}{L_4} & \frac{\partial y_{m_1}}{L_5} & \frac{\partial y_{m_1}}{L_6} & \frac{\partial y_{m_1}}{L_7} & \frac{\partial y_{m_1}}{L_8} \\ .. & .. & .. & .. & .. & .. & .. & .. \end{bmatrix} \tag{3.18}$$

L represents the observation vector shown in equation 3.19

$$L = \begin{bmatrix} x_{m_1} & y_{m_1} & \dots & \dots \end{bmatrix}^T \tag{3.19}$$

and v is the residual vector shown in equation 3.20

$$v = \begin{bmatrix} v_{xm_1} & v_{ym_1} & \dots & \dots \end{bmatrix}^T \tag{3.20}$$

Substituting these matrices in equation 3.17 leads to equation 3.21

$$\begin{bmatrix} \frac{\partial x_{m_1}}{\partial L_1} & \frac{\partial x_{m_1}}{L_2} & \frac{\partial x_{m_1}}{L_3} & 0 & 0 & 0 & \frac{\partial x_{m_1}}{L_7} & \frac{\partial x_{m_1}}{L_8} \\ 0 & 0 & 0 & \frac{\partial y_{m_1}}{L_4} & \frac{\partial y_{m_1}}{L_5} & \frac{\partial y_{m_1}}{L_6} & \frac{\partial y_{m_1}}{L_7} & \frac{\partial y_{m_1}}{L_8} \\ .. & .. & .. & .. & .. & .. & .. & .. \end{bmatrix}_{n_e \times 8} \begin{bmatrix} L_1 \\ L_2 \\ L_3 \\ L_4 \\ L_5 \\ L_6 \\ L_7 \\ L_8 \end{bmatrix}_{8 \times 1} = \begin{bmatrix} x_{m_1} \\ y_{m_1} \\ .. \\ .. \end{bmatrix}_{n_e \times 1} \tag{3.21}$$

Where, n_e = number of equations and $n_e/2$ is the number of targets on the plate.

The weight matrix P = I. The projective matrix elements L_i can then be obtained by using a least squares adjustment using the formula provided in equation 3.22. Initial projection matrix was assumed as a unit matrix.

$$\hat{x} = (A^T A)^{-1} A^T L \tag{3.22}$$

Once the projective matrix elements L_i are obtained, they can be use to calculate the physical parameters of rotation, $R_{mc}(\omega_{mc}, \phi_{mc}, \kappa_{mc})$, and translation, $T_{mc}(X_{mc}, Y_{mc}, Z_{mc})$, based on the following collinearity condition for x_m and y_m and X_{tar} and Y_{tar} (equation 3.23).

$$\begin{aligned} x_m &= x_p - f\frac{m_{mc11}(X_{tar}-X_{mc}) + m_{mc12}(Y_{tar}-Y_{mc}) + m_{mc13}(-Z_{mc})}{m_{mc31}(X_{tar}-X_{mc}) + m_{mc32}(Y_{tar}-Y_{mc}) + m_{mc33}(-Z_{mc})} \\ y_m &= y_p - f\frac{m_{mc21}(X_{tar}-X_{mc}) + m_{mc22}(Y_{tar}-Y_{mc}) + m_{mc23}(-Z_{mc})}{m_{mc31}(X_{tar}-X_{mc}) + m_{mc32}(Y_{tar}-Y_{mc}) + m_{mc33}(-Z_{mc})} \end{aligned} \tag{3.23}$$

where,

x_p and y_p are principal point coordinates of the image plane and f is the focal length of the camera.

$$R_{mc} = \begin{bmatrix} m_{mc11} & m_{mc12} & m_{mc13} \\ m_{mc21} & m_{mc22} & m_{mc23} \\ m_{mc31} & m_{mc32} & m_{mc33} \end{bmatrix} \tag{3.24}$$

and,

$$
\begin{aligned}
m_{mc11} &= cos\phi_{mc}cos\kappa_{mc} \\
m_{mc12} &= cos\omega_{mc}sin\kappa_{mc} + sin\omega_{mc}sin\phi_{mc}cos\kappa_{mc} \\
m_{mc13} &= sin\omega_{mc}sin\kappa_{mc} - cos\omega_{mc}sin\phi_{mc}cos\kappa_{mc} \\
m_{mc21} &= -cos\phi_{mc}sin\kappa_{mc} \\
m_{mc22} &= cos\omega_{mc}cos\kappa_{mc} - sin\omega_{mc}sin\phi_{mc}sin\kappa_{mc} \\
m_{mc23} &= sin\omega_{mc}cos\kappa_{mc} + cos\omega_{mc}sin\phi_{mc}sin\kappa_{mc} \\
m_{mc31} &= sin\phi_{mc} \\
m_{mc32} &= -sin\omega_{mc}cos\phi_{mc} \\
m_{mc33} &= cos\omega_{mc}cos\phi_{mc}
\end{aligned}
\tag{3.25}
$$

Using homogeneous coordinate representation, equation 3.23 can be written as equation 3.26:

$$
\begin{bmatrix} x_m \\ y_m \\ 1 \end{bmatrix} = \lambda K \begin{bmatrix} m_{mc11} & m_{mc12} & -(m_{mc11}X_{mc} + m_{mc12}Y_{mc} + m_{mc13}Z_{mc}) \\ m_{mc21} & m_{mc22} & -(m_{mc21}X_{mc} + m_{mc22}Y_{mc} + m_{mc23}Z_{mc}) \\ m_{mc31} & m_{mc32} & -(m_{mc31}X_{mc} + m_{mc32}Y_{mc} + m_{mc33}Z_{mc}) \end{bmatrix} \begin{bmatrix} X_{tar} \\ Y_{tar} \\ 1 \end{bmatrix} \tag{3.26}
$$

where K is the intrinsic matrix, $K = \begin{bmatrix} 1 & 0 & \frac{-x_p}{f} \\ 0 & 1 & \frac{-y_p}{f} \\ 0 & 0 & \frac{-1}{f} \end{bmatrix}$

and λ is the scale factor.

Comparing equation 3.14 and equation 3.26, equation 3.27 is obtained.

$$\begin{bmatrix} L_1 & L_2 & L_3 \\ L_4 & L_5 & L_6 \\ L_7 & L_8 & 1 \end{bmatrix} = \lambda K \begin{bmatrix} m_{mc11} & m_{mc12} & -(m_{mc11}X_{mc} + m_{mc12}Y_{mc} + m_{mc13}Z_{mc}) \\ m_{mc21} & m_{mc22} & -(m_{mc21}X_{mc} + m_{mc22}Y_{mc} + m_{mc23}Z_{mc}) \\ m_{mc31} & m_{mc32} & -(m_{mc31}X_{mc} + m_{mc32}Y_{mc} + m_{mc33}Z_{mc}) \end{bmatrix} \quad (3.27)$$

Equating the first two columns on each side in equation 3.27 gives equation 3.28.

$$\begin{bmatrix} m_{mc11} & m_{mc12} \\ m_{mc21} & m_{mc22} \\ m_{mc31} & m_{mc32} \end{bmatrix} = \frac{1}{\lambda} K^{-1} \begin{bmatrix} L_1 & L_2 \\ L_4 & L_5 \\ L_7 & L_8 \end{bmatrix} \quad (3.28)$$

Equation 3.28 can be rewritten as equation 3.29.

$$\begin{bmatrix} m_{mc11} & m_{mc12} \\ m_{mc21} & m_{mc22} \\ m_{mc31} & m_{mc32} \end{bmatrix} = \frac{1}{\lambda} \begin{bmatrix} C_{11} & C_{12} \\ C_{21} & C_{22} \\ C_{31} & C_{32} \end{bmatrix} \quad (3.29)$$

where,

$$C = \begin{bmatrix} C_{11} & C_{12} \\ C_{21} & C_{22} \\ C_{31} & C_{32} \end{bmatrix} = K^{-1} \begin{bmatrix} L_1 & L_2 \\ L_4 & L_5 \\ L_7 & L_8 \end{bmatrix} \quad (3.30)$$

Due to the orthogonality conditions of the columns of the rotation matrix R_{mc}, equation 3.31 is obtained

$$m_{mc11}^2 + m_{mc21}^2 + m_{mc31}^2 = m_{mc12}^2 + m_{mc22}^2 + m_{mc32}^2 = 1 \quad (3.31)$$

From equation 3.29 and equation 3.31, the scale factor λ can be calculated as shown in equation 3.32,

$$\lambda = \left(C_{11}^2 + C_{21}^2 + C_{31}^2\right)^{1/2} = \left(C_{12}^2 + C_{22}^2 + C_{32}^2\right)^{1/2} \tag{3.32}$$

Substituting equation 3.32 in equation 3.29, equation 3.33 is obtained (Abdel-Aziz and Karara, 1971, Seedahmed and Habib, 2002).

$$\begin{bmatrix} m_{mc11} & m_{mc12} \\ m_{mc21} & m_{mc22} \\ m_{mc31} & m_{mc32} \end{bmatrix} = \begin{bmatrix} \frac{C_{11}}{\left(C_{11}^2+C_{21}^2+C_{31}^2\right)^{1/2}} & \frac{C_{12}}{\left(C_{12}^2+C_{22}^2+C_{32}^2\right)^{1/2}} \\ \frac{C_{21}}{\left(C_{11}^2+C_{21}^2+C_{31}^2\right)^{1/2}} & \frac{C_{22}}{\left(C_{12}^2+C_{22}^2+C_{32}^2\right)^{1/2}} \\ \frac{C_{31}}{\left(C_{11}^2+C_{21}^2+C_{31}^2\right)^{1/2}} & \frac{C_{32}}{\left(C_{12}^2+C_{22}^2+C_{32}^2\right)^{1/2}} \end{bmatrix} \tag{3.33}$$

Comparing equation 3.33 to the trigonometric values of the elements of rotation matrix, equations 3.34, 3.35 and 3.36 are obtained which can be used to calculate the physical angles of the rotation matrix $(\omega_{mc}, \phi_{mc}, \kappa_{mc})$.

$$\phi_{mc} = sin^{-1}\left(\frac{C_{31}}{\left(C_{11}^2 + C_{21}^2 + C_{31}^2\right)^{1/2}}\right) \tag{3.34}$$

$$\omega_{mc} = sin^{-1}\left(\frac{-C_{32} * sec(\phi_{mc})}{\left(C_{12}^2 + C_{22}^2 + C_{32}^2\right)^{1/2}}\right) \tag{3.35}$$

$$\kappa_{mc} = sin^{-1}\left(\frac{-C_{21} * sec(\phi_{mc})}{\left(C_{11}^2 + C_{21}^2 + C_{31}^2\right)^{1/2}}\right) \tag{3.36}$$

The translation matrix can be calculated from the scale factor, rotation matrix and projection matrix elements L_3 and L_6 using equation 3.37

$$T_{mc} = \begin{bmatrix} X_{mc} \\ Y_{mc} \\ Z_{mc} \end{bmatrix} = -\frac{1}{\lambda} R_{mc}^{T} K^{-1} \begin{bmatrix} L_3 \\ L_6 \\ 1 \end{bmatrix} \tag{3.37}$$

X_{mc} and Y_{mc} calculated here represent the deviation of the mirror vertex from the optical axis of the camera on the local X and Y axis, respectively. Z_{mc} represents the distance between the top plate and camera lens and needs to be corrected to obtain the distance between camera lens and mirror base. This can easily be done by subtracting those two values as shown in equation 3.38.

$$Z_{mc(Corrected)} = Z_{mc(Obtained)} - h_m - d_{pm} \tag{3.38}$$

The distance between camera lens and mirror base ($Z_{mc(Corrected)}$) will be represented as Z_{mc} in the following chapters since that is the value required for further calculations.

where, h_m= mirror height =78mm as described in Section 3.1, and

d_{pm} is the distance between top plate and mirror base.

Once R_{mc} and T_{mc} are obtained, the catadioptric camera can be considered as a monolithic system in order to perform calculations.

Chapter 4

Navigation and Mapping using Catadioptric Camera

Following the mirror-camera calibration, the position of the catadioptric system in the object space can be determined using control points (CP's), which are targetted points in the object space with known coordinates. This is repeated for several positions of the system. The images captured from these positions are then used to obtain the 3D coordinates of common features forming a sparse point cloud using epipolar geometry. These calculated coordinates can then be used to position the catadioptric camera once it has moved to its next location. These steps are repeated and constitute a sequential process for navigation and mapping.

4.1 Calculation of Mirror Coordinates of Control Points

As mentioned, the relative angular and linear displacements between the mirror and the camera as obtained from calibration can be used to combine the camera and mirror into a single monolithic system - the catadioptric camera. This is done by establishing a relationship between the image coordinates and the corresponding mirror coordinates of the control points (Figure 4.1). Essentially, the mirror coordinate of a CP is the intersection between the image ray emanating from the CP and the surface of the mirror. Using the collinearity equations (Wolf et al., 2014) and the shape of the mirror, a one-to-one relationship is established between the two sets of coordinates.

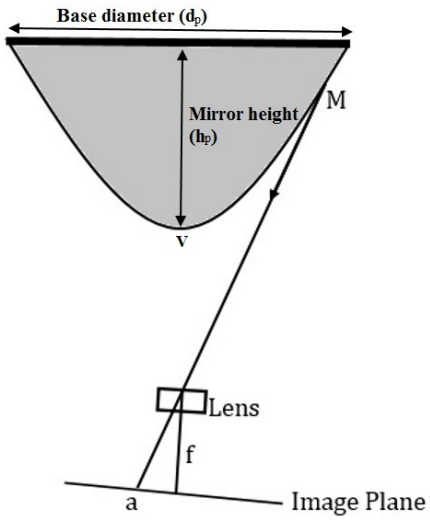

Figure 4.1: Mirror-Image Relationship

The objective is to determine the unknown mirror coordinates in the catadioptric coordinate system of the control points (X_{mi}, Y_{mi}, Z_{mi}), where i refers to the control point. The control point is reflected in the mirror at these mirror coordinates and then recorded in the image. The image coordinates x_{ai} and y_{ai} can be measured and are utilized to obtain mirror coordinates along with the already calculated rotation and translation matrices: $R_{mc}(\omega_{mc}, \phi_{mc}, \kappa_{mc})$ and $T_{mc}(X_{mc}, Y_{mc}, Z_{mc})$. The mirror coordinates are determined from these known parameters using their relationship as described by the collinearity equation and the equation of the mirror.

The two collinearity equations are:

$$x_{ai} = x_p - f\frac{m_{mc11}(X_{mi} - X_{mc}) + m_{mc12}(Y_{mi} - Y_{mc}) + m_{mc13}(Z_{mi} - Z_{mc})}{m_{mc31}(X_{mi} - X_{mc}) + m_{mc32}(Y_{mi} - Y_{mc}) + m_{mc33}(Z_{mi} - Z_{mc})} \tag{4.1}$$

$$y_{ai} = y_p - f\frac{m_{mc21}(X_{mi} - X_{mc}) + m_{mc22}(Y_{mi} - Y_{mc}) + m_{mc23}(Z_{mi} - Z_{mc})}{m_{mc31}(X_{mi} - X_{mc}) + m_{mc32}(Y_{mi} - Y_{mc}) + m_{mc33}(Z_{mi} - Z_{mc})} \tag{4.2}$$

and the equation of the paraboloid (surface of the mirror) is:

$$Z_{mi} - t_z = c_x(X_{mi} - t_x)^2 + c_y(Y_{mi} - t_y)^2 \tag{4.3}$$

where, x_p and y_p are principal point coordinates,

f represents the focal length of the camera

t_x, t_y and t_z are the x, y and z coordinates of the vertex V of the mirror, and

c_x and c_y describe the shape (curve) of the parabola along x and y axis respectively, such that $c_x = c_y = \frac{h_p}{\left(\frac{d_p}{2}\right)^2}$

Since the vertex of the mirror is the origin of the catadioptric coordinate system, $t_x = t_y = t_z = 0$

Therefore, the equation of the paraboloid can also be written as:

$$Z_{mi} = c_x(X_{mi}^2 + Y_{mi}^2) \tag{4.4}$$

Using the measurements of the paraboloid, 78 mm in diameter and 38 mm in height, c_x was determined to be 0.025.

The three equations 4.1, 4.2 and 4.4 yield a unique solution for each object point. A M_i (X_{mi}, Y_{mi}, Z_{mi}) is obtained for each a_i(x_{ai},y_{ai}). The image coordinate of each point are measured by the operator.

The coordinates of the camera lens in the catadioptric camera coordinate system are also known to be C($-X_{mc}, -Y_{mc}, -Z_{mc}$). In the next section C and M_i will be used to determine the position of the camera in the world coordinate system or the system of the indoor environment.

4.2 Positioning of the Catadioptric System

Once the camera catadioptric camera has been calibrated, it can be used for the purposes of positioning, mapping and navigation. Positioning involves using previously known co-ordinates of control points to obtain the coordinates of the catadioptric camera in the world coordinate system. Mapping uses stereo pairs of these positions to obtain 3D coordinates of common features. These common points are called "tie-points." Navigation can also be termed as "Incremental Positioning" since it uses the same mathematical model as positioning, the only difference being that the control used for navigation step is the coordinates of tie-points determined from mapping. This can be described using figures 4.2, 4.3 and 4.4.

In figure 4.2, previously set=up control points are used to calculate the coordinates of the catadioptric camera at two separate locations.

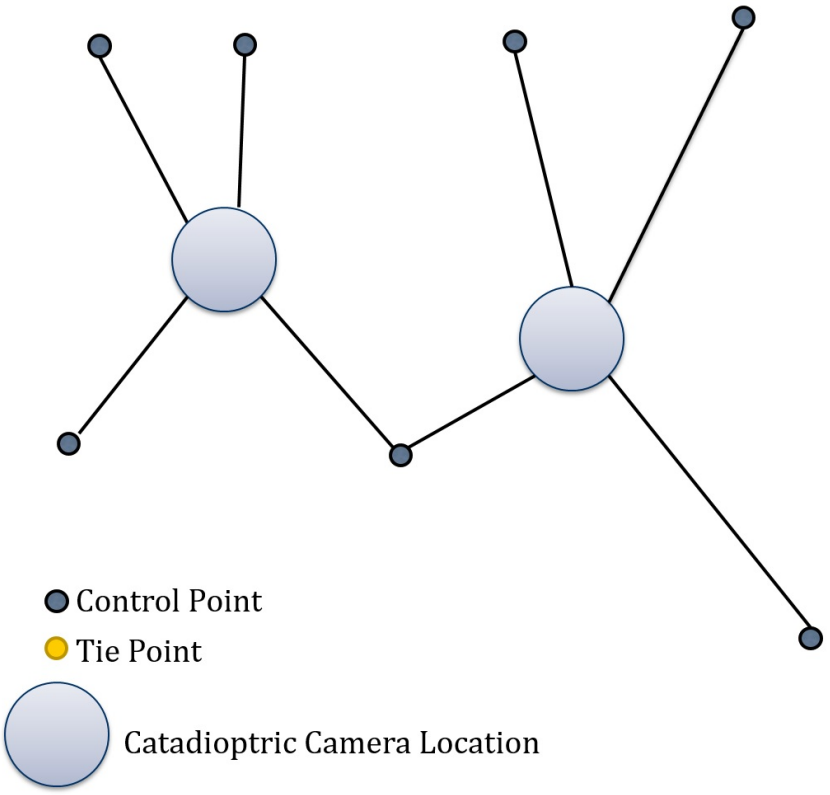

Figure 4.2: Positioning

In figure 4.3, the two positions are used in stereo to determine coordinates of four tie-points in the local environment.

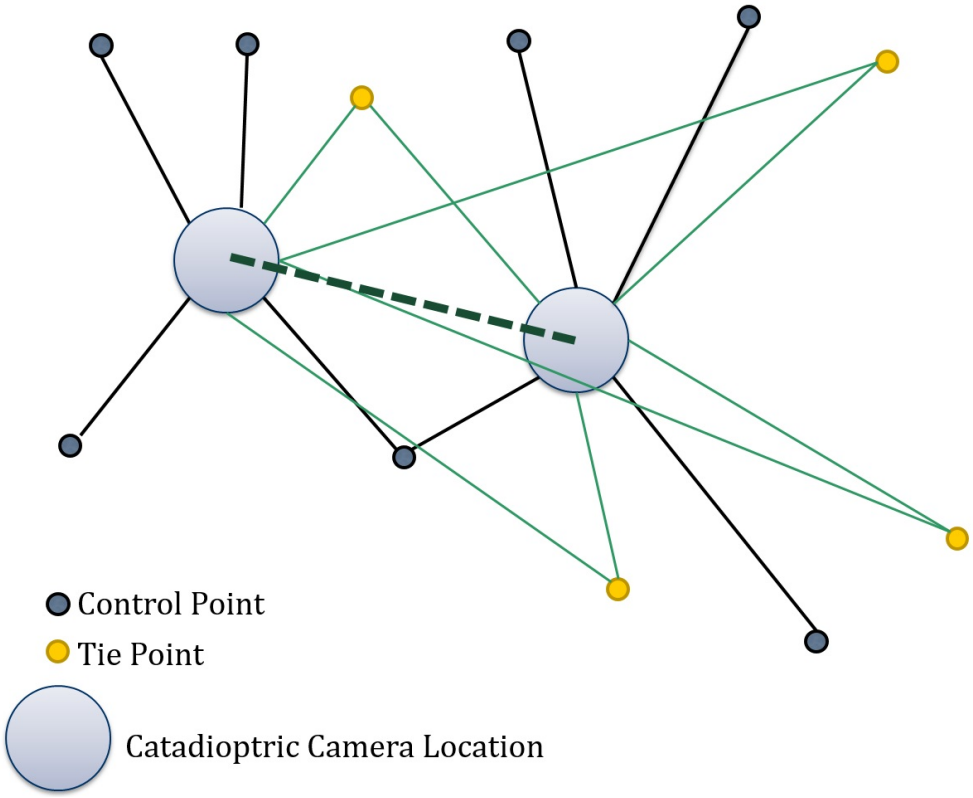

Figure 4.3: Mapping

In figure 4.4, the four tie-points, which were determined in the previous step are used to calculate the coordinates of the catadioptric camera at a new location. It should be noted that positioning and navigation (incremental positioning) make use of only one catadioptric image, whereas mapping requires at least two.

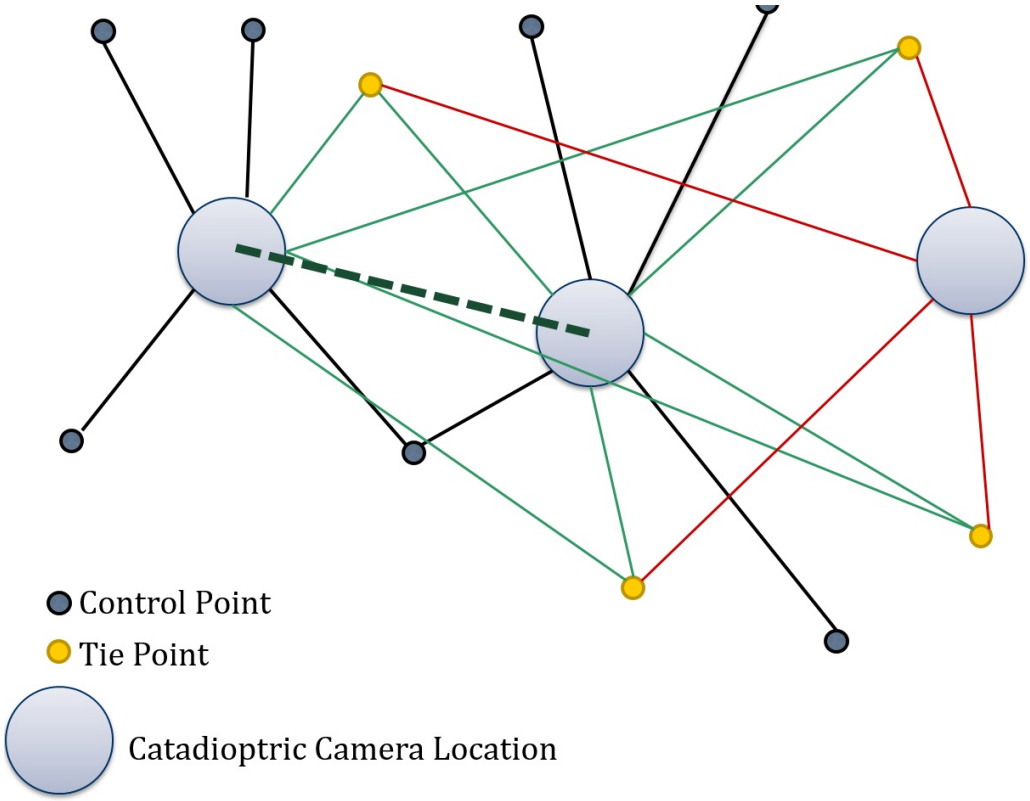

Figure 4.4: Navigation

Positioning of the catadioptric camera follows a very similar procedure as space re-sectioning. Multiple control points with known coordinates are used to obtain the 3D coordinates of the catadioptric camera in the world coordinate system. Due to the addition of a mirror, this process is more complex than space re-sectioning using a perspective camera. To account for this complexity, the reflective properties of the mirror are utilized. A detailed methodology to obtain the 3D coordinates of catadioptric camera in a local environment is discussed in subsection 4.2.1.

4.2.1 3D coordinates of the camera in the world coordinate system

For the purpose of positioning the catadioptric camera in the world coordinate system, the coordinates of the camera lens, expressed by C($-X_{mc}, -Y_{mc}, -Z_{mc}$) and mirror coordinates

in local coordinate system $M_i(X_{mi}, Y_{mi}, Z_{mi})$ are utilized. The coordinates of CP's in world coordinate system will also be required. These are described as $P_i(X_{pi}, Y_{pi}, Z_{pi})$.

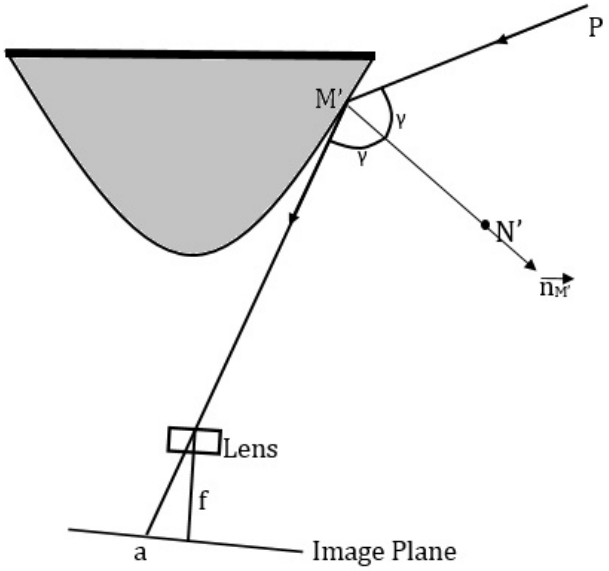

Figure 4.5: CP reflection on mirror (Camera View)

Since the system of the catadioptric camera is to be positioned in the world coordinate system, there are 6 unknown parameters to be determined, namely 3 rotational parameters ($R(\omega, \phi, \kappa)$) and 3 translation parameters ($T(X_T, Y_T, Z_T)$). These are solved using the mirror's reflective properties. R and T are then used to calculate C in world coordinate system (C'), which represents the position of the catadioptric camera.

C=$(X_C, Y_C, Z_C) = (-X_{mc}, -Y_{mc}, -Z_{mc})$

Camera lens coordinates in world coordinate system are determined by a 3D similarity transform (equation 4.5),

$$C' = \begin{bmatrix} X'_C \\ Y'_C \\ Z'_C \end{bmatrix} = R \begin{bmatrix} X_C \\ Y_C \\ Z_C \end{bmatrix} + \begin{bmatrix} X_T \\ Y_T \\ Z_T \end{bmatrix} \tag{4.5}$$

Similarly, the corresponding mirror coordinates in wold coordinate system of the control points can be determined by equation 4.6.

$$M_i' = \begin{bmatrix} X_{mi}' \\ Y_{mi}' \\ Z_{mi}' \end{bmatrix} = R \begin{bmatrix} X_{mi} \\ Y_{mi} \\ Z_{mi} \end{bmatrix} + \begin{bmatrix} X_T \\ Y_T \\ Z_T \end{bmatrix} \tag{4.6}$$

where,

$$R = \begin{bmatrix} m_{11} & m_{12} & m_{13} \\ m_{21} & m_{22} & m_{23} \\ m_{31} & m_{32} & m_{33} \end{bmatrix} \tag{4.7}$$

where,

$$\begin{aligned} m_{11} &= cos\phi.cos\kappa \\ m_{12} &= cos\omega.sin\kappa + sin\omega.sin\phi.cos\kappa \\ m_{13} &= sin\omega.sin\kappa - cos\omega.sin\phi.cos\kappa \\ m_{21} &= -cos\phi.sin\kappa \\ m_{22} &= cos\omega.cos\kappa - sin\omega.sin\phi.sin\kappa \\ m_{23} &= sin\omega.cos\kappa + cos\omega.sin\phi.sin\kappa \\ m_{31} &= sin\phi \\ m_{32} &= -sin\omega.cos\phi \\ m_{33} &= cos\omega.cos\phi \end{aligned} \tag{4.8}$$

Since the mirror surface is perfectly reflective, it is known that the incident angle (γ) between the vector $\overrightarrow{P_iM_i'}$ and the normal vector of the surface on that point n_{Mi}' is the same as the

reflected one between $\overrightarrow{C'M'_i}$ and n'_{Mi} (Figure 4.5). However, the normal vector in the world coordinate system is not known but can easily be derived as the normal vector to the mirror surface at point M' (equation 4.11). Therefore, to obtain the normal vector, the equation of the mirror in the world coordinate system and the coordinates of the point are required. These, however, are yet to be calculated after the rotation and translation matrix are obtained. Therefore the only way to use n'_{Mi}, and the condition of equal angles, is by having n'_{Mi} as a function of R and T.

The normal vector, n'_{Mi}, is first calculated in the coordinate system of the catadioptric camera. N_i is a point at unit distance along the normal vector from M_i (in catadioptric coordinate system).

Equation 4.9 gives the equation of the paraboloid (shape of the mirror)

$$Z_{mi} = c_x(X_{mi}^2 + Y_{mi}^2) \tag{4.9}$$

Using the equation of the paraboloid, the normal unit vector in the catadioptric coordinate system at the mirror coordinate M_i can be represented by equation 4.10

$$\hat{n_{Mi}} = \left(\frac{\nabla Z_{mi}}{||\nabla Z_{mi}||}\right)_{M_i} = \overrightarrow{M_i N_i} \tag{4.10}$$

where $\nabla = \begin{bmatrix} -\partial f/\partial x \\ -\partial f/\partial y \\ -1 \end{bmatrix}$

M_i was calculated using equations 4.1, 4.2 and 4.4.

The normal vector (in world coordinate system) can be represented by using equation 4.11

$$n'_{Mi} = \left(\frac{\nabla Z'_{mi}}{||\nabla Z'_{mi}||} \right)_{M'_i} \tag{4.11}$$

But as described before M'_i is not known. An alternative way to describe n'_{Mi} is required. n'_{Mi} can be described as a function of the rotation matrix as follows:

$$n'_{Mi} = \overrightarrow{M'_i N'_i} = (RN_i + T) - (RM_i + T) = R(N_i - M_i) = R(\overrightarrow{M_i N_i}) = R\hat{n_{Mi}} \tag{4.12}$$

Therefore, the relationship between the normal vector in the catadioptric coordinate system ($\hat{n_{Mi}}$) and normal vector in world coordinate system (n'_{Mi}) can be described by equation 4.13.

$$n'_{Mi} = R.\hat{n_{Mi}} \tag{4.13}$$

Since, the incident angle (γ) between the vector $\overrightarrow{P_i M'_i}$ and n'_{Mi} is the same as the reflected one between $\overrightarrow{C' M'_i}$ and n'_{Mi}, equation 4.14 is obtained.

$$\frac{\overrightarrow{C' M'_i}.n'_{Mi}}{||C' M'_i||} = \frac{\overrightarrow{P_i M'_i}.n'_{Mi}}{||P_i M'_i||} \tag{4.14}$$

Equation 4.14 can be rewritten as equation 4.15. This is done to obtain the residuals in the units of distance.

$$||P_i M'_i|| - \left(\frac{\overrightarrow{P_i M'_i}.n'_{Mi}}{\overrightarrow{C' M'_i}.n'_{Mi}} \right) ||C' M'_i|| \tag{4.15}$$

Another observation that can be made is that the three vectors (reflection, incidence and normal) lie in the same plane, therefore the coplanarity condition can be applied as shown in equation 4.16.

$$\overrightarrow{C'M'_i}.(n'_{Mi} \times \overrightarrow{P_iM'_i}) = 0 \tag{4.16}$$

C' and M'_i are substituted from equations 4.5 and 4.6 in equations 4.15 and 4.16 to obtain R and T, respectively. However, since there are only two equations and 6 unknowns $(\omega, \phi, \kappa, X_T, Y_T, Z_T)$, at least 3 CP's and the corresponding mirror coordinates are required. Therefore $i \geq 3$. More control points were used to obtain an over-determined result. There are also restrictions on which control points can be used based on their geometry. For example, collinear control points cannot be used since that leads to an ill-conditioned numerical solution. Control points spread out in different directions and at different elevations are preferred.

Figure 4.6 below displays how the catadioptric system is positioned using targetted CP in the indoor environment.

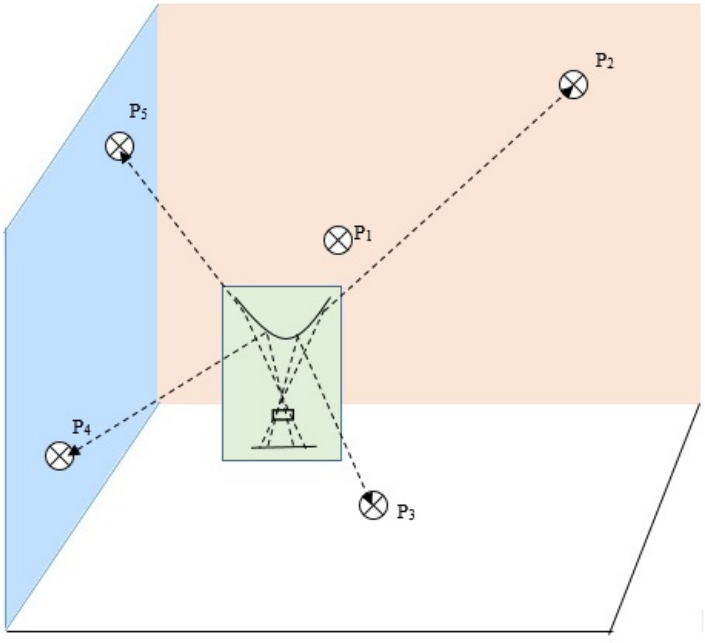

Figure 4.6: Indoor Environment

The above equations for all points can be rewritten in the form of equation 4.17.

$$By = 0 \tag{4.17}$$

where y represents the unknowns and shown in equation 4.18.

$$y = \begin{bmatrix} \omega & \phi & \kappa & X_T & Y_T & Z_T \end{bmatrix}^T_{6\times 1} \tag{4.18}$$

and B represents the design matrix shown in 4.19.

$$B = \begin{bmatrix} \frac{\partial f_i}{\partial \omega} & \frac{\partial f_i}{\partial \phi} & \frac{\partial f_i}{\partial \kappa} & \frac{\partial f_i}{\partial X_T} & \frac{\partial f_i}{\partial Y_T} & \frac{\partial f_i}{\partial Z_T} \\ \frac{\partial g_i}{\partial \omega} & \frac{\partial g_i}{\partial \phi} & \frac{\partial g_i}{\partial \kappa} & \frac{\partial g_i}{\partial X_T} & \frac{\partial g_i}{\partial Y_T} & \frac{\partial g_i}{\partial Z_T} \\ .. & .. & .. & .. & .. & .. \end{bmatrix}_{(n_P/2)\times 6} \tag{4.19}$$

Where n_p is number of CP's

These can then be solved together for all unknowns using all points by using least squares adjustment. The initial parameters for each location were approximated as the center of the room with no rotation.

It should be noted, however, that least squares works optimally for systems where certain assumptions can be made. One of these assumptions being that X and Y are identically distributed without any bias. In this case, distribution along X and Y is different because of the shape of mirror, i.e. objects in the local environment appear distorted in the image of the mirror. This is the image which is used for measurements. However, least squares was still assumed with the assumption that such distortions have minimal effect on the results.

4.3 Mapping using Catadioptric System

Once R and T have been calculated, the position of the catadioptric camera in the world coordinate system can be obtained. The position of camera lens, C'(RC + T) and the mirror coordinates of the CP's, $M_i'(RM_i + T)$ can also be calculated. Following an identical process for an image taken from a different position, using the same or different targets, the position coordinates for the catadioptric camera at a different position can be determined. Since system settings might change at a different location, there might be a need to repeat calibration and make use of those parameters while determining the new position. Therefore two (or more) images taken from different positions are used to obtain 3D coordinates of common features. This is done by space intersection using coplanarity conditions.

4.3.1 Space intersection using coplanarity

Space intersection makes use of known or previously determined exterior orientation of at least two exposure stations along with measured image coordinates of object points to determine their coordinates. This is done using the coplanarity condition which mathematically describes the relationship between three vectors $\overrightarrow{B}$, $\overrightarrow{U_1}$ and $\overrightarrow{U_2}$ lying in the same plane (Figure 4.7), where $\overrightarrow{B}$ is the image base connecting the left camera location L_1 and right camera location L_2, $\overrightarrow{U_1}$ is the ray vector connecting L_1 with the object point A and $\overrightarrow{U_2}$ is the ray vector connecting L_2 with A. The images of A on left and right images are a_1 and a_2 respectively.

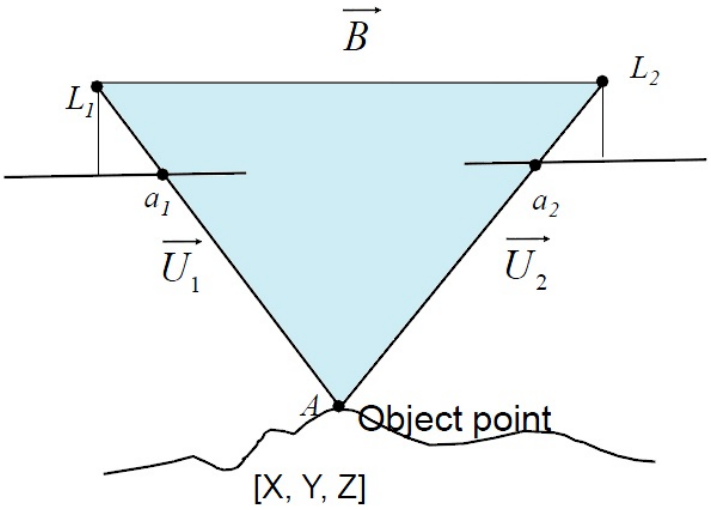

Figure 4.7: Coplanarity Condition

From Figure 4.7, equations 4.20, 4.21, 4.22 and 4.23 can be observed, that:

$$\overrightarrow{B} = \overrightarrow{L_2} - \overrightarrow{L_1} \tag{4.20}$$

$$\overrightarrow{L_1A} = \overrightarrow{U_1} = \Lambda_1 \overrightarrow{a_1} \tag{4.21}$$

$$\overrightarrow{L_2A} = \overrightarrow{U_2} = \Lambda_2 \overrightarrow{a_2} \tag{4.22}$$

$$\overrightarrow{B} - \overrightarrow{U_1} + \overrightarrow{U_2} = 0 \tag{4.23}$$

where Λ_1 and Λ_2 are the corresponding scale factors.

Substituting equations 4.21 and 4.22 in equation 4.23, equation 4.24 is obtained.

$$\overrightarrow{B} - \Lambda_1 \overrightarrow{a_1} + \Lambda_2 \overrightarrow{a_2} = 0 \tag{4.24}$$

where,

$$\overrightarrow{a_1} = \overrightarrow{L_1 a_1} \tag{4.25}$$

and

$$\overrightarrow{a_2} = \overrightarrow{L_2 a_2} \tag{4.26}$$

Based on the coplanarity condition $\Lambda_1$and Λ_2 can be determined from equation 4.24, which can then be used to determine A by using equations 4.21 or 4.22. The mathematical model developed for catadioptric camera is very similar. However, a couple of modifications are made. Firstly, mirror coordinates instead of image coordinates are used and secondly, as will be shown the vectors analogous to $\overrightarrow{a_1}$ and $\overrightarrow{a_2}$ will be the reflection vectors, extending from the reflection of the object in the mirror in the direction of the object. A detailed explanation is given in the following subsection.

4.3.2 Obtaining 3D coordinates of objects in the local environment

In order to calculate the 3D coordinates of a point Q (Figure 4.8), two calculated positions of the catadioptric camera in the world coordinate system and corresponding images C_1 and C_2 can be used. For this, the image coordinates of the point Q in each of the two images are measured: $q_1(x_{q_1}, y_{q_1})$ in the first image from first position, and $q_2(x_{q_2}, y_{q_2})$ in the second

image from the second position. The corresponding mirror coordinate for these points can be obtained from equations 4.1, 4.2 and 4.4. These corresponding mirror coordinates (in the world coordinate system) are referred as $M_{1q}(X_{M_{1q}}, Y_{M_{1q}}, Z_{M_{1q}})$ and $M_{2q}(X_{M_{2q}}, Y_{M_{2q}}, Z_{M_{2q}})$. The normal vectors at M_{1q} and M_{2q} are referred to as $\hat{n_{1q}}$ and $\hat{n_{2q}}$. The normal vectors can be calculated since the surface of the paraboloid and coordinates of the mirror points are known. Also, since C_1, C_2, M_{1q} and M_{2q} are known, the reflection vector from the each of the mirror coordinates to Q can be determined. This derivation is given next.

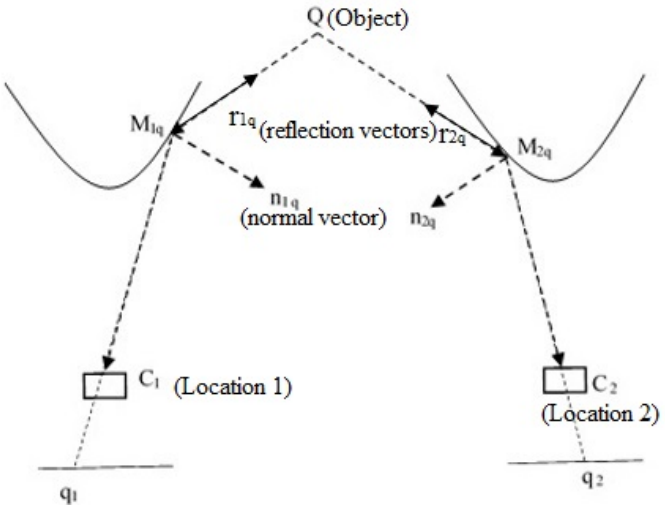

Figure 4.8: Mapping using 2 positions of the catadioptric sensor

The direction of a reflection vector can be determined from the incidence vector and the normal vector using equation 4.27 (de Greve, 2007).

$$r = i - 2(i.\hat{n})\hat{n} \tag{4.27}$$

where r, $\hat{n}$ and i are the reflection, unit normal and incidence vectors respectively.

Equation 4.27 can be utilized for calculating the direction of the unknown vector, r_{1q} and

r_{2q}, to the point Q from its corresponding mirror coordinate. This vector can then be used to calculate the coordinates of the point.

Rearranging equation 4.27 and introducing the calculated values of the normal vector, mirror and lens coordinates equations 4.28 and 4.29 are obtained.

$$r_{1q} = 2(\overrightarrow{M_{1q}C_1}.\hat{n_{1q}})\hat{n_{1q}} - \overrightarrow{M_{1q}C_1} \tag{4.28}$$

$$r_{2q} = 2(\overrightarrow{M_{2q}C_2}.\hat{n_{2q}})\hat{n_{2q}} - \overrightarrow{M_{2q}C_2} \tag{4.29}$$

where,

- vectors $\overrightarrow{M_{1q}C_1}$ and $\overrightarrow{M_{2q}C_2}$ are vectors from the corresponding mirror coordinates of Q to the camera lens at locations C_1 and C_2 respectively
- vectors $\hat{n_{1q}}$ and $\hat{n_{2q}}$ are unit normal vectors from the corresponding mirror coordinates of Q at locations 1 and 2 respectively
- $\overrightarrow{r_{1q}}$ is a vector from M_{1q} in the direction of Q and $\overrightarrow{r_{2q}}$ is a vector from M_{2q} in the direction of Q. However, the vectors most likely differ in magnitudes from $\overrightarrow{M_{1q}Q}$ and $\overrightarrow{M_{2q}Q}$

Therefore, the relationship between the two pairs of vectors can be represented by equations 4.30 and 4.31 by introducing the corresponding scale factors.

$$\overrightarrow{M_{1q}Q} = Q - M_{1q} = \lambda_1 r_{1q} \tag{4.30}$$

$$\overrightarrow{M_{2q}Q} = Q - M_{2q} = \lambda_2 r_{2q} \tag{4.31}$$

where λ_1 and λ_2 are unknown scale factors.

If λ_1 and λ_2 are determined, the coordinates of Q can be calculated using equation 4.30 or 4.31, or from both by averaging the result. The scale factors $\lambda_1$and λ_2 can be determined by making use of the co-planarity condition between $\overrightarrow{M_{1q}Q}$, $\overrightarrow{M_{2q}Q}$ and $\overrightarrow{M_{1q}M_{2q}}$ (equation 4.32).

$$\overrightarrow{M_{1q}M_{2q}}.(r_{1q} \times r_{2q}) = 0 \tag{4.32}$$

Since all these vectors are 3D vectors, equations 4.30 and 4.31 can be re-written as in equation 4.33

$$\begin{bmatrix} X_{M_{1q}} \\ Y_{M_{1q}} \\ Z_{M_{1q}} \end{bmatrix} - \begin{bmatrix} X_{M_{2q}} \\ Y_{M_{2q}} \\ Z_{M_{2q}} \end{bmatrix} = \lambda_1 r_{1q} - \lambda_2 r_{2q} \tag{4.33}$$

$$\begin{bmatrix} X_{M_{1q}} \\ Y_{M_{1q}} \\ Z_{M_{1q}} \end{bmatrix} - \begin{bmatrix} X_{M_{2q}} \\ Y_{M_{2q}} \\ Z_{M_{2q}} \end{bmatrix} - \lambda_1 \begin{bmatrix} r_{1qx} \\ r_{1qy} \\ r_{1qz} \end{bmatrix} + \lambda_2 \begin{bmatrix} r_{2q_x} \\ r_{2q_y} \\ r_{2q_z} \end{bmatrix} = 0 \tag{4.34}$$

Therefore four equations derived from 4.32 and 4.33 are used to solve for two unknowns $\lambda_1$and λ_2. Once $\lambda_1$and λ_2 are determined, the 3D coordinates of the point Q can be calculated using equation 4.34

$$\begin{bmatrix} X_Q \\ Y_Q \\ Z_Q \end{bmatrix} = \left(\begin{bmatrix} X_{M_{1q}} \\ Y_{M_{1q}} \\ Z_{M_{1q}} \end{bmatrix} - \lambda_1 r_{1q} + \begin{bmatrix} X_{M_{2q}} \\ Y_{M_{2q}} \\ Z_{M_{2q}} \end{bmatrix} - \lambda_2 r_{2q} \right) /2 \tag{4.35}$$

This can be done for any common detected points in the two images.

The above equations 4.32 and 4.33 are then rewritten in the form of equation 4.36 to solve using least squares adjustment

$$A_2 x_2 = 0 \tag{4.36}$$

where x_2 represents the unknowns and is shown in equation 4.37

$$x_2 = \begin{bmatrix} \lambda_1 \\ \lambda_2 \end{bmatrix} \tag{4.37}$$

and A_2 represents the design matrix and is shown in equation 4.38

$$A_2 = \begin{bmatrix} \frac{\partial f}{\partial \lambda_1} & \frac{\partial f}{\partial \lambda_2} \\ \frac{\partial g_x}{\partial \lambda_1} & \frac{\partial g_x}{\partial \lambda_2} \\ \frac{\partial g_y}{\partial \lambda_1} & \frac{\partial g_y}{\partial \lambda_2} \\ \frac{\partial g_z}{\partial \lambda_1} & \frac{\partial g_z}{\partial \lambda_2} \end{bmatrix} \tag{4.38}$$

where, $f(\lambda_1, \lambda_2) = (\lambda_1 r_{1q} - \lambda_2 r_{2q}).(r_{1q} \times r_{2q})$, and

$$\begin{bmatrix} g_x(\lambda_1, \lambda_2) \\ g_y(\lambda_1, \lambda_2) \\ g_z(\lambda_1, \lambda_2) \end{bmatrix} = \begin{bmatrix} X_{M_{1q}} \\ Y_{M_{1q}} \\ Z_{M_{1q}} \end{bmatrix} - \begin{bmatrix} X_{M_{2q}} \\ Y_{M_{2q}} \\ Z_{M_{2q}} \end{bmatrix} - \lambda_1 \begin{bmatrix} r_{1qx} \\ r_{1qy} \\ r_{1qz} \end{bmatrix} + \lambda_2 \begin{bmatrix} r_{2q_x} \\ r_{2q_y} \\ r_{2q_z} \end{bmatrix}$$

Equation 4.36 can then be solved together for all unknowns using all points by using least squares adjustment. Initial parameters of each mapped point were based on their position in the room and were approximated using the wall or object they were placed on.

4.4 Image Unwrapping

An additional step involves unwrapping of the catadioptric images obtained from the system. It was observed in several studies (Dupuis et al., 2014, Scaramuzza et al., 2007) that feature detection and matching is easier in unwrapped images than original catadioptric images. When images are unwrapped, they represent a perspective panoramic view. Although the unwrapped images have imperfections and distortions, the characteristics and attributes of features, such as their shape, are more accurately preserved than in catadioptric images. This is the reason unwrapped images are preferred for feature detection and matching. Even though automated feature detection is not made use of in current experiments, it will be very helpful in any future work involving automation and is discussed in Section 6. The method used for unwrapping the obtained catadioptric images is described below.

4.4.1 Unwrapping Images Using Perspective Geometry

Figure 4.9: Catadioptric Image

The idea is to use the perspective geometry in order to rectify the image. The objective is to 'unwrap' the image seen in Figure 4.9. This is to be done using vanishing point geometry. All vertical parallel lines are assumed to intersect at the center. For example, the vertical ends of the checkered paper shown in Figure 4.9 are parallel. The desired transformation required for that part of the image is approximated in Figure 4.10.

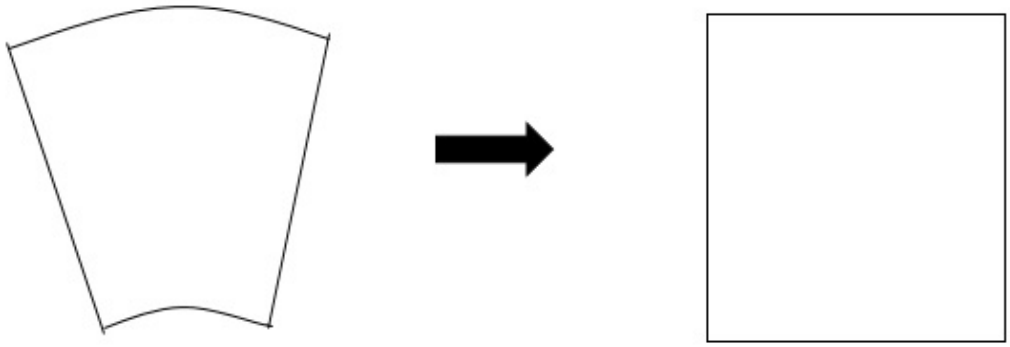

Figure 4.10: Mathematical transformation for rectification

Using the characteristics of the object, width and length, a mathematical function was obtained using this desired transformation as shown in equation 4.39 and 4.40. Since the width and the length of checkered paper were known, the image of the object was transformed to a scaled version of the object in the new image as shown in Figure 4.11. The same mathematical function was applied to the rest of the image as well. Nearest neighbor approach is used for interpolation.

In equation 4.39, pixel values of ends of checkered paper in the unwrapped image were calculated as $\left(p'_{cbx}, p'_{cby}\right)$ using its characteristics and compared to measured pixel values in the catadioptric image $\left(p_{cbx}, p_{cby}\right)$. Several points like these are used to calculate the transformation function f, the inverse of which is then applied to obtain other pixels in the unwrapped image (equation 4.40) using nearest neighbour (Altman, 1992) approach.

$$\begin{aligned} p'_{cbx} &= p_{cbx}.f(p_x, p_y) \\ p'_{cby} &= p_{cby}.f(p_x, p_y) \end{aligned} \tag{4.39}$$

$$\begin{aligned} p'_x &= p_x.f^{-1}(p_x, p_y) \\ p'_y &= p_y.f^{-1}(p_x, p_y) \end{aligned} \tag{4.40}$$

The final result obtained is observed in Figure 4.12.

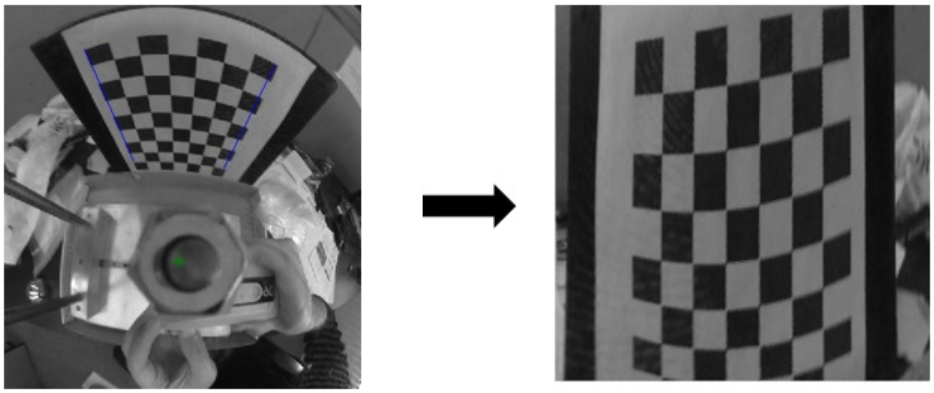

Figure 4.11: Solution applied to Figure 4.9

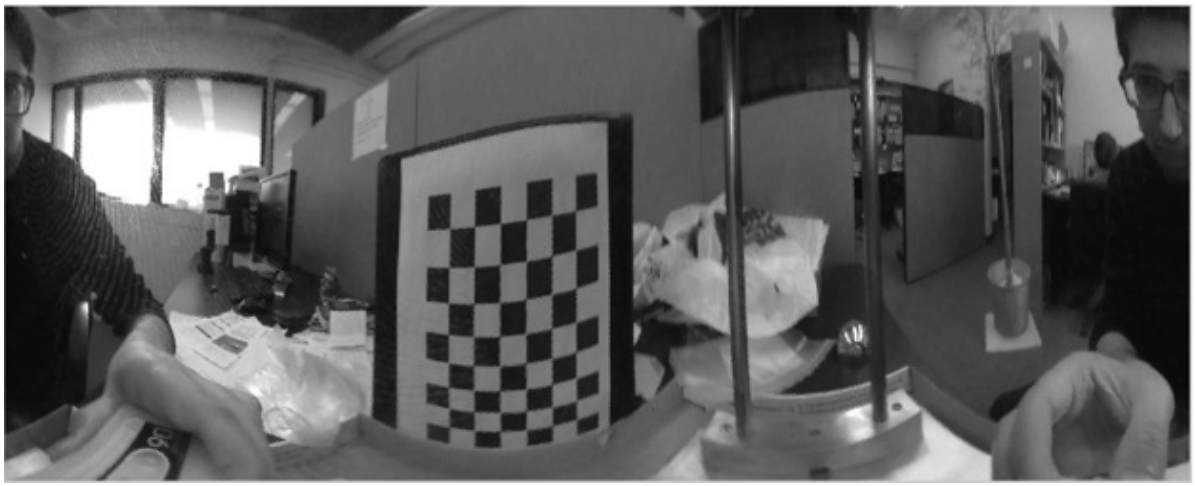

Figure 4.12: Unwrapping result for Figure 4.9

As can be observed, errors and distortion still exist in the image. Firstly, even though the vertical lines are parallel, the horizontal lines are not. They seem to be getting more curved as you go lower. Secondly it is observed that lower checkerboard boxes seem to be smaller than the higher ones. Both these distortions occur due to the shape of the mirror. Because the mirror is not spherical, rather more parabolic, the distortion is not equidistant, that is the distortion continually changes as the distance from the center of the mirror changes.

This is why there is a change along the vertical axis. A proposed solution for this problem involves making use of the horizontal lines, which are ideally supposed to be parallel and implementing it along with the previous mathematical transformation. An alternate solution would be performing cylindrical projection using two different cylinders on the two halves of the image (top and bottom). These ideas can be implemented in the future work performed on the system.

Chapter 5

Implementation and Results

After the aforementioned mathematical models were formulated, experiments were performed to conduct an actual application. The set-up of these experiments and the results are described in this chapter along with the analysis of the results. While the mathematical models were being formulated, simulations were performed. Those simulation results are provided in section 5.1 describing various stages in obtaining the position of the camera, navigating it and mapping points. In section 5.2 numerical results for the experiments performed in different environments are provided. Descriptions of these environments are also provided. Finally, an analysis of these numerical results is performed discussing the errors and efficiency.

5.1 Simulation results

For validation the mathematical models described in Chapters 3 and 4, were tested in simulated environments. The application procedures and results are given in this section.

5.1.1 Calibration

The first step in navigation and mapping involves the calibration of the catadioptric camera system. As described in Chapter 3, the image and object coordinates of target on the top plate of the constructed system are compared to obtain the relative orientation and translation of mirror and camera coordinate reference system.

A simulation of the calibration process is shown in Figure 5.1. The target coordinates were inputted and corresponding image coordinates were selected manually. A projection matrix describing the relationship between these was obtained using least squares adjustment. This projection matrix was used to obtain the relative rotation and translation parameters. At least 3 corresponding sets of coordinates (image and targets) are required for this purpose. The blue point at the bottom represents the camera lens, the squares, the image coordinates and the red points, the target coordinates. In the close up image on the right, the errors can also be observed, since in an over-determined system they are not perfectly aligned.

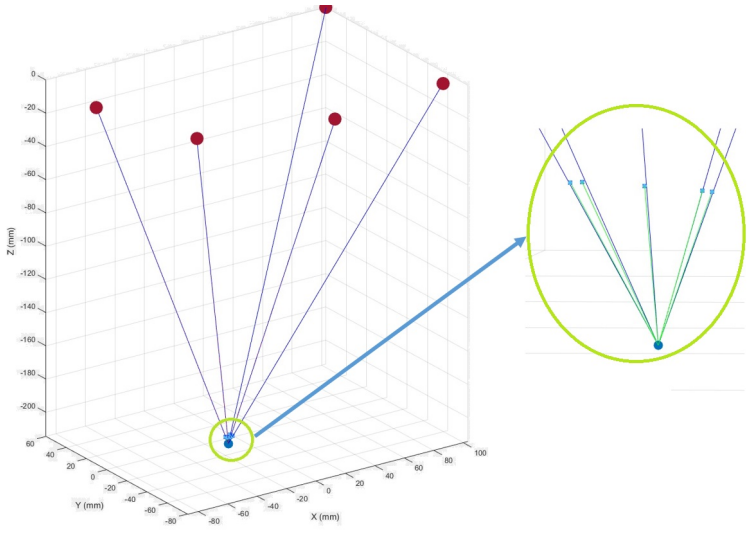

Figure 5.1: Mirror-Camera Calibration Simulation

A fine adjustment procedure is then employed on these results to obtain more accurate results.

This is done by inputting image coordinates of visually identifiable points on the mirror (such as the centre) and seeing where they are placed on the simulation model of the mirror. In addition to this, an assumption is made that there is no rotation about either of the three axes and determining the translation matrix by observing the edges and center of the catadioptric mirror. Based on the the construction of the system it is known that there is no rotation about the x or y local axis and the camera was placed such that it's axis was parallel to the z axis, the assumption that the rotation matrix is an identity matrix is a safe assumption. The results for translation matrix can be estimated and then changed such that the image below (on the right) is obtained, where it can be seen in simulation that the center and edges were correctly estimated. Therefore, it can be concluded that the calibration results thus obtained improve the overall accuracy. After performing several validation tests and proceeding to next steps, this was observed to be an efficient way to calibrate the system. This is considered more efficient than the previous method since the previous method has a very high sensitivity and a one millimetre error in translation or a one degree error in rotation is propagated and in an average size room can lead to an error of several decimeters. This is discussed further in the error analysis section. Therefore this additional method was used for this purpose. However, this only works if their is no change in relative orientation and translation of mirror and camera upon movement of the system, which is the case with the current constructed system.

Figure 5.2 displays the above mentioned alternative methodology, showing a point which is selected in the left image and the simulated view on the right. The mirror model was simulated using the dimensions of the parabolic mirror used in the experiments..

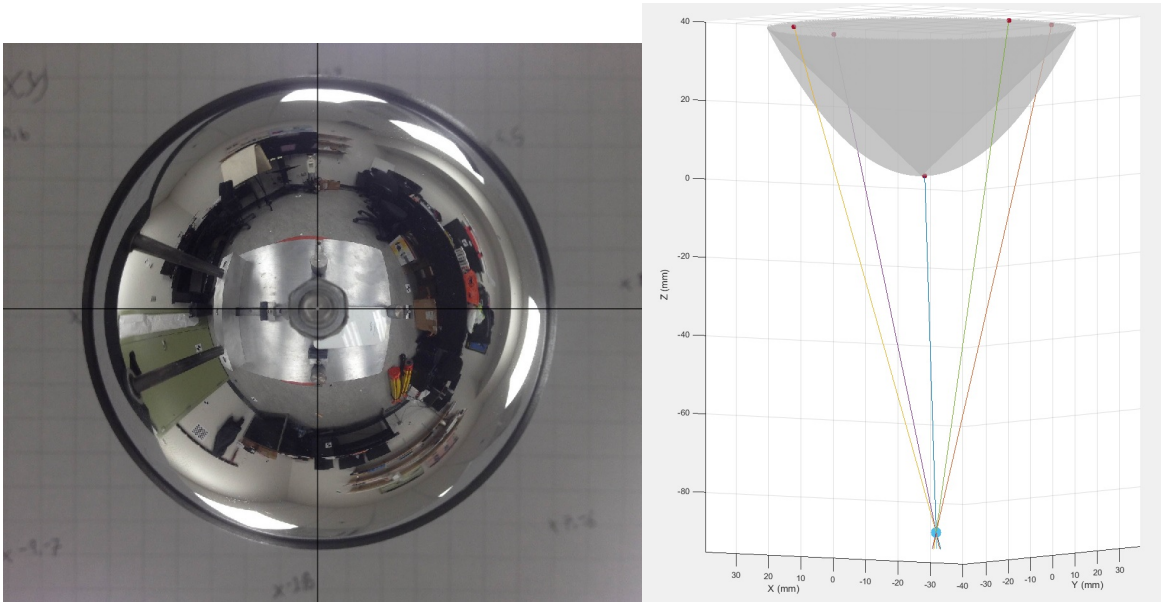

Figure 5.2: Refining the Calibration Manually

5.1.2 Calculation of Mirror Coordinates of Control Points (CP's)

The next step in the methodology involved selecting the image coordinates of CP's and obtaining their corresponding mirror coordinates. This was detailed in Section 4.1.

Once the image coordinates of the control point were measured as shown in image on the left in Figure 5.1, a one-to-one relationship using collinearity equations and the shape of the mirror was used to obtain the corresponding mirror coordinate as shown on the right.This step is later used for mapping as well.

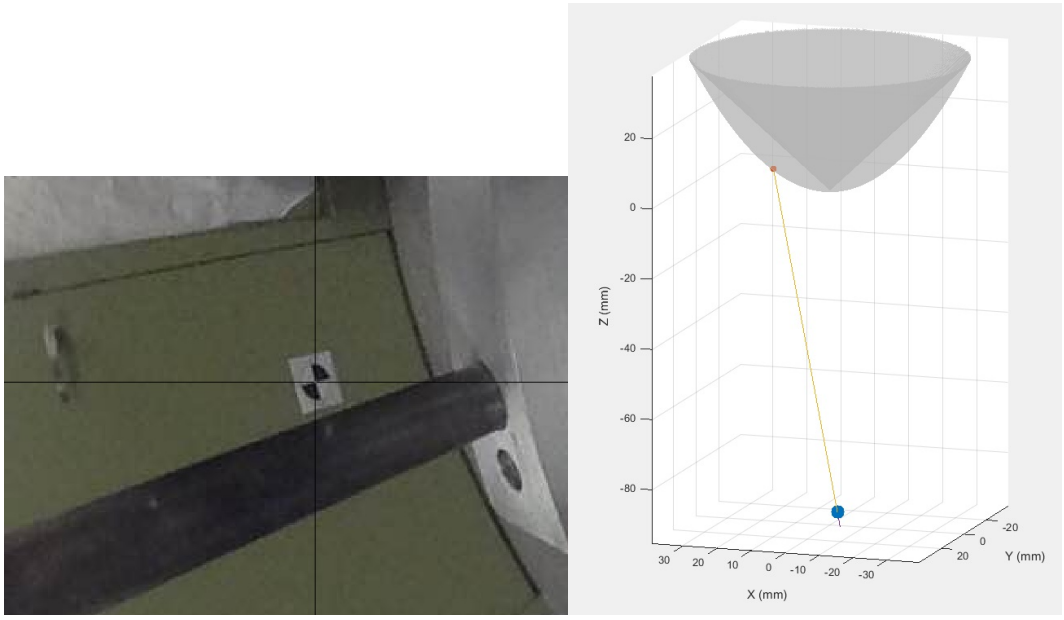

Figure 5.3: Selection of Mirror Coordinates

5.1.3 Positioning

Following the calculation of the mirror coordinates of the control points, the coordinates of catadioptric system in the world coordinate system are calculated. This is done by calculating the relative orientation and translation between the catadioptric system and the world coordinate system. The known coordinates of the control points in the world coordinate system are utilized for this purpose along with the previously determined corresponding mirror coordinates.

A simulation of the experiment is shown in Figure 5.4. The catadioptric system centered initially at its own vertex was moved to its position in Figure 5.4 using reflection constraints from lens coordinate, to mirror coordinates and corresponding object coordinates. A close up of the catadioptric system is shown in Figure 5.5.

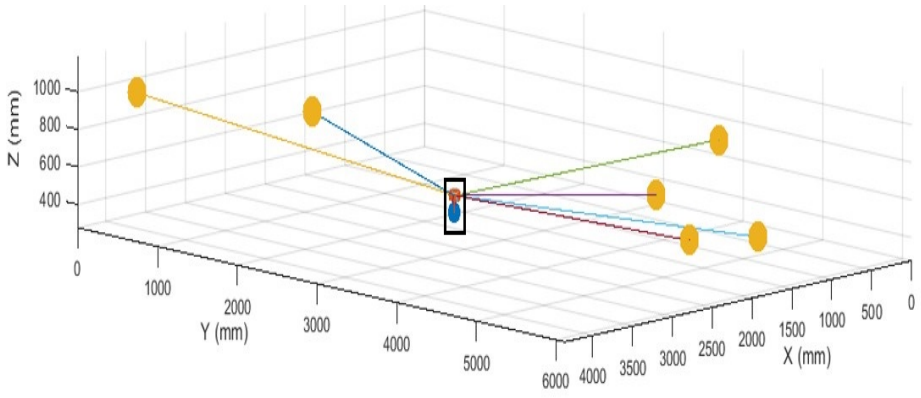

Figure 5.4: Positioning using CP's

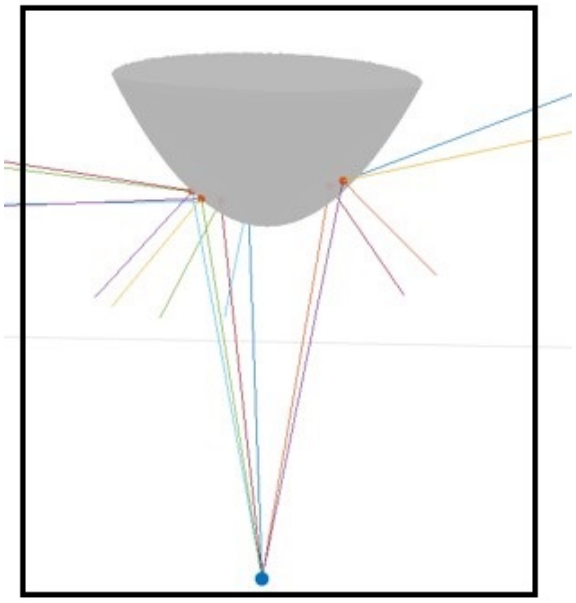

Figure 5.5: Mirror Reflection of CP's

5.1.4 Mapping Simulation

The next step was the estimation of the object coordinates in the room/hallway. A simulation environment was set up in order to test and validate the mathematical model described in Section 4.3 which was to be used for this purpose. A target coordinate was assumed along

with two positions of the catadioptric system. Corresponding mirror coordinates of the target were calculated for each of the positions manually. The math model was then employed to see if it would provide the same results, i.e. the same target coordinate for the given mirror coordinates. The result was successfully obtained and is shown in Figure 5.6. Since, no manual training was involved, no errors were introduced in the simulation.

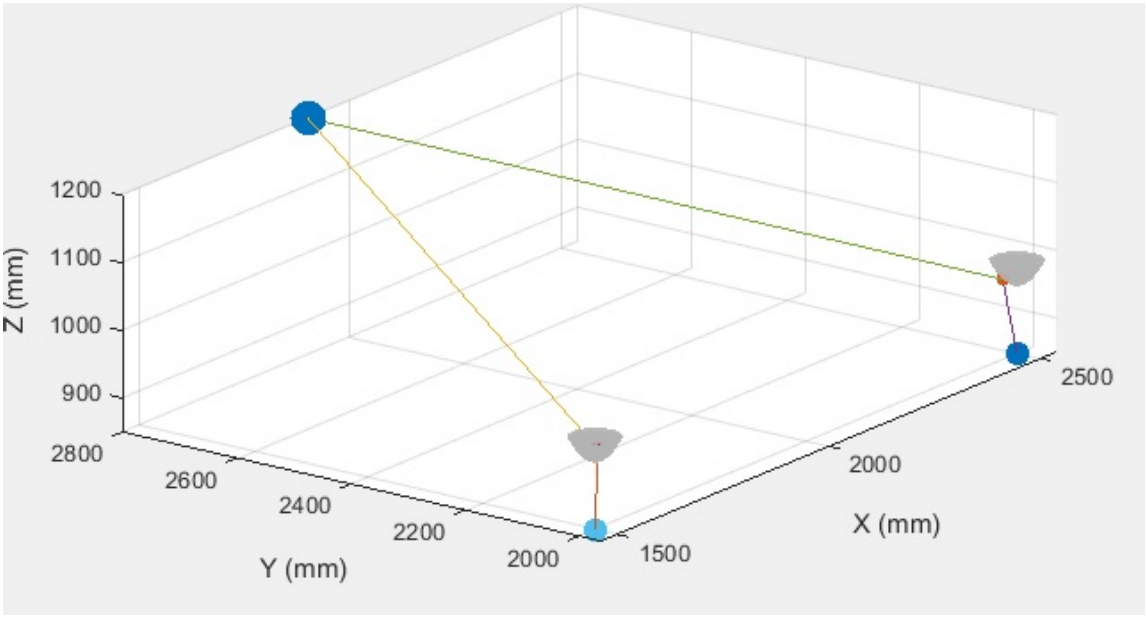

Figure 5.6: Mapping Simulation

5.2 Experimental Set ups and Results

Two experimental set ups were performed, both in the Petrie Science and Engineering building in York University. The first set up, in Site 1, involves the movement of the catadioptric system on a mobile platform along and into the cubicles. This setup enables a good approximation of a possible application, i.e., the movement of a robot along the hallways and entering in various rooms. The second, in Site 2 involves navigation and mapping within a room from different locations. Therefore, two of the most anticipated applications are explored in these

two experimental set-ups. The numerical results are provided along with images taken from each set-up.

Sites and locations are referred with the prefix S and L respectively for brevity.

5.2.1 Site 1 Test

In the first experiment, in Site 1, the catadioptric camera was set up at five different locations. The experiment was performed in a room consisting of a straight pathway and three cubicles on each side. Figure 5.7 shows a few images of the site. Four locations were determined using the CPs and one from the 3D points calculated from these four locations. These locations are denoted as L1, L2, L3, L4 and L5 respectively.

Figure 5.7: Site 1

5.2.1.1 Determination of the Position of the Catadioptric Camera

In this subsection, different locations are displayed along with the rotation and position results obtained for that location. The catadioptric image taken from that location is shown along with the unwrapped image, which makes it easier to visually identify the placement of the catadioptric camera. The unwrapped image looks like a panoramic image, however, it is slightly distorted especially from top and bottom corners. Several control points were set up in the room, some along the cubicle wall panels and some inside the cubicle. Three of the locations (L1, L2 and L4) lie in a straight line along the pathway, whereas L3 is inside one of the cubicles. L5 also lies along the pathway, however at a different alignment than L1, L2 and L4. The coordinates L1, L2, L3 and L4 were determined using control points and the coordinates of L5 were determined using the 3D points obtained from images captured at the other four locations of the mobile platform.

Since the first step, in the process of navigation and mapping was calibration, the following table shows the calibration result. As mentioned before, since all three rotation angles were assumed to be zero (and the camera was physically placed accordingly) in order to obtain more accurate calibration results, only translation results are shown below. These results show the relative translation between the camera and the mirror. Using these values the camera coordinate system is positioned in the mirror coordinate system which is then referred to as the catadioptric coordinate system. Table 5.1 describes the translation between the camera and the mirror coordinate system. The calibration results are the same for all the locations on Site 1. The images and results of the locations are provided in the following subsections.

Camera (mm)	
X_{mc}	-2.9
Y_{mc}	2.8
Z_{mc}	-91

Table 5.1: S1 Calibration Results

5.2.1.1.1 Location 1

Images Figure 5.8 shows the image taken at Site 1 Location 1 and Figure 5.9 shows the panoramic image of Site 1 Location 1 image.

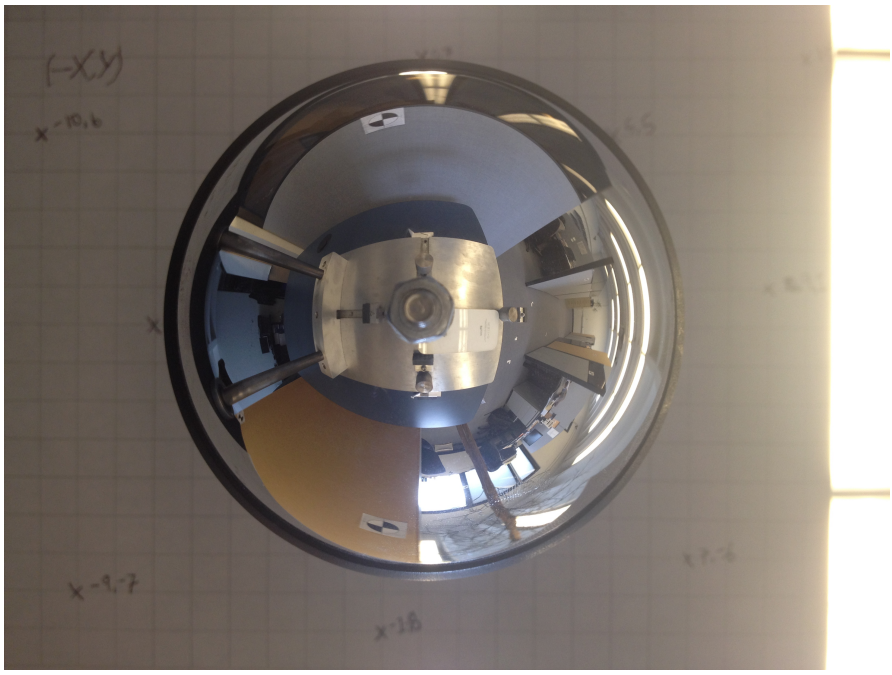

Figure 5.8: Site 1 Location 1 Image

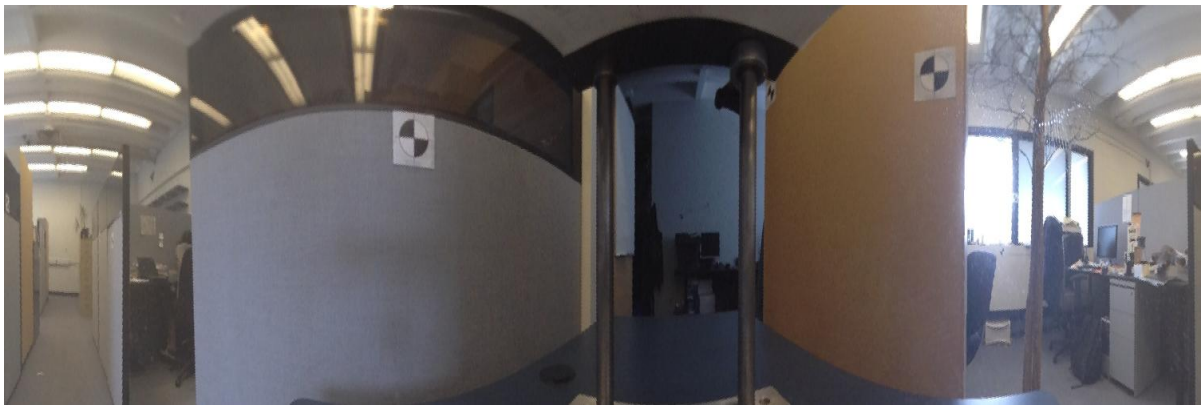

Figure 5.9: Site 1 Location 1 Unwrapped Image

Results

Table 5.2 gives the estimate rotation angles of the catadioptric system when positioned in the world coordinate system, i.e. relative orientation between the catadioptric coordinate system and world coordinate system. Since several control points were available, four experiments were performed for each location. Different combination of control points was used in each experiment. These orientation results can be validated in several ways. One of the ways would be by placing the the system on a tilting plane/table and measuring the tilts directly. Another possibility is using a simulated environment which can be transformed using observed orientation and using the rotated coordinates of known points for the recovery of orientation of the system. The results provided were calculated by taking the average of obtained parameters from these experiments. The standard deviation of these results is also provided. Table 5.3 gives the actual position of the catadioptric system at that location in world coordinate system. This is followed by the Table 5.4 which provides the positioning results of different experiments and accompanied by their average and standard deviation. The results from Table 5.3 and 5.4 are compared to obtain the average error which is given in Table 5.5.

In Table 5.2 below, the standard deviation represents the deviation of results obtained from

the four experiments. It should be noted that unlike positioning results, the orientation results are not compared to and ideal/actual value, since the method used to determine these values is the only way to measure these angles. In addition to that, during positioning the catadioptric system is considered as a monolithic system and estimated as a point (centered at vertex of the mirror).

Rotation Angles	Average (degrees)	Standard Deviation (degrees)
ω	-0.65	1.05
ϕ	-5.4	0.42
κ	-92.35	0.25

Table 5.2: Site 1 Location 1 Rotation Results

Measured (mm)	
X_T	870
Y_T	435
Z_T	870

Table 5.3: Site 1 Location 1 Actual Position

Experiment	1	2	3	4	Average	Standard Deviation
$X_T(mm)$	979.1	985.4	949.7	987.9	975.53	17.61
$Y_T(mm)$	305.1	315.6	318.4	482.2	355.33	84.78
$Z_T(mm)$	759.5	761.6	748.3	715.8	746.3	21.15

Table 5.4: Site 1 Location 1 Calculated Positions

The errors are the difference between the actual reference value and the average calculated value, which is the average of the values obtained from different experiments.

Δ_{X_T}, Δ_{Y_T} and Δ_{Z_T} represent the error in displacement along X, Y and Z axis respectively.

Δ_{X_T,Y_T,Z_T}= Reference X_T, Y_T, Z_T - Calculated Average X_T, Y_T, Z_T

Δ_{S_T} is the overall positioning error, that is the 3D displacement error in the position of the point and is given by equation 5.1

$$\Delta_{S_T} = \sqrt{(\Delta_{X_T})^2 + (\Delta_{Y_T})^2 + (\Delta_{Z_T})^2} \tag{5.1}$$

Error (mm)	
Δ_{X_T}	-105.5
Δ_{Y_T}	79.7
Δ_{Z_T}	123.7
Δ_{S_T}	181.1

Table 5.5: Site 1 Location 1 Positioning Error

5.2.1.1.2 Location 2

Images Figure 5.10 shows the image taken at Site 1 Location 2 and Figure 5.11 shows the panoramic image of Site 1 Location 2 image.

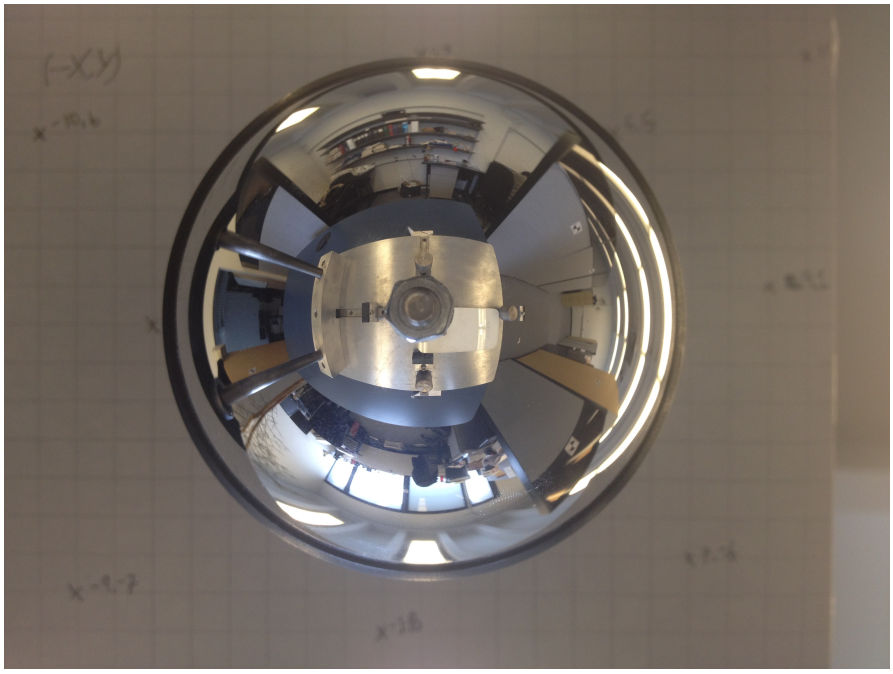

Figure 5.10: Site 1 Location 2 Image

Figure 5.11: Site 1 Location 2 Unwrapped Image

Results

Table 5.6 gives the estimate rotation angles of the catadioptric system at Site 1 Location 2. Table 5.7 gives the actual position of the catadioptric system at that location in world coordinate system. This is followed by the Table 5.8 which provides the positioning results of different experiments and accompanied by their average and standard deviation. The results from Table 5.7 and 5.8 are compared to obtain the average error which is given in Table 5.9.

Rotation Angles	Average (degrees)	Standard Deviation (degrees)
ω	-0.85	2.99
ϕ	-3.58	0.99
κ	-89.65	0.13

Table 5.6: Site 1 Location 2 Rotation Results

Measured (mm)	
X_T	2048
Y_T	472
Z_T	870

Table 5.7: Site 1 Location 2 Measured Positions

Experiment	1	2	3	4	Average	Standard Deviation
$X_T(mm)$	2012.1	2022.1	1892.1	1951.2	1969.38	60.3
$Y_T(mm)$	373.8	390.7	466.9	391.2	405.65	41.63
$Z_T(mm)$	684.4	697.2	685	765.7	708.08	38.87

Table 5.8: Site 1 Location 2 Calculated Positions

Error (mm)	
Δ_{X_T}	78.6
Δ_{Y_T}	66.4
Δ_{Z_T}	161.9
Δ_{S_T}	191.8

Table 5.9: Site 1 Location 2 Positioning Error

5.2.1.1.3 Location 3

Images Figure 5.12 shows the image taken at Site 1 Location 3 and Figure 5.13 shows the panoramic image of Site 1 Location 3 image.

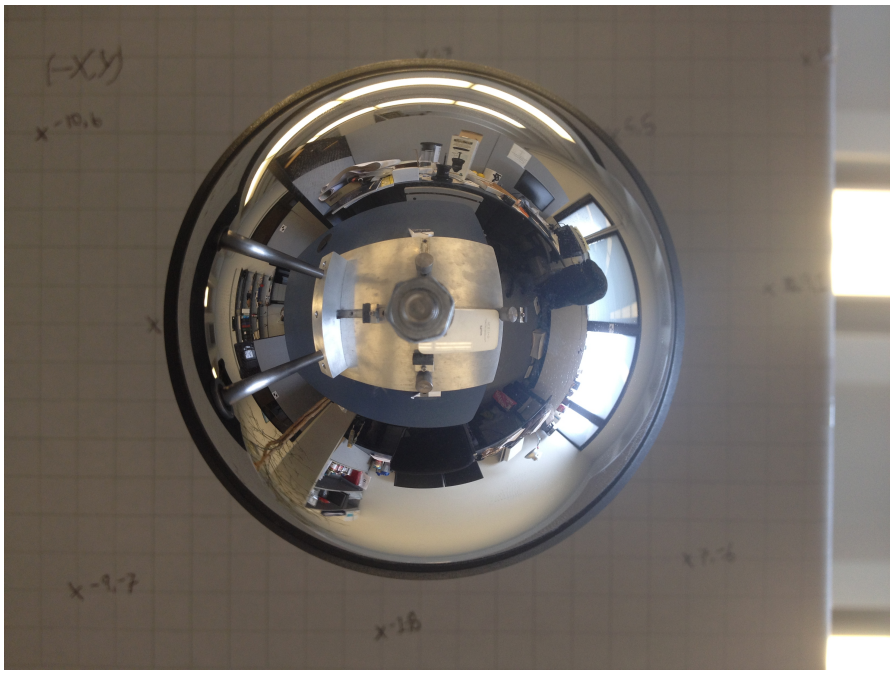

Figure 5.12: Site 1 Location 3 Image

Figure 5.13: Site 1 Location 3 Unwrapped Image

Results

Table 5.10 gives the estimate rotation angles of the catadioptric system at Site 1 Location 3. Table 5.11 gives the actual position of the catadioptric system at that location in world coordinate system. This is followed by the Table 5.12 which provides the positioning results of different experiments and accompanied by their average and standard deviation. The results from Table 5.11 and 5.12 are compared to obtain the average error which is given in Table 5.13.

Rotation Angles	Average (degrees)	Standard Deviation (degrees)
ω	-0.83	1.2
ϕ	-2.7	0.8
κ	-178.55	0.37

Table 5.10: Site 1 Location 3 Rotation Results

Measured (mm)	
X_T	1800
Y_T	1800
Z_T	870

Table 5.11: Site 1 Location 3 Measured Positions

Experiment	1	2	3	4	Average	Standard Deviation
$X_T(mm)$	1954.4	1954.8	1953.1	1980.4	1960.675	13.17
$Y_T(mm)$	1801	1841.8	1673.5	1727.9	1761.05	75.01
$Z_T(mm)$	645.9	662.6	685.9	705.7	675.025	26.22

Table 5.12: Site 1 Location 3 Calculated Positions

Error (mm)	
Δ_{X_T}	-160.7
Δ_{Y_T}	39.0
Δ_{Z_T}	195.0
Δ_{S_T}	255.6

Table 5.13: Site 1 Location 3 Positioning Error

5.2.1.1.4 Location 4

Images Figure 5.14 shows the image taken at Site 1 Location 4 and Figure 5.15 shows the panoramic image of Site 1 Location 4 image.

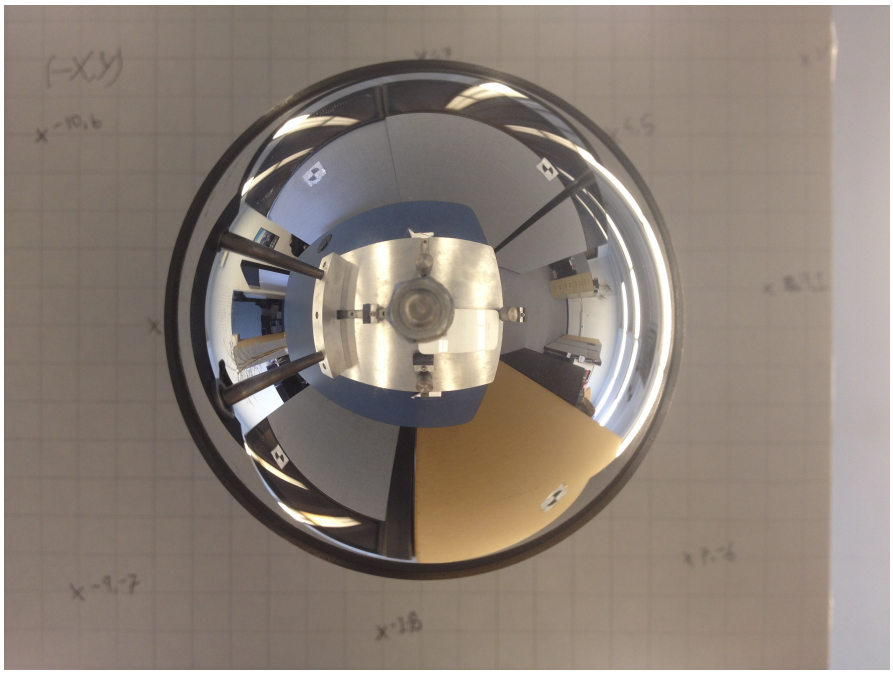

Figure 5.14: Site 1 Location 4 Image

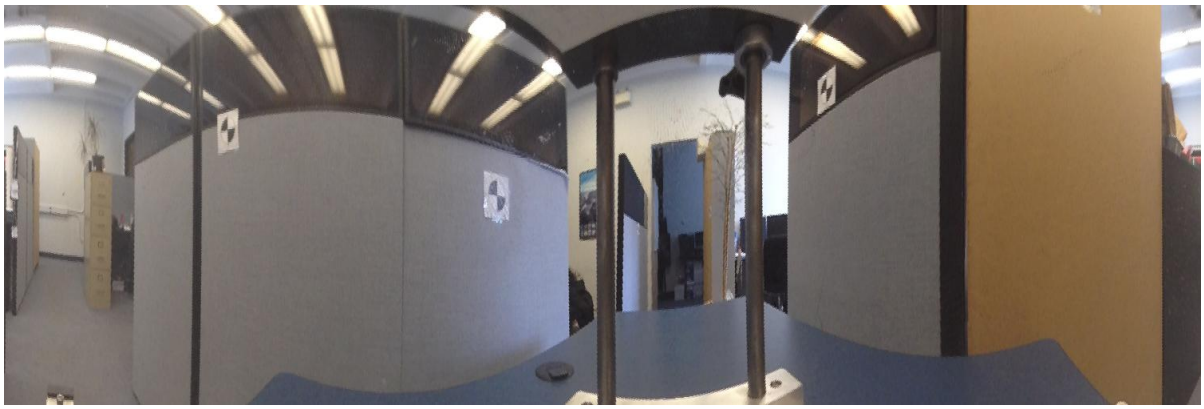

Figure 5.15: Site 1 Location 4 Unwrapped Image

Results

Table 5.14 gives the estimate rotation angles of the catadioptric system at Site 1 Location 4. Table 5.15 gives the actual position of the catadioptric system at that location in world coordinate system. This is followed by the Table 5.16 which provides the positioning results of different experiments and accompanied by their average and standard deviation. The results from Table 5.15 and 5.16 are compared to obtain the average error which is given in Table 5.17.

Rotation Angles	Average (degrees)	Standard Deviation (degrees)
ω	1.58	2.85
ϕ	−1.45	0.56
κ	−92.33	0.95

Table 5.14: Site 1 Location 4 Rotation Results

Measured (mm)	
X_T	3313
Y_T	505
Z_T	870

Table 5.15: Site 1 Location 4 Measured Positions

Experiment	1	2	3	4	Average	Standard Deviation
$X_T(mm)$	3399.1	3364.3	3363.7	3298.7	3356.45	41.91
$Y_T(mm)$	536.3	518.4	522	506.3	520.75	12.35
$Z_T(mm)$	838.7	822.1	819.7	828.7	827.3	8.5

Table 5.16: Site 1 Location 4 Calculated Positions

Error (mm)	
Δ_{X_T}	-43.5
Δ_{Y_T}	-15.8
Δ_{Z_T}	42.7
Δ_{S_T}	62.9

Table 5.17: Site 1 Location 4 Positioning Error

Summary of Results

Table 5.18 gives the positioning results of the catadioptric system, comparing the measured coordinates with calculated coordinates obtained from positioning using CP's from the results obtained for each location.

Location	Measured (mm)			Calculated (mm)			Error (Meas. - Calc.) (mm)		
	X	Y	Z	X	Y	Z	ΔX	ΔY	ΔZ
L1	870	435	870	975.53	355.33	746.3	-105.5	79.7	123.7
L2	2048	472	870	1969.38	405.65	708.08	78.6	66.4	161.9
L3	1800	1800	870	1960.67	1761.05	675.03	-160.67	39.0	195.0
L4	3313	505	870	3356.45	520.75	827.3	-43.5	-15.8	42.7
Mean Error (mm)							-57.77	42.33	130.83
Std. Dev. (mm)							102.74	42.3	65.57

Table 5.18: S1 Positioning Results and Errors

In Figure 5.16, the planimetric (XY plane) results are visually displayed.

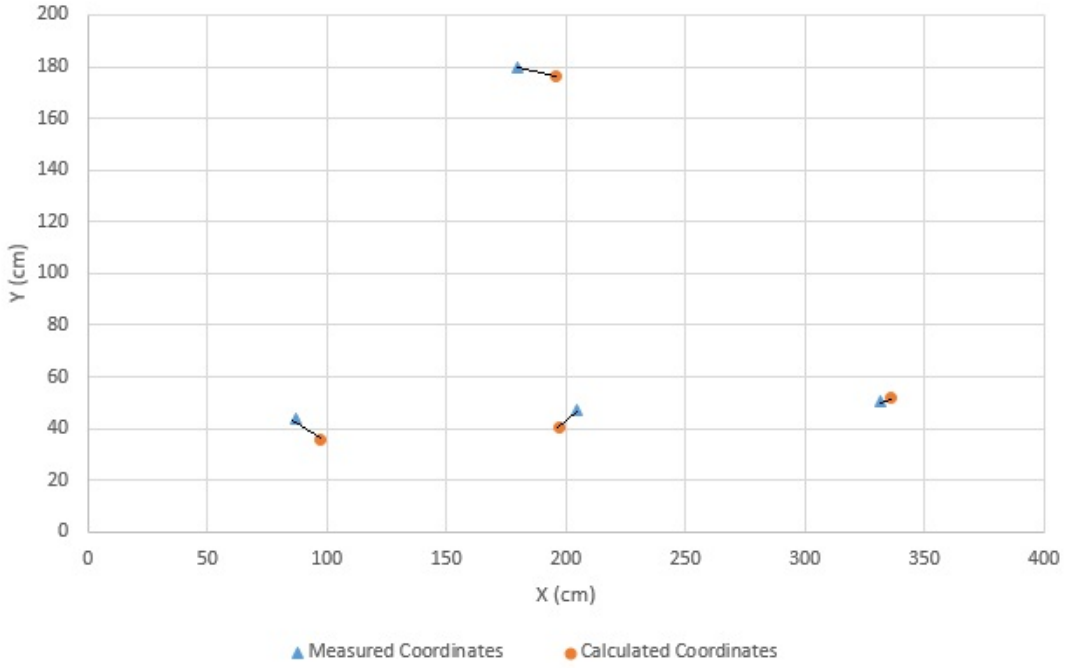

Figure 5.16: S1 Planimetric errors

The following Figure 5.17 describes elevation positioning results. Z represents elevation and S represents the 2D distance along X-Y axes (S = $\sqrt{x^2 + y^2}$).

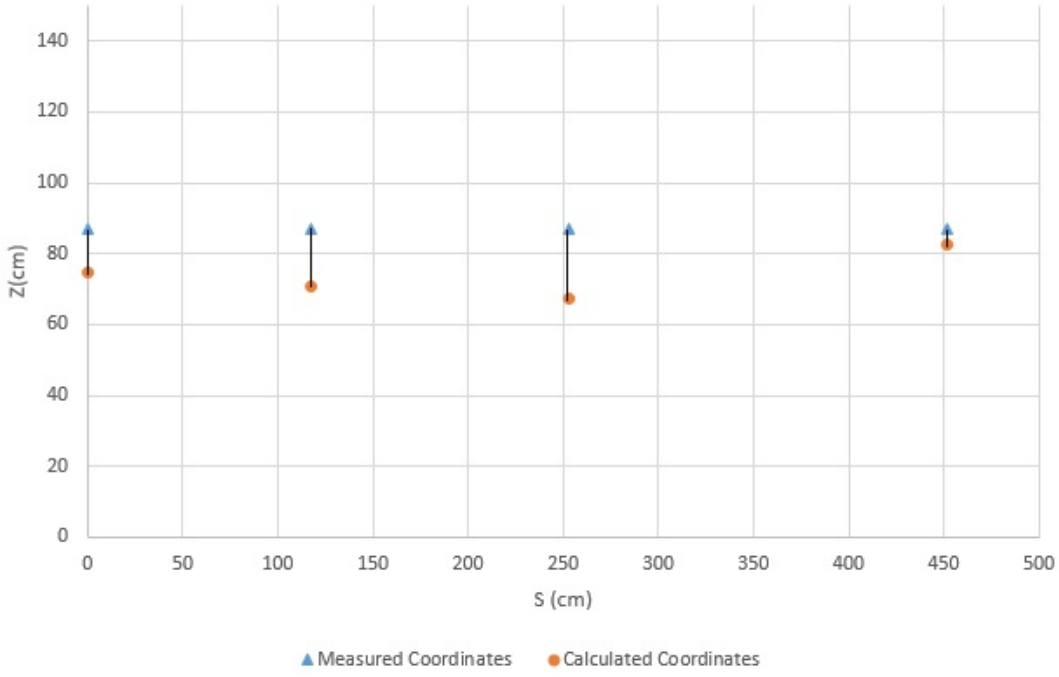

Figure 5.17: S1 Vertical errors

5.2.1.2 S1 Mapping Results

For the mapping test the 3D coordinates of common tie points captured from two location of the catadioptric system were estimated. Table 5.19 provides the measured and calculated coordinates of the mapped points along with errors.

Point	Measured (mm)			Calculated (mm)			Error (Meas- Calc) (mm)		
	X	Y	Z	X	Y	Z	ΔX	ΔY	ΔZ
TP1	807.0	-60.0	1107.0	909.2	-55.1	1079.9	-102.2	-4.9	27.1
TP2	55.0	885.0	1433.0	-243.2	996.8	1567.6	298.2	-111.8	-134.6
TP3	808.0	885.0	1184.0	851.9	945.1	1157.8	-43.9	-60.1	26.2
TP4	2785.0	1103.0	1250.0	2718.0	1098.3	1268.8	67.0	4.7	-18.8
TP5	2909.0	-60.0	1048.0	2965.0	47.1	1104.1	-56.0	-107.1	-56.1
TP6	3714.0	1123.0	1367.0	3853.2	1257.7	1566.4	-139.2	-134.7	-199.4
TP7	3837.0	-60.0	1151.0	3789.6	105.5	1280.2	47.4	-165.5	-129.2
TP8	1770.0	3996.0	1569.0	1774.3	3913.5	1555.4	-43.0	82.5	13.6
TP9	1463.0	3695.0	908.0	1506.7	3697.1	1005.5	-43.7	-2.1	-97.5
TP10	2490.0	1103.0	1200.0	2501.7	1057.5	1187.4	-11.7	45.5	12.6
TP11	2474.0	-60.0	1173.0	2539.5	-9.8	1189.9	-65.5	-50.2	-16.9
TP12	3245.0	1103.0	1200.0	3242.6	1129.8	1256.5	2.4	-26.8	-56.5
Mean Error (mm)							-4.3	-44.2	-52.5
Std. Dev. (mm)							111.5	75.0	73.7

Table 5.19: S1 Mapping Results and Errors

Figure 5.18 shows the mapped points plotted along with their measured coordinates in the XY plane. The mapped points are plotted along with their actual measured coordinates in order to analyze the results.

Figure 5.19 shows the elevation errors in all of 12 mapped points. These errors (along the y-axis) are the difference between the measured and calculated elevations of the points (named along x-axis in the plot).

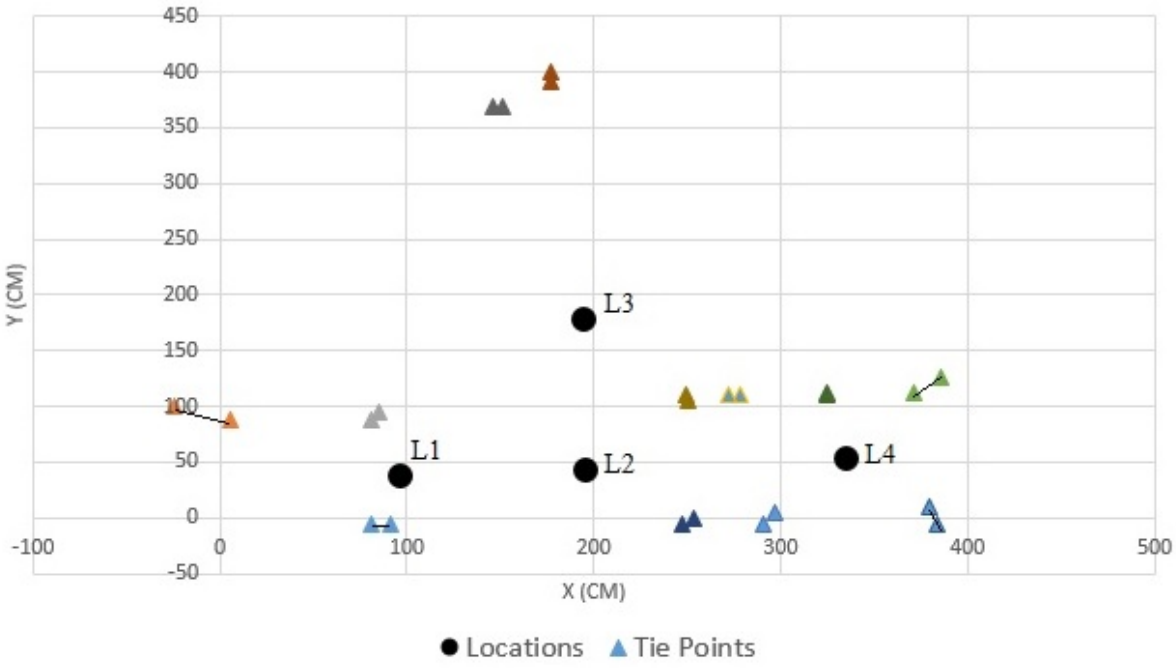

Figure 5.18: S1 Mapping errors (Planimetry)

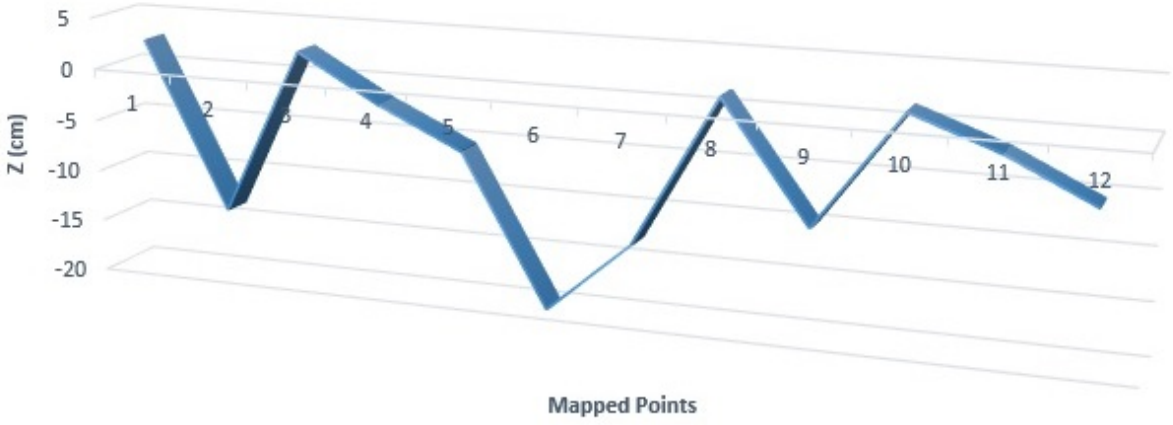

Figure 5.19: S1 Mapping errors (Elevation)

5.2.1.3 S1 Navigation Results

Table 5.20 gives the measured and calculated coordinates of catadioptric system at Location 5, which were determined using the 3D points (tie-points) obtained from images captured at L1, L2, L3 and L4. The errors along each axis are also given in the table.

Location	Measured (mm)			Calculated (mm)			Error (Meas - Calc) (mm)		
	X	*Y*	*Z*	*X*	*Y*	*Z*	ΔX	ΔY	ΔZ
L5	1985	869	870	2274.7	682.9	921.1	-289.7	186.1	-51.1

Table 5.20: S1 Navigation Results and Errors

Figure 5.20 shows the position of an additional point (Location 5) which was calculated using four tie points (obtained from the other four locations). No CP's were used to calculate this location. A detailed error analysis is provided in Section 5.3.

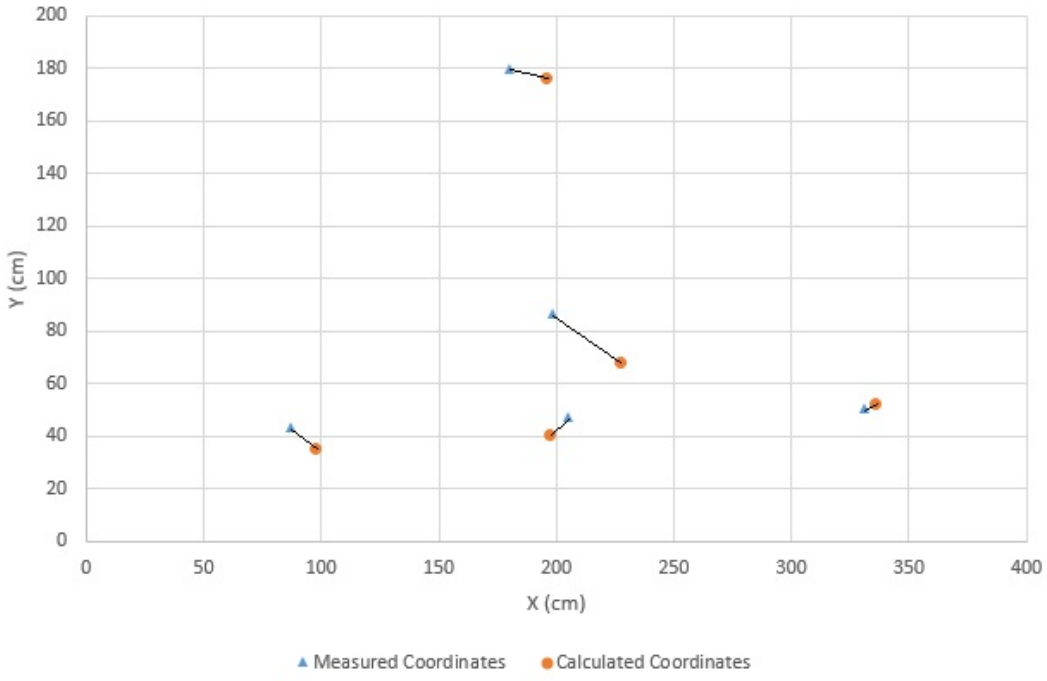

Figure 5.20: S1 Navigation Results (Planimetry)

The following Figure 5.21 describes elevation navigation results. Z represents elevation and

S represents the 2D distance along X-Y axes (S = $\sqrt{x^2 + y^2}$).

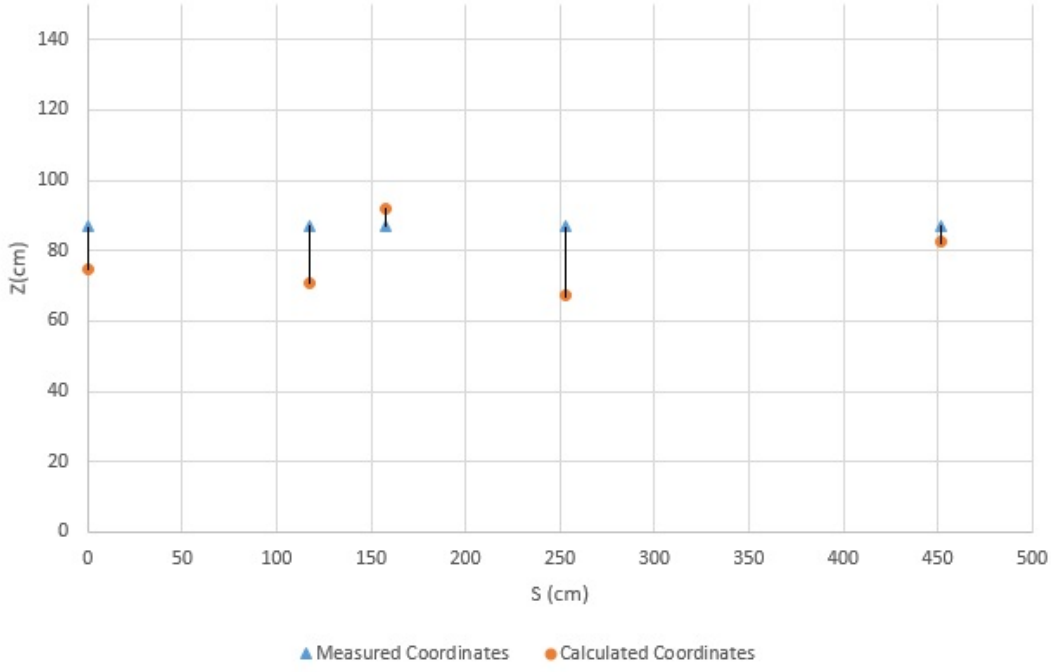

Figure 5.21: S1 Navigation Results (Elevation)

5.2.2 Site 2

In the second experiment, in Site 2, the catadioptric camera was set up as shown in three different locations. All three are determined using the CP's set up within the room. Location 2 is calculated, again, from the 3D points (tie-points) obtained from the other two locations of the mobile platform. Site 2 is a room, approximately 6m x 4m x 6m in dimension. Few of the images of site 2 are shown in Figure 5.22.

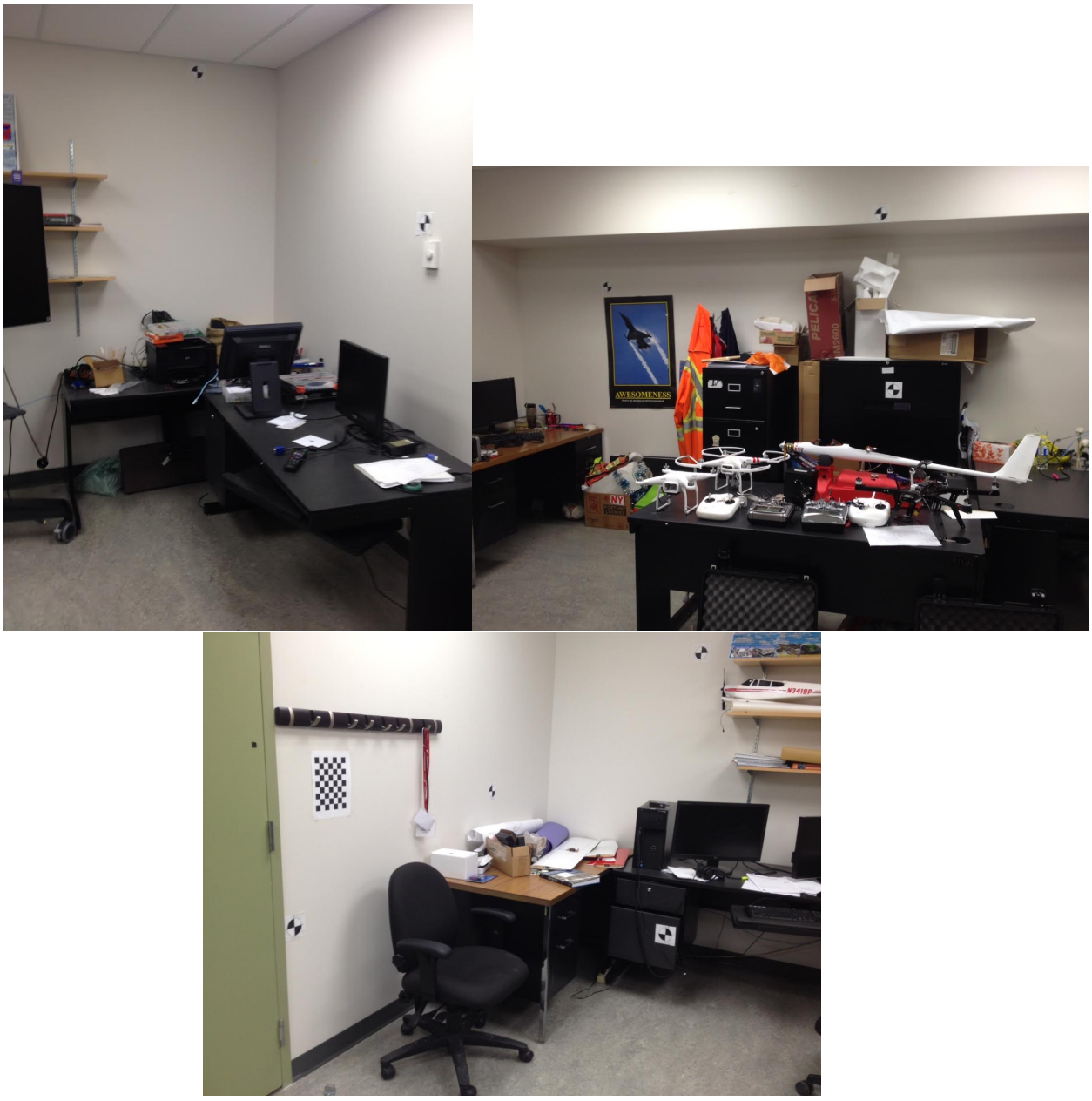

Figure 5.22: Site 2

5.2.2.1 Positioning Results

In this subsection, different locations are displayed along with the rotation and position results obtained for that location. The catadioptric image taken from that location is shown along

with the unwrapped image, which makes it easier to visually identify the placement of the catadioptric camera. The rectified image looks like a panoramic image, however, it is slightly distorted especially from top and bottom corners. There are three different locations taken in an average sized (approximately 6m x 4m x 4m) room. T. Eighteen control points were set up in the room and the mobile platform with the catadioptric camera was moved to three different location (L1, L2, L3), these positions were calculated and also measured manually and the two were compared. All three locations are approximately along a line, i.e. their X axis values are almost the same and they are approximately 1m apart along the Y axis. The images captured from these positions are shown in Figures 5.23, 5.25 and 5.27.

Since the first step, in the process of navigation and mapping was calibration, table 5.21 shows the calibration result. As mentioned before, since all three rotation angles were assumed to be zero (and the camera was physically placed accordingly) in order to obtain more accurate calibration results, only translation results are shown below. These results show the relative translation between the camera and the mirror. Using these values the camera coordinate system is positioned in the mirror coordinate system which is then referred to as the catadioptric coordinate system. Therefore, the following describe the relation between the camera and the mirror coordinate system. It is also observed that these results are the same as those obtained for Site 1.

Camera (mm)	
X_{mc}	-2.9
Y_{mc}	2.8
Z_{mc}	-91

Table 5.21: S2 Calibration Results

The results and images for each location are provided in the same manner as for Site 1.

5.2.2.1.1 Location 1

Images Figure 5.23 shows the image taken at Site 2 Location 1 and Figure 5.24 shows the panoramic image of Site 2 Location 1 image.

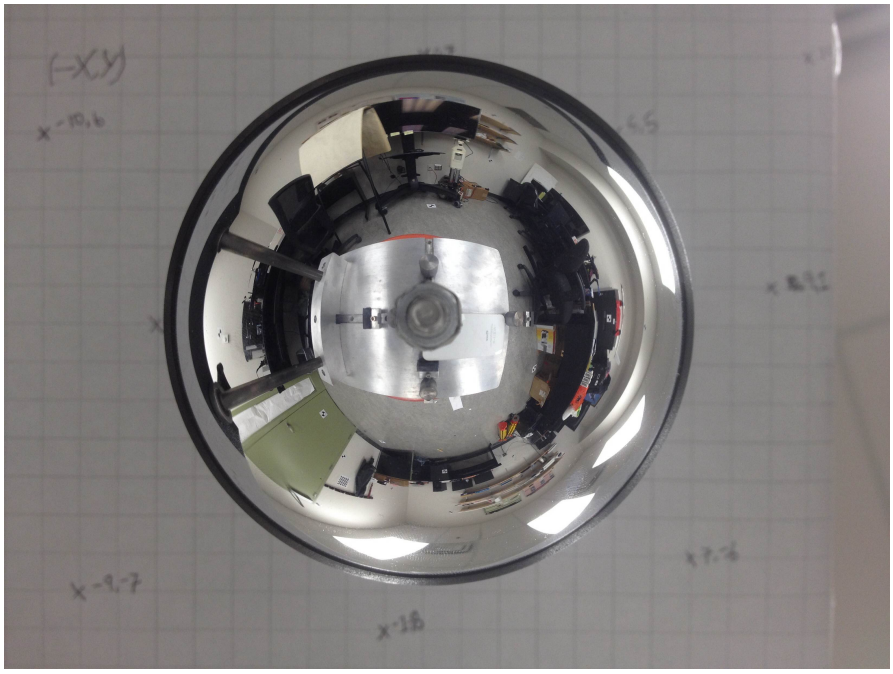

Figure 5.23: Site 2 Location 1 Image

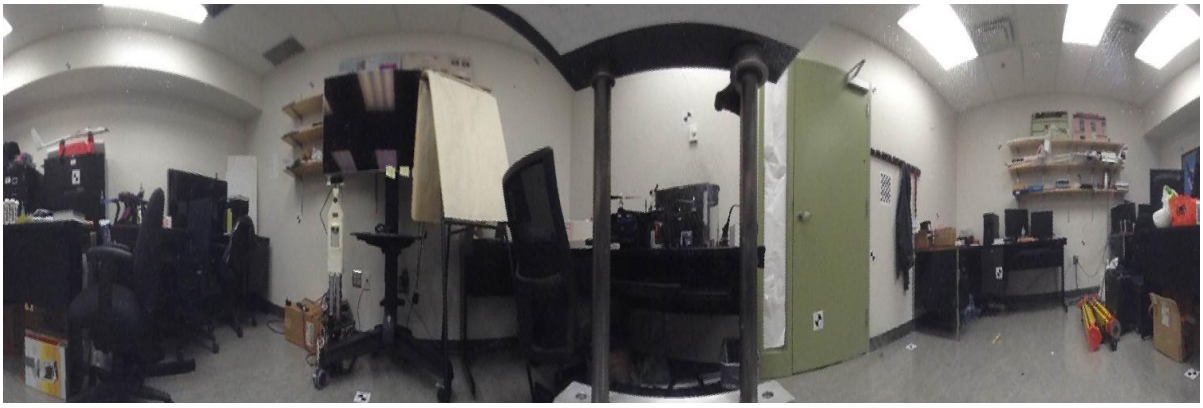

Figure 5.24: Site 2 Location 1 Unwrapped Image

Results

Table 5.22 gives the estimate rotation angles of the catadioptric system at Site 2 Location 1.

Table 5.23 gives the actual position of the catadioptric system at that location in world coordinate system. This is followed by the Table 5.24 which provides the positioning results of different experiments and accompanied by their average and standard deviation. The results from Table 5.23 and 5.24 are compared to obtain the average error which is given in Table 5.25.

Rotation Angles	Average (degrees)	Standard Deviation (degrees)
ω	-6.13	0.93
ϕ	-4.75	0.17
κ	-108.45	0.59

Table 5.22: Site 2 Location 1 Rotation Results

Measured (mm)	
X_T	1870
Y_T	2055
Z_T	671

Table 5.23: Site 2 Location 1 Measured Positions

Experiment	1	2	3	4	Average	Standard Deviation
$X_T(mm)$	1734.6	1734.6	1707.7	1615.1	1698	56.7
$Y_T(mm)$	1829.8	1829.8	1893.5	1854.2	1851.83	30.07
$Z_T(mm)$	481.4	481.4	463.6	492.6	479.75	12

Table 5.24: Site 2 Location 1 Calculated Positions

Error (mm)	
Δ_{X_T}	200.7
Δ_{Y_T}	212.0
Δ_{Z_T}	178.6
Δ_{S_T}	342.4

Table 5.25: Site 2 Location 1 Positioning Error

5.2.2.1.2 Location 2

Images Figure 5.25 shows the image taken at Site 2 Location 2 and Figure 5.26 shows the panoramic image of Site 2 Location 2 image.

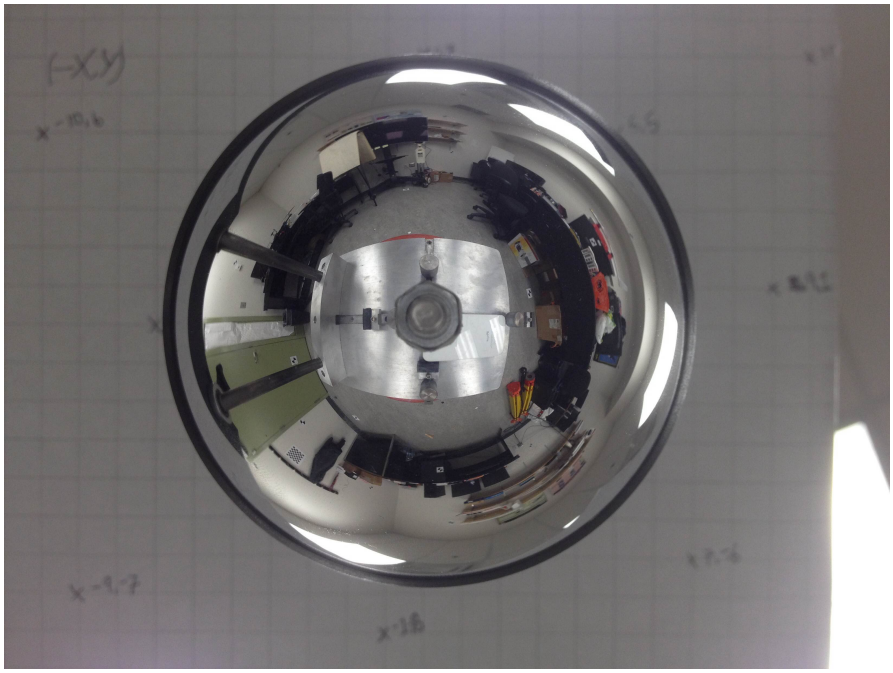

Figure 5.25: Site 2 Location 2 Image

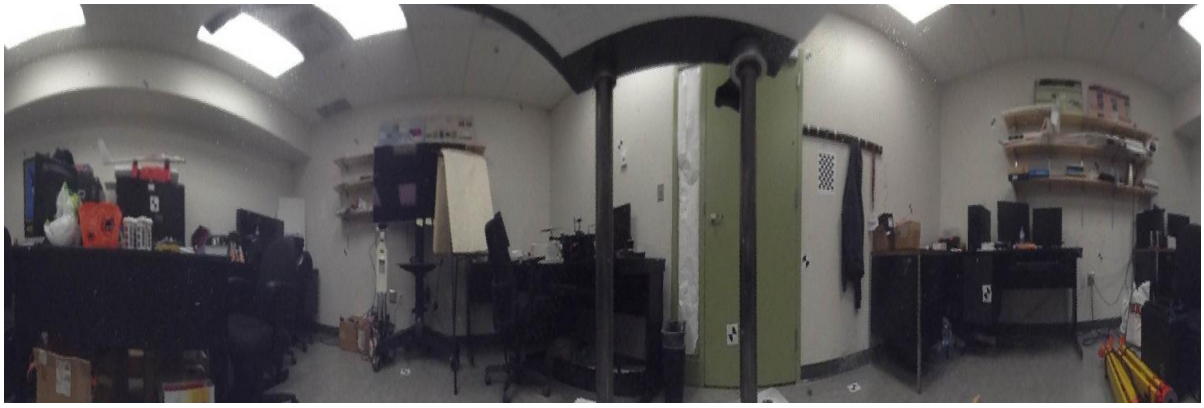

Figure 5.26: Site 2 Location 2 Unwrapped Image

Results

Table 5.26 gives the estimate rotation angles of the catadioptric system at Site 2 Location 2.

Table 5.27 gives the actual position of the catadioptric system at that location in world coordinate system. This is followed by the Table 5.28 which provides the positioning results of different experiments and accompanied by their average and standard deviation. The results from Table 5.27 and 5.28 are compared to obtain the average error which is given in Table 5.29.

Rotation Angles	Average (degrees)	Standard Deviation (degrees)
ω	-5.525	0.49
ϕ	-3.275	0.33
κ	-111.35	0.29

Table 5.26: Site 2 Location 2 Rotation Results

Measured (mm)	
X_T	1870
Y_T	3140
Z_T	671

Table 5.27: Site 2 Location 2 Measured Positions

Experiment	1	2	3	4	Average	Standard Deviation
$X_T(mm)$	1678	1740.7	1605.1	1576.5	1650.08	74
$Y_T(mm)$	2813.8	2858.5	2897.6	2848.6	2854.63	34.47
$Z_T(mm)$	468.6	442.4	399	401.9	427.98	33.55

Table 5.28: Site 2 Location 2 Calculated Positions

Error (mm)	
Δ_{X_T}	219.9
Δ_{Y_T}	285.4
Δ_{Z_T}	242.0
Δ_{S_T}	434.0

Table 5.29: Site 2 Location 2 Positioning Error

5.2.2.1.3 Location 3

Images Figure 5.27 shows the image taken at Site 2 Location 3 and Figure 5.28 shows the panoramic image of Site 2 Location 3 image.

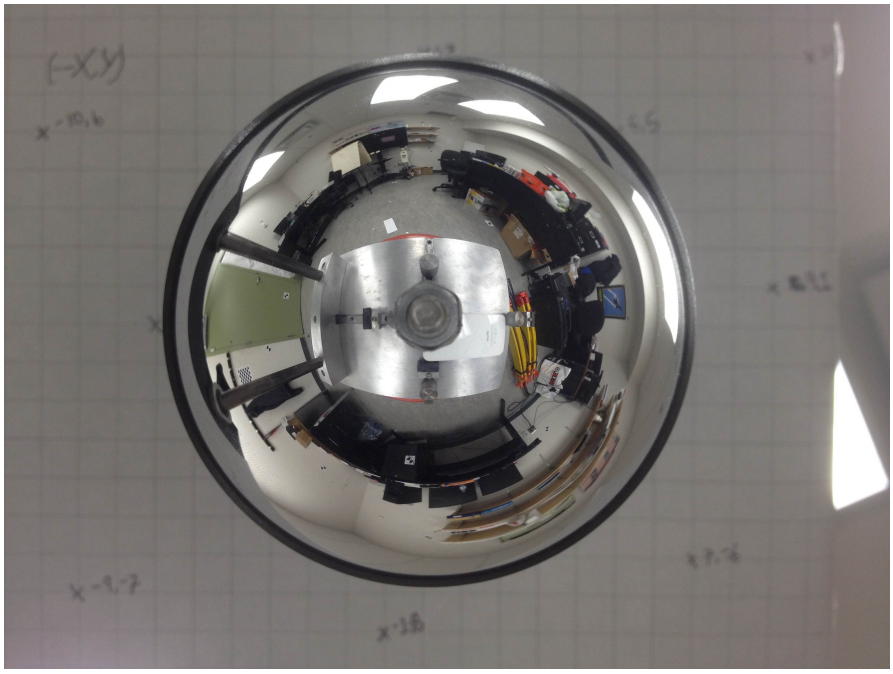

Figure 5.27: Site 2 Location 3 Image

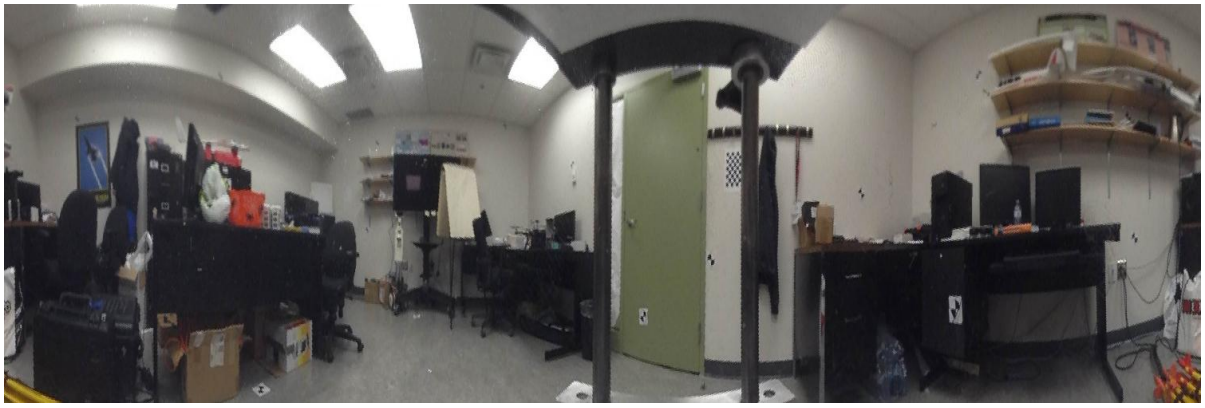

Figure 5.28: Site 2 Location 3 Unwrapped Image

Results

Table 5.30 gives the estimate rotation angles of the catadioptric system at Site 2 Location 3.

Table 5.31 gives the actual position of the catadioptric system at that location in world coordinate system. This is followed by the Table 5.32 which provides the positioning results of different experiments and accompanied by their average and standard deviation. The results from Table 5.31 and 5.32 are compared to obtain the average error which is given in Table 5.33.

Rotation Angles	Average (degrees)	Standard Deviation (degrees)
ω	-3.43	0.41
ϕ	-0.5	0.54
κ	-111.88	0.33

Table 5.30: Site 2 Location 3 Rotation Results

Measured (mm)	
X_T	1870
Y_T	4115
Z_T	671

Table 5.31: Site 2 Location 3 Measured Positions

Experiment	1	2	3	4	Average	Standard Deviation
$X_T(mm)$	1621.7	1667.9	1622	1599.8	1627.85	28.65
$Y_T(mm)$	3926.3	3951.4	3972.9	3898.3	3937.23	32.19
$Z_T(mm)$	385.1	391.5	404	360	385.15	18.51

Table 5.32: Site 2 Location 3 Calculated Positions

Error (mm)	
Δ_{X_T}	242.2
Δ_{Y_T}	177.8
Δ_{Z_T}	284.9
Δ_{S_T}	414.0

Table 5.33: Site 2 Location 3 Positioning Error

Summary of Results

Table 5.34 gives the positioning results of the catadioptric system (at Site 2), comparing the measured coordinates with calculated coordinates obtained from positioning using CP's from the results shown in the second and third table of each location.

Location	Measured (mm)			Calculated (mm)			Error (Meas. - Calc.) (mm)		
	X	*Y*	*Z*	*X*	*Y*	*Z*	ΔX	ΔY	ΔZ
L1	1870	2055	671	1698	1851.83	479.75	200.7	212.0	178.6
L2	1870	3140	671	1650.08	2854.63	427.98	220	285.4	242.0
L3	1870	4115	671	2854.63	3937.23	385.15	242.2	177.8	284.9
Mean Error (mm)							220.97	225.07	235.17
Std. Dev. (mm)							20.77	54.98	53.48

Table 5.34: S2 Positioning Results and Errors

Figure 5.29 shows the locations of the catadioptric system on Site 2, comparing the measured coordinates with calculated coordinates obtained from positioning using CP's.

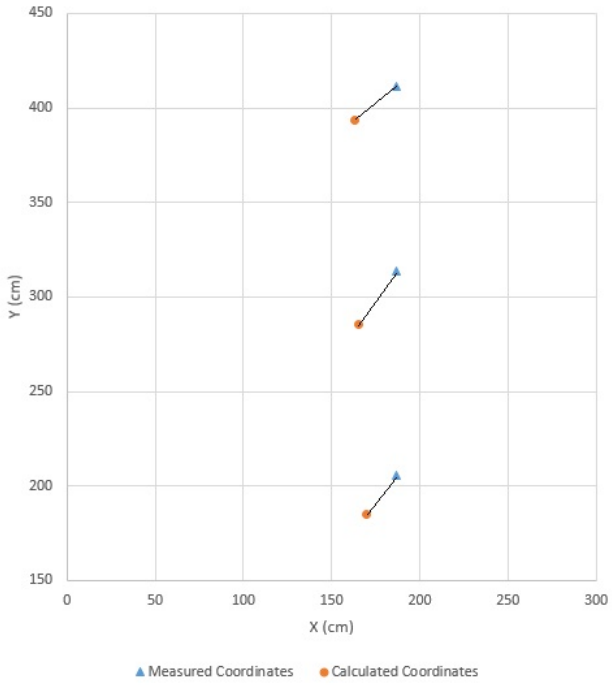

Figure 5.29: S2 Path Analysis (Planimetry)

The following Figure 5.30 describes elevation positioning results. In the plot, Z represents

elevation and S represents the 2D distance along X-Y axes (S = $\sqrt{x^2 + y^2}$).

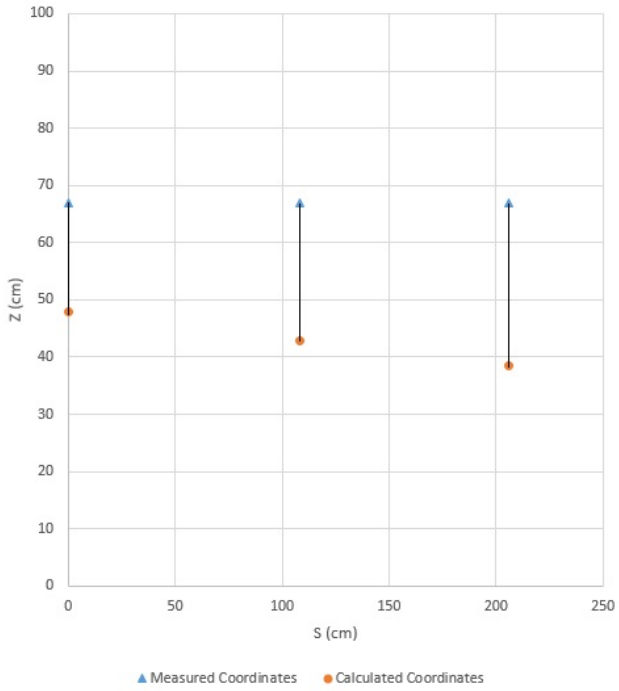

Figure 5.30: S2 Path Analysis (Elevation)

5.2.2.2 Mapping Results

For the mapping test the 3D coordinates of common tie points captured from two location of the catadioptric system were estimated. Table 5.35 provides the measured and calculated coordinates of the mapped points (at Site 2) along with errors.

Figure 5.31 shows the mapped points plotted along with their measured coordinates in order to assess any positional differences. Some of the mapped points were visually identifiable points obtained from both images and some were just recalculated CP's using the average positioning results. A detailed error analysis is provided in section 5.3.

Point	Measured (mm)			Calculated (mm)			Error (Meas - Calc) (mm)		
	X	*Y*	*Z*	*X*	*Y*	*Z*	Δ*X*	Δ*Y*	Δ*Z*
TP1	0	1639.0	1675.0	-189.6	1555.9	1697.9	189.6	83.1	-22.9
TP2	1009.0	6111.0	2022.0	1101.2	5978.5	1960.0	-92.2	132.5	62.0
TP3	2734.0	6111.0	1532.0	2780.3	6259.2	1695.6	-46.3	-148.2	-163.6
TP4	4952.0	5272.0	1911.0	5012.1	5450.4	2126.0	-60.1	-178.4	-215.0
TP5	4374.0	3016.0	2290.0	4362.2	3105.2	2196.8	11.8	-89.2	93.2
TP6	3362.0	0	2267.0	3414.5	58.1	2237.3	-52.5	-58.1	29.7
TP7	0	3695.0	680.0	-136.9	3670.8	709.2	136.9	24.2	-29.2
TP8	0	5262.0	1139.0	95.3	5145.3	1135.1	-95.3	116.7	3.9
TP9	0	2910.0	309.0	-245.3	2867.1	340.3	245.3	42.9	-31.3
TP10	3612.0	0	922.0	3692.5	-139.4	1175.5	-80.5	139.4	-253.5
Mean Error (mm)							15.7	6.5	-52.7
Std. Dev. (mm)							127.0	117.0	118.0

Table 5.35: S2 Mapping Results and Errors

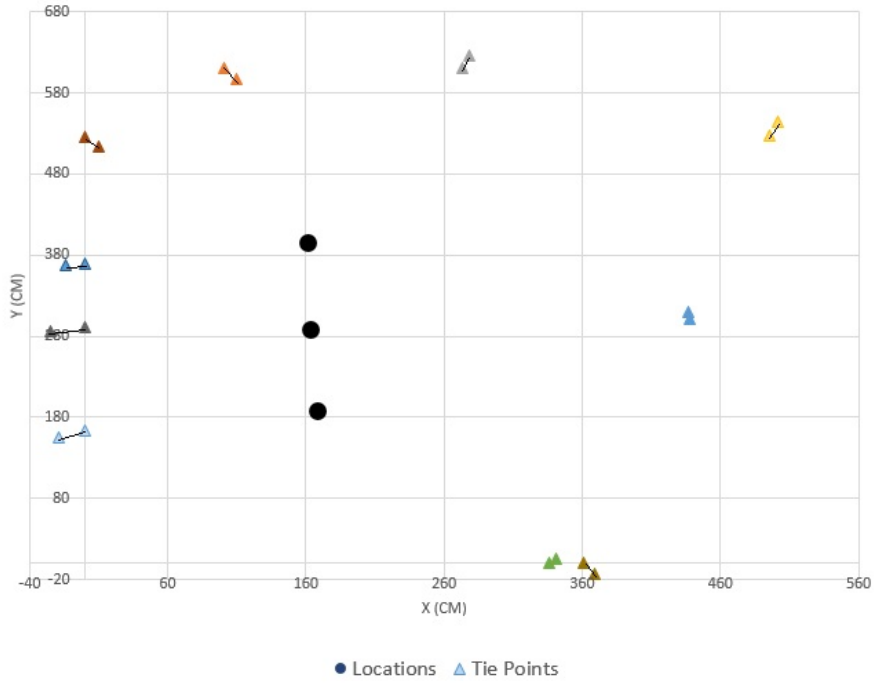

Figure 5.31: S2 Mapping errors (Planimetry)

Figure 5.32 shows the elevation errors in all of 10 mapped points. These errors (along the y-axis) are the difference between the measured and calculated elevations of the points (named

along x-axis in the plot).

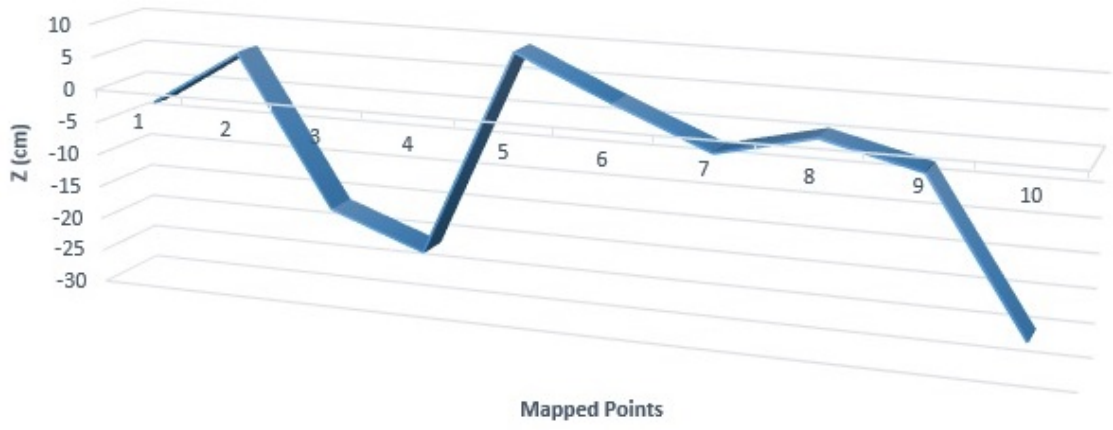

Figure 5.32: S2 Mapping errors (Elevation)

5.2.2.3 Navigation Results

Table 5.36 shows the position and errors of catadioptric system at Location 2 when it is calculated using four tie points which were determined from the other two locations. These results are visually displayed in Figure 5.33 (XY plane) and Figure 5.34 (elevation)

Location	Measured (mm)			Calculated (mm)			Error (Meas - Calc) (mm)		
	X	*Y*	*Z*	*X*	*Y*	*Z*	ΔX	ΔY	ΔZ
L2	1870	3140	670	1655.5	2869.1	393	214.5	270.9	277.0

Table 5.36: S2 Navigation Results and Errors

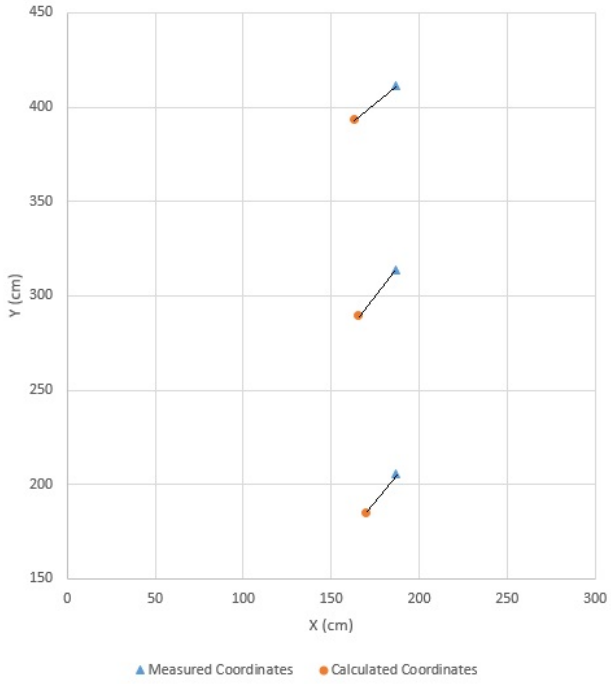

Figure 5.33: S2 Navigation results (Planimetry)

Figure 5.34 describes elevation navigation results. In the plot, Z represents elevation and S represents the 2D distance along X-Y axes (S = $\sqrt{x^2 + y^2}$).

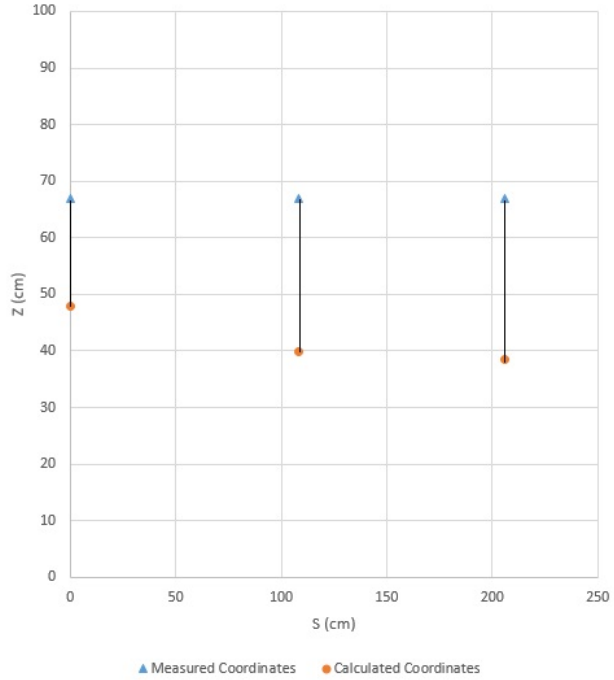

Figure 5.34: S2 Navigation results (Elevation)

5.3 Error and Sensitivity Analysis

In this section, the results presented in the previous section are analyzed.

5.3.1 Positioning Analysis

Table 5.37 shows the average positioning errors of the four locations of Site 1.

Average Positioning Error (mm)	
ΔAX_T	97.1
ΔAY_T	50.2
ΔAZ_T	130.8
ΔAS_T	172.9

Table 5.37: S1 Positioning Errors

where,

$$\Delta AX_T = \sum_{i=1:4} |\Delta X_T(S1Li)|/4$$
$$\Delta AY_T = \sum_{i=1:4} |\Delta Y_T(S1Li)|/4$$
$$\Delta AZ_T = \sum_{i=1:4} |\Delta Z_T(S1Li)|/4$$
$$\Delta AS_T = \sum_{i=1:4} |\Delta S_T(S1Li)|/4$$

Table 5.38 shows the average positioning errors of the three locations of Site 2.

Average Positioning Error (mm)	
ΔAX_T	220.9
ΔAY_T	225.1
ΔAZ_T	235.2
ΔAS_T	396.8

Table 5.38: S2 Positioning Errors

where,

$$\Delta AX_T = \sum_{i=1:4} |\Delta X_T(S2Li)|/3$$
$$\Delta AY_T = \sum_{i=1:4} |\Delta Y_T(S2Li)|/3$$
$$\Delta AZ_T = \sum_{i=1:4} |\Delta Z_T(S2Li)|/3$$
$$\Delta AS_T = \sum_{i=1:4} |\Delta S_T(S2Li)|/3$$

One of the things observed in comparing the two tables 5.37 and 5.38, is that the positioning results of Site 1 (average positioning error, ΔAS_T = 17.29 cm) are much more accurate than those of the 3 location in Site 2 (ΔAS_T = 39.68 cm). This can be attributed to the spaciousness of the test area, i.e. the distance of the camera system from the targets and is the most decisive factor in accuracy of the results. This is also observed when different results for the same location are compared. The results which were obtained using nearby targets are much closer to the reference of position than the ones obtained farther targets. Since the distance from targets is the main source of error, the positioning error can be calculated in terms of

the average distance of targets used, which gives the result as 1/12, which is the ratio of displacement error to the average distance of targets used.

Distance from targets is not the only factor which impacts the results. Another very important factor is the geometry from the location to the targets. It is observed that if the targets are well distributed in all directions from the mirror, much better results are obtained. However, if they are concentrated on one side, the error is high. This is because it leads to less constraint which results in more freedom of movement and a weak solution. Another important factor which affects the results is the number of CP's used. Generally the more CP's, the better the result, however, there needs to be caution on the CP's used. CP's nearer to the camera and ones which improve the geometry are preferred.

A few additional observations can be made by looking at the results and comparing the results of the two experiments with each other. Even though, the positions results of Site 1 are more accurate than those of Site 2, as described above, the variance in the results of Site 1 is higher than that of those in Site 2 as seen in table 5.18 and 5.34. This can be attributed to the diversity of the geometry and distance of CP's used in Site 1. In Site 2 the camera system is located near the centre and the geometry of the room allows control points to be distributed evenly throughout which results in consistency of results obtained from different sets of control points. In Site 1, however, a whole different set of CP's results in a different value. For example, replacing a nearby target, with a farther away one changes the result significantly as compared to replacing it with one at similar distance. These results can be improved, for both sites, by using a higher number of control points.

5.3.2 Mapping Analysis

Table 5.39 shows the average mapping errors of all twelve tie-points on Site 1(calculated from Table 5.19).

Average Mapping Error (mm)	
ΔMX_T	73.5
ΔMY_T	66.3
ΔMZ_T	65.7
ΔMS_T	118.8

Table 5.39: S1 Average Mapping Errors

Table 5.40 shows the average mapping errors of all ten tie-points on Site 2 (calculated from Table 5.35).

Average Mapping Error (mm)	
ΔMX_T	101.1
ΔMY_T	101.2
ΔMZ_T	90.4
ΔMS_T	169.2

Table 5.40: S2 Average Mapping Errors

where,

$$\Delta MX_T = \sum_{i=1:n} |\Delta X_T(TPi)|/n$$

$$\Delta MY_T = \sum_{i=1:n} |\Delta Y_T(TPi)|/n$$

$$\Delta MZ_T = \sum_{i=1:n} |\Delta Z_T(TPi)|/n$$

$$\Delta MS_T = \sum_{i=1:n} |\Delta S_T(TPi)|/n$$

Where n, represents the number of mapped points.

The mapping results are displayed in the previous section in a plot for each experiment. However, observing tables 5.39 and 5.40, it is noted that Site 1 has an average mapping

error (ΔMS_T) of 11.88 cm and Site 2, an average mapping error of 16.92 cm. This error is the average displacement for the position of the 3D points. The main reason for better results in mapping in Site 1 is because of better system positioning results. However, it is observed that mapping is more accurate than positioning for both rooms. This is an important conclusion, especially for Site 2 where the difference between the two is much more. Even though positioning results are used for the mapping operation, there is an improvement since the positioning errors tend to balance each other out, when used for mapping. This is due to the added constraints in using a stereo system geometry For example, an estimation error of the rotation angle at a location might lead to a high positioning error, but the same error is negated when images captured from two of the locations, having the same rotation error, are used for mapping.

There are three main factors which affect the mapping results: distance, distribution of targets, and elevation of the tie-points. Similar to positioning, where closer CP's provide better results, in mapping closer targets are more accurately determined. This is again because of propagation error. The error might be in part due to the initial calibration error, the propagated positioning error or an image coordinates measuring error. Outliers can easily be determined by reviewing the results and thus are eliminated. An example of a outlier might be the selection of a wrong target or a mismatch of targets. An outlier detection method such as RANSAC (Random Sample Consensus) might be used for this purpose. The geometry of the network of tie-points used plays a very important role in accuracy. An example of weak geometry is a target on the same side of both mirrors as this often results in large errors. This is because a slight error in the reflection angle results in a high propagation of error in that particular direction. Targets in the middle of two set-up locations have been determined with high accuracy.

Finally, elevation of the targets also affects the accuracy of the mapped point. The higher the

elevation of the point, the lower the accuracy. This is because of the shape of the mirror and because the change in reflection angle is more pronounced at a point reflected higher up on the mirror. Therefore points which have a lower elevation are mapped more accurately. This is also true for positioning where CP's with lower elevation give a more accurate result for the location.

As was mentioned before, the mapped points consisted of both CP's and new points which were visible in both images being used. Even though these CP's were used in order to determine the position of the catadioptric camera, no favorable bias in their error values is found, that is they are not more accurate. The error values of tie points lie within the range of error values of mapped coordinates of CP's. In fact the average error of tie points is lower. However this is only because they were closer and at better geometry. Therefore, it can be safely concluded that whether the point was used in determination of the position does not impact its mapped result using the average position of the catadioptric camera.

5.3.3 Navigation Analysis

In both experiments, in Site 1 and 2, navigation results are obtained by calculating the coordinates of locations (i.e. positioning) using mapped points (control point generation and densification). These mapped points are common points viewed from two or more locations, calculated as described in mapping. In Site 1 for experimental purposes, an extra location, Location 5, was added and was determined using four mapped points shown in figure 5.18. This location is included in the figure 5.20. It can be observed that the accuracy of this location as compared to the actual measured value is lower than those of points obtained by positioning. The displacement error of Location 5 using tie-points is 34.81 cm (Table 5.41) as compared to the average displacement errors of other points, which is 17.29 cm. This is as expected, since the inputs for positioning, i.e. the CP's are more accurate than tie-points.

The measured coordinates of control points were used in positioning, whereas, the mapping errors (average = 11.88 cm) lead to a higher error in positioning L5. The factors affecting navigation results are the same as those affecting positioning, i.e. the number of the control points used, distance between the camera and control points and the geometry of the network.

Average Error (mm)	
ΔX_T	-289.7
ΔY_T	186.1
ΔZ_T	-51.1
ΔS_T	348.1

Table 5.41: S1L5 Positioning Error

In the case of Site 2 (Table 5.42), Location 2 was calculated from tie points obtained from Location 1 and Location 3. By observing the result, it can be concluded that the position of Location 2 obtained using CP's is more accurate than one obtained using tie-points. The difference, however, is relatively little (44.29 cm as compared to 43.4 cm). It is also approximately 5 cm higher than the average positioning error of Site 1. This is expected since, again, tie points are less accurate than CP's. Even though the average mapping error for Site 1 was 16.29 cm and factors in the accuracy of navigation, the accuracy of navigation also depends on the geometry and number of tie-points used. Therefore, the displacement error in the position of tie points might cancel out while navigation and provide a result which is very similar to positioning, as in this case.

As in the case of the positioning error, the navigation error can be calculated in terms of the average distance of targets used, which gives the result as 1/5.5, which is the ratio of displacement error to the average distance of targets used.

Average Error (mm)	
ΔX_T	214.5
ΔY_T	270.9
ΔZ_T	277.0
ΔS_T	442.9

Table 5.42: Site 2 Location 2 Positioning Error (using tie-points)

The following is the list which describes the possible error sources in the experiments:

- Calibration errors in calculation of intrinsic and/or extrinsic parameters. These are the main sources of errors and lead to larger errors in positioning and mapping and are discussed in detail in next section.
- Measurement Errors in measurement of pixel coordinates for obtaining corresponding mirror coordinates. Different users might obtain different results. Additional measurement errors might occur in measurement of coordinates of the positions and of tie-points.
- Further errors might be introduced due to the movement of the system, i.e. a slight change in configuration during motion from one location to another.
- Errors might also be introduced because of certain assumptions in calculations, such as the least squares assumption and the assumption that the system is stable when moved from one location to another.

5.3.4 Sensitivity Analysis

A sensitivity analysis was performed on the calibration (of mirror-camera system) simulation model. This was done in order to determine calibration errors would affect the positioning

and mapping results. For this task, translation and orientation errors were introduced in the simulation model of the catadioptric system used for the experiments. From this sensitivity analysis, it is observed that an error of a degree in relative rotation, or of a few millimetres in translation in calibration, result in an error of decimeters in object space in navigation and mapping. This is primarily due to the shape of the omnidirectional mirror and the set up of the catadioptric system. A slight translation error leads to a miscalculation of mirror coordinate of the object. Due to the reflection property of the mirror, the error in positioning of the catadioptric system or mapping of a tie point increases proportionally with the distance between the camera and the object. In, summary, estimation errors of rotation angle of the camera relative to the mirror or in relative translation, changes the estimated projection of mirror point in the image and this further translates into an error in navigation and mapping. For example, a miscalculation of 1 mm in position of camera leads to an average of 18 cm change in the elevation of a point on a wall 3 meters away (Figure 5.35). Similar planimetric errors are obtained for estimation errors along the XY plane. This high error propagation is due to the change in the reflection angle at different points on the mirror. This means that a one mm error in translation (during calibration of mirror-camera system) causes a miscalculation of mirror coordinate, which in turn causes an error in estimated reflection angle which leads to increasing positioning error proportional to object-camera distance. Since the change in the reflection angle is significant (about 5^0 at median height of the mirror, i.e., 19 mm) the error is significant. This error exists in both navigation and mapping as well.

This error value decreases at points located on the higher end of the mirror and increases at points located on the lower end of the mirror, i.e., the points reflected on the lower end of the mirror are affected much more by this miscalculation than the points affected on higher end of the mirror. However the relationship is not linear since it depends on the reflection angle as well. The reflection angle ranges ideally from -90^0 to 52.5^0 (However the visibility of some of the lower points is limited). A one mm miscalculation in position of the camera at a point

reflected on 5 mm height of the mirror results in change in reflection angle of about $6^0(-53^0$ to $-59^0)$ which propagates to approximately change in position of a point of about 100 cm whereas the same miscalculation affects the position of a point reflected on the higher end of the camera, 38 mm by only 13 cm.

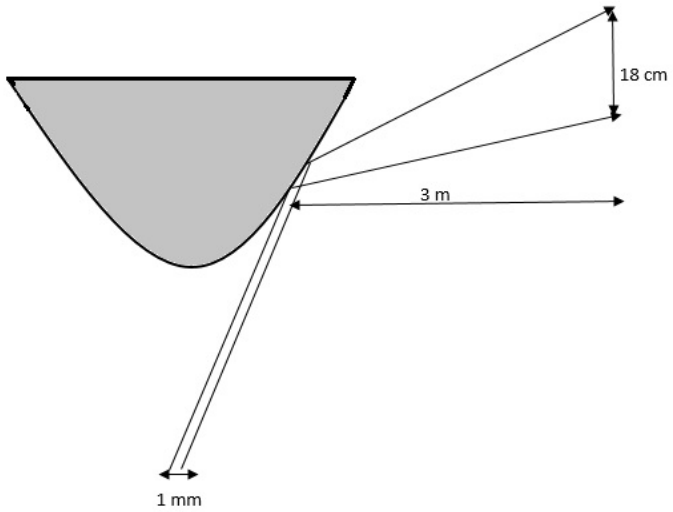

Figure 5.35: Sensitivity Analysis (Translation Error)

A detailed analysis of positioning error caused due to translation error in calibration is provided in Figure 5.36. The contour lines represent the propagated error (in mm's). The figure consists of the errors in objects at different mirror coordinates (Z_{MC}).

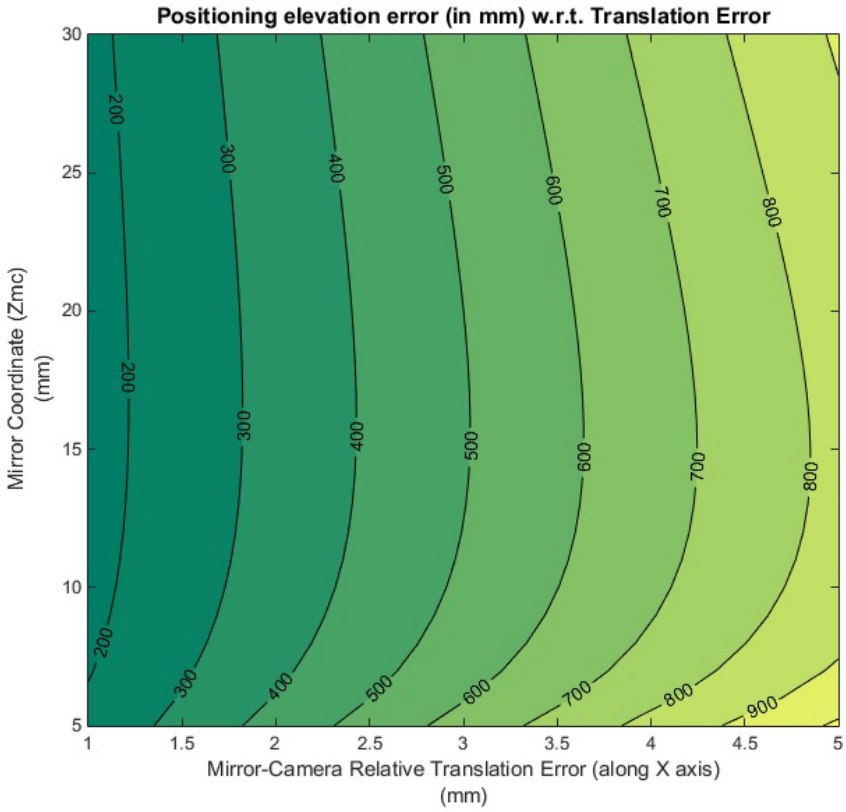

Figure 5.36: Detailed Sensitivity Analysis (Translation Error)

The positioning results are also very sensitive to estimation errors in the calculation of relative rotation between the camera and mirror during calibration. For example, a miscalculation of 0.4^0 in rotation about x or y axis (ω or ϕ) for a projected point at height of about 19 mm on the mirror would cause the same error of approximately 18 cm in the calculation of the elevation coordinate of a point 3 m away (Figure 5.37). Similar errors are obtained for estimation errors along other axes. The error increases for points reflected lower on the mirror since the reflection angle changes more drastically.

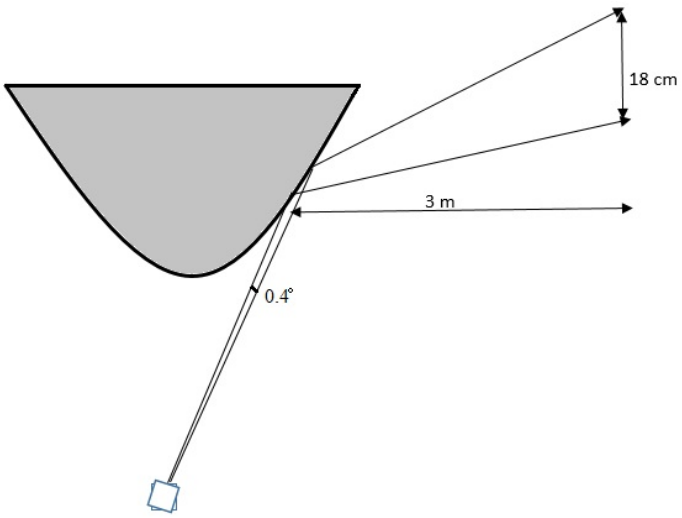

Figure 5.37: Sensitivity Analysis (Rotation Error)

A detailed analysis of positioning error caused due to orientation error in calibration is provided in Figure 5.38.

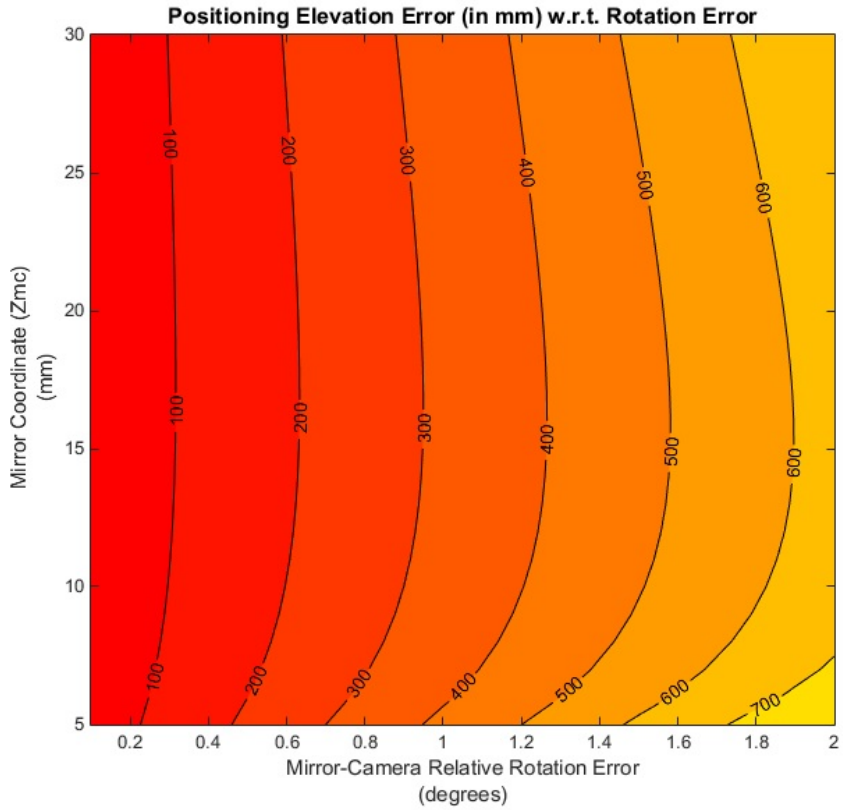

Figure 5.38: Detailed Sensitivity Analysis (Rotation Error)

Miscalculations in position and orientation of camera with respect to the mirror can also cause planimetric errors in positioning as shown Figure 5.39. However, these errors depend heavily on the environment and the position of the camera within the indoor environment. A miscalculation of 0.5^0 in rotation can lead to a planimetric (position along XY axis) error of 2.6 cm for a point positioned 3m away. Miscalculation in translation causes more severe errors. Translation miscalculation affect obtained coordinates of points at lower elevation (and obtained coordinates of camera due to these points) much more than those at higher elevation. This is because, a small error of 1mm, causes a rotation error of approximately 10^0 at a point viewed on cameras lowest point as compared to only 1.5^0 at a point located at mirror's highest point, due to shape of the paraboloid (the circumference increases as elevation increases).

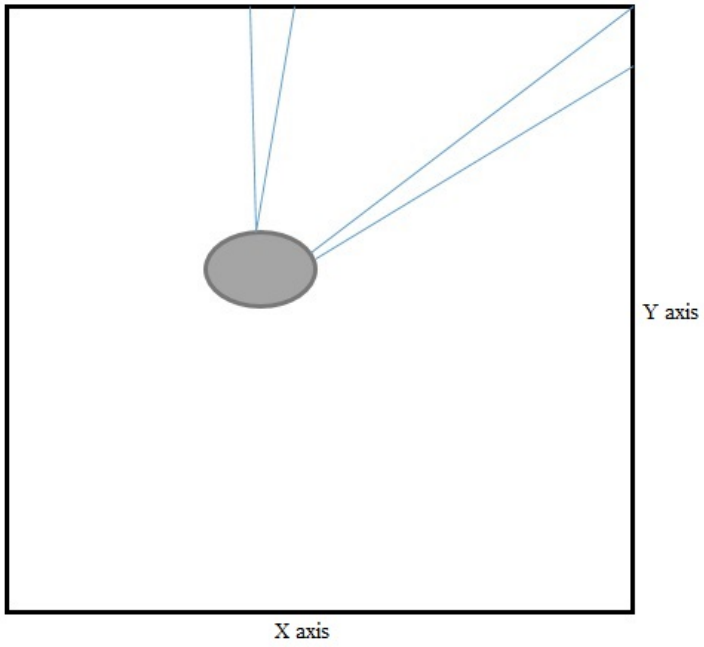

Figure 5.39: Planimetric Sensitivity

Figure 5.40 shows the planimetric error due to 1mm translation miscalculation at a point 3m away.

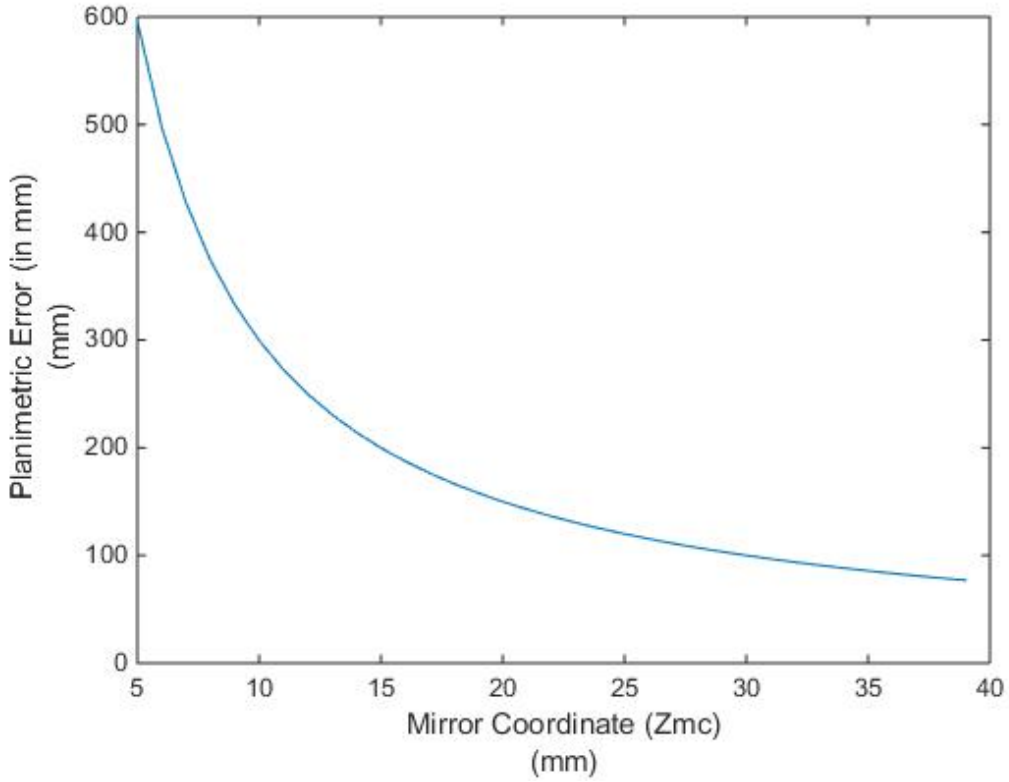

Figure 5.40: Planimetric Sensitivity

A combination of the errors caused by translation and rotation errors can lead to even larger errors. When these errors combine they increase the error not just linearly. Meaning, if there is a position error of 1 mm for the camera along the X axis and a 0.4^0 rotation angle along the Y axis for a projected point at a height of about 19 mm on the mirror, the total error in calculated elevation of a point located 3 m away from the camera would be approximately 36 cm. It is therefore very important to obtain accurate calibration results since the rest of the results will depend on it, and because there is a high propagation of error from calibration to other processes. This is the reason why the calibration of the catadioptric system was performed using the targets on the top plate and then refined using the visual fine adjustment method in order to better estimate the rotation and translation matrices. Since the results were obtained manually, it can be approximated that they have sub-mm accuracy.

Chapter 6

Conclusions and Future Work

6.1 Conclusion

Mathematical models were developed to evaluate vision based navigation and mapping using catadioptric cameras. This was done in four major steps: calibration, positioning, navigation and mapping. A low cost, highly flexible system was constructed in order to test these mathematical models. Several experiments were performed at two sites. A paraboloid mirror was used for the experiments such that the mirror-camera combination, catadioptric camera is a non central camera so that the math models are generic and can be implemented on a variety of camera-mirror systems involving mirrors of different shapes such as sphere, hyperbolic and elliptical.

6.1.1 Calibration

In calibration, the relative orientation and translation of the mirror coordinate system and camera coordinate system (the image coordinate system) were determined, that is, their relationship was established so that the system could be treated as a single monolithic unit (a

catadioptric camera). This was done using a combination of two methods. The first one utilizes the image coordinates of the targets placed on the mirror mounted plate using projective geometry and collinearity conditions. The second involved the use of those estimated results as a-priori values and further refining them by manual simulation.

6.1.2 Positioning of the catadioptric camera

To position the catadioptric camera, the mathematical model utilized two conditions, both contingent upon the reflection of the mirror. The first one was the collinearity equations linking the mirror coordinates of the CP's, that is the reflection of CP in the mirror as seen in the image, to the CP's. The second exploited the co-planarity of the three points: mirror coordinate, CP and Lens coordinate. At least 3 CP's were required to obtain the position of the catadioptric camera. The mirror coordinates of the CP's were determined before this step directly from their respective image coordinates using a collinearity equation and the shape of the paraboloid. If a different mirror is used this change will be required and the rest of the steps remain same. This will be explored more in the next section. Therefore the position of the catadioptric camera was thus obtained in a world coordinate system. Several locations in each of the experiments were established and their positions determined using the same mathematical model with same or different CP's placed on that site. An average positioning accuracy of about 17 cm was obtained for Site 1 with errors ranging from 4cm to 25 cm. For Site 2 the average positioning error was about 40 cm. The primary causes being the geometry of and distance of the control points from the catadioptric system.

6.1.3 Mapping using stereo set-ups

These different system set-ups were then used to map points in the room. Therefore, a few common points visible in two or more images were mapped. This was done using space intersection based on epipolar geometry. Two or even three sometimes, positions were used in order to determine each point. The coplanarity of the respective mirror coordinate (of the point to be determined) on each of the locations along with the point itself was used to determine the coordinate itself. Another input which was required to obtain the result was the calculated reflection angle for the point from the lens of the camera to the mirror to the point to be determined. This vector was utilized in the coplanarity equation in order to determine the coordinate of the point. An average mapping error of about 12 cm was obtained for Site 1 by analyzing more than 12 mapped points. Whereas for Site 2, it was 16 cm due to the higher positioning error.

6.1.4 Navigation (Positioning using tie-points)

These densified control points were then used to calculate the position of the catadioptric camera when placed at a different location. Therefore navigation involves sequential and simultaneous positioning and mapping. This process was performed several times in order to represent and simulate the route of a mobile platform on which the system would be placed. Experiments were performed in order to compare these determined positions with positioning results so as to understand the efficiency of the system.

Finally the results from each of the stages were obtained. The navigation results were less accurate than the positioning results. They were calculated in the same way, using mapped points as targets. The results for Site 1 and Site 2 were 35 cm and 44cm respectively. The positions of each of the locations was obtained and represented in a navigation route along

with respective errors. Similar graphic was provided for the mapped points. The errors in positioning and mapping were obtained and discussed for each of the experiments. The efficiency of the process was evaluated and compared with other works.

6.2 Future Work

A navigation and mapping system, using a catadioptric camera system, was developed and implemented. However, many additions and modifications can be made to the system which can potentially help to reduce the manual work involved and increase the efficiency and accuracy of the vision-based system. These additions and modifications will allow the system to be used for a wider array of applications, and are discussed in this section. Since the experiments performed consisted of a specific camera and a specific mirror, the flexibility of the system will be discussed along with other options which might provide better results. Finally the potential improvement of the whole system due to a possible combination with other sensors used in navigation and mapping will be discussed.

6.2.1 Automation

Automation of any system is usually preferred over any involved manual training. The automation of the current system would involve three major things which are discussed below.

6.2.1.1 Implementation on a mobile robot

The first step in automation of the catadioptric camera involves its implementation on a mobile platform. This can be done on the mobile robot as shown in Chapter 3. The mobile

platform not only provides the system with mobility but also acts as a fixed system with certain geometric constraints which would be helpful especially in calibration of the system and would save time and manual labor from re-calibrating the system for each location. The mobile platform will make the vision based system useful in its application in areas such as nursing homes and mines as discussed in Chapter 1. Implementation on the robot would also make the experiments performed here easier although it might reduce the flexibility. A specific camera and a specific mirror (at least in terms of size) would be used. This is not necessarily a disadvantage, since the best combination can be tried and implemented.

Several other sensors can also be implemented on the mobile robot such as laser scanners and odometer. More equipment such as tablets can be added on it for various other applications.

6.2.1.2 Automatic Processing

This is another key step in automation of the system. Manual selection, especially that of image coordinates of control points and targets, was used in several steps which were performed as a part of calibration, positioning and mapping. A step required before automatic feature detection (detection of control points in the image) is the unwrapping of images which is discussed in last section of Chapter 4. To solve this a highly accurate feature detection code would be required since the size of the visible targets is relatively small. Therefore, a future work would involve development of a feature detection code for this purpose. One of the things which might assist in this are set up of bigger and more specific targets such that using their design as template a search could be performed in the image of the mirror in order to determine their reflection location. The distortion of the target due to its reflection in the paraboloid mirror does make this harder especially since the target is distorted differently at different locations. The use of SURF (Speeded Up Robust Features) (Bay et al., 2006) and SIFT (Scale-invariant feature transform) (Lowe, 2004) might be helpful with this. It is

also very important to note that different identification marks will be required for different CP's and targets. One of the SURF matching results performed to obtain common features between two overlapping images is shown in Figure 6.2.

Some of the feature detection codes were designed to use two or three images with common features in order to obtain the 3D coordinates of these common points (i.e. mapping). These mapped points can be used as tie-points for navigation. However, these codes need to be refined to eliminate all mismatched points, so that the obtained results for mapping can be used as a whole in the next step.

Figure 6.1: SURF Matching rectified images

6.2.1.3 Real Time

Finally, the automation of the system will require real-time processing. Not only does this require a higher processing power from on-board system on the mobile robot but also but also a general initialization which will be suitable for all environments such that wherever the CP's are provided, the mobile robot can start processing. The initial requirement would be either CP's or previously established mapped points by the system. The mapped points might not be as accurate as the CP's but are sufficient for functioning. The results can then be

improved once CP's are detected later in the environment. Therefore, certain familiarity with the environment is necessary in any case even in an automated scenario. Storage memory might also be an issue for real time processing, depending on the size of the environment and the format data is stored in. There is definitely a lot of room for work in this area, perhaps the most out of all the aforementioned stages.

6.2.2 Camera Flexibility and Additional Sensors

6.2.2.1 Flexibility

Camera and mirror flexibility was a key aspect of the construction of the system. Since different applications may have different requirements, camera and mirror flexibility is important. The mathematical models developed allow for this flexibility.

As was mentioned in the earlier chapters, the mathematical model allows for use of different mirror shapes and sizes. Even though the experiments were performed using paraboloid shaped mirror, with only a few changes a spherical, a hyperbolic or an elliptical mirror can be used.

The changes will be made when there is a relationship established between the image coordinates and the respective mirror coordinates of points in the environment. This happens after calibration and during positioning and throughout the whole procedure. The one to one relationship is established by making use of collinearity equations and the mathematical shape of the mirror. So in the experiments discussed above the shape of the mirror is represented by the following equation:

$$Z_{mi} = 0.025(X_{mi}^2 + Y_{mi}^2) \tag{6.1}$$

Therefore in case a spherical mirror was being used, the above equation can be replaced by the following in those steps:

$$Z_{mi} = c^2 - (X_{mi}^2 + Y_{mi}^2) \tag{6.2}$$

where c represents the radius of the sphere and in case an ellipsoid was being used:

$$Z_{mi}^2 = c^2(\frac{X_{mi}^2}{a^2} + \frac{Y_{mi}^2}{b^2}) \tag{6.3}$$

where a, b and c represent the length of semi principal axis of the ellipsoid.

Therefore, the substitution of an equation in the algorithm will allow the user flexibility in mirror shape.

The system is also flexible for any cameras. Since all radial distortion and alignment errors are accounted for, any conventional perspective camera can be used.

6.2.2.2 Odometers and Laser Scanners

Using additional sensors such as odometers, Infra red (IR) sensors and laser scanners can prove to be a major help in improving the accuracy of the system and in its automation. These sensors can be mounted on the mobile platform along with the catadioptric system. An initial calibration to determine the relative translation and orientation of the catadioptric system with respect to each sensor would be required in order to co register the data.

Odometers can be very helpful to determine the relative motion of the mobile platform, that is the system from the initial point. This information can serve not only as initial estimate to

improve upon but in certain scenarios, depending upon the accuracy of the odometer, can be taken as the new position, thus changing the functioning of the whole system and making it more focused for a certain task for better accuracy. Another approach use would be to use them to provide an initial estimate and thus a constraint for calculation of the position of the system.

Laser scanners can be utilized in several ways. Since 3D laser scanners are relatively expensive and bulky, using 2D laser scanners (range finders) would be more practical, especially in for proposed applications since the mobile platform navigates in a 2D plane. One of the range finders (weight - 160g, Figure 6.2) was used on the mobile robot provided by CrossWing. Also, more than one laser scanner can be used. The use of two laser scanners simultaneously can be very helpful, especially in the case of traversing a hallway. Usually the two walls are close enough to stay within the range of laser scanner, so putting them at a certain angle from each other can provide the distance of walls on either side thus providing a constraint for the targets located on these walls (Figure 6.3). This improves the calculation of their coordinates, i.e. mapping accuracy, thus improving navigation and the whole process.

Figure 6.2: Hokuyo URG-04LX-UG01 Range Finder (Robotshop, 2015)

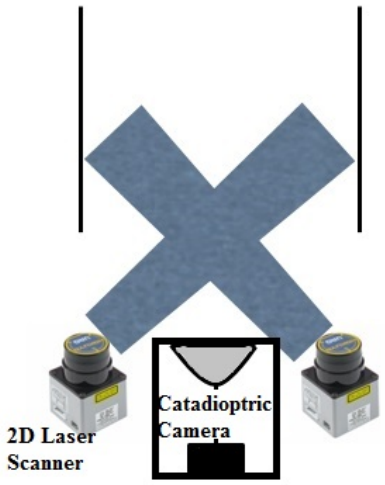

Figure 6.3: Using Catadioptric Camera with 2D range finders

Bibliography

[1] Abdel-Aziz, Y. I. and Karara, H. M. (1971). Direct linear transformation from comparator coordinates into object-space coordinates in close-range photogrammetry. American Society of Photogrammetry, Symposium on Close-Range Photogrammetry, Falls Church, Virginia. 433 pages: 1–18.

[2] Aliaga, D.G. (2001). Accurate Catadioptric Calibration for Real-time Pose Estimation in Room-size Environments. Computer Vision, 2001. ICCV 2001. Proceedings. Eighth IEEE International Conference on Volume 1 pp. 127-134.

[3] Aliakbarpour, H., Tahri, O., Araujo, H., 2014. Visual Servoing of Mobile Robots using Non-Central Catadioptric Cameras. Robotics and Autonomous Systems - Volume 62, Issue 11, November 2014, pp. 1613–1622.

[4] Altman, N. S. (1992). An introduction to kernel and nearest-neighbor nonparametric regression. The American Statistician. 46 (3): 175–185.

[5] Baker, S. & Nayar, S.K., (1999). A Theory of Single-Viewpoint Catadioptric Image Formation, International Journal of Computer Vision , pp. 35-175.

[6] Baker, S. & Nayar, S.K., (2001). Single Viewpoint Catadioptric Cameras, Panoramic Vision: Sensors, Theory, Applications, Ryad Benosman and Sing Bing Kang, ed., Springer-Verlag, 2001, pp. 39-71.

[7] Barreto, J.P. and Araujo, H. (2001). Issues on the geometry of central catadioptric image formation. Computer Vision and Pattern Recognition, Proceedings / CVPR, IEEE Computer Society Conference on Computer Vision and Pattern Recognition. IEEE Computer Society Conference on Computer Vision and Pattern Recognition 2:422-427.

[8] Bauer, J. C. (2007). The future of medical robotics: Creating synergy in the interaction of patients, caregivers, and intelligent machines. Retrieved from http://www.intouchhealth.com/TEWSClinicalRobotics.pdf (last accessed 23 June 2015).

[9] Bay, H., Tuytelaars, T. and Van Gool, L. (2006). SURF: Speeded Up Robust Features, Computer Vision – ECCV 2006, Volume 3951 of the series Lecture Notes in Computer Science pp 404-417.

[10] Bouguet, J.Y. (2015), Camera Calibration Toolbox for Matlab, Retrieved from http://www.vision.caltech.edu/bouguetj/calib_doc/index.html (last accessed Dec 16th 2016).

[11] Bourgeois, P. Rodriguez, P. and Ragot, N., (2011). Omnidirectional Catadioptric Image Unwrapping via Total Variation Regularization. Robotic and Sensors Environments (ROSE), 2011 IEEE, pp. 220-225.

[12] Brown, D. C. (1966). Decentering distortion of lenses (PDF). Photogrammetric Engineering. 32 (3): 444–462.

[13] Castañón–Puga, M., Salazar, A., Aguilar, L., Gaxiola-Pacheco, C. and Licea, G (2015), A novel hybrid intelligent indoor location method for mobile devices by zones using Wi-Fi signals, Sensors. pp. 30142–30164.

[14] Chou, Y.S. and Liu, J.S. (2013). A robotic indoor 3d mapping system using a 2d laser range finder mounted on a rotating four-bar linkage of a mobile platform. Int. J. Adv. Robot. Syst., 10.

[15] de Greve, B. (2007) Reflections and Refractions in Ray Tracing, Retrieved from http://www.bramz.net/data/writings/reflection _transmission.pdf (last accessed 28 February 2016).

[16] Dupuis, Y., Quispe, A.Mendoza, Vasseur, P., Castaneda, B., Ragot, N., (2014). Enhanced omnidirectional image unwrapping for face detection, 2014 IEEE International Conference on Image Processing (ICIP), pp. 263-267

[17] Fischler, M.A. and Bolles, R.C. (1981). Random Sample Consensus: A Paradigm for Model Fitting with Applications to Image Analysis and Automated Cartography (PDF). Comm. of the ACM 24 (6), pp. 381–395.

[18] Gaspar, J. and Victor, J.S. (1999). Visual Path Following with a Catadioptric Panoramic Camera. International Symposium on Intelligent Robotic systems, pp. 139-147.

[19] Gerstweiler, G., Vonach, E. and Kaufmann, H. (2016), Hymotrack: A mobile AR navigation system for complex indoor environments. Sensors. 2016, pp. 16-17.

[20] Geyer, C. and Daniilidis, K (1999). Catadioptric Camera Calibration. Computer Vision, 1999. The Proceedings of the Seventh IEEE International Conference on (Volume:1), pp. 398-404.

[21] Geyer, C. and Daniilidis, K (2000). A Unifying Theory for Central Panoramic Systems and Practical Applications. Proceedings of the 6th European Conference on Computer Vision-Part II, pp. 445-461.

[22] Geyer, C. and Daniilidis, K (2003). Mirrors in Motion: Epipolar Geometry and Motion Estimation. Proc. IEEE Int'l Conf. Computer Vision, pp. 766-773.

[23] Ghilani, C.D. (2011). "Adjustment Computations: Spatial Data Analysis", John Wiley & Sons.

[24] Grisetti, G., Kummerle, R., Stachniss, C., and Burgard, W. (2010). A tutorial on graph-based SLAM. Intelligent Transportation Systems Magazine, IEEE, 2(4), 31-43.

[25] Ilizirov, G, Filin, S., (2016), Pose Estimation and Mapping Using Catadioptric Cameras with Spherical Mirrors, ISPRS - International Archives of the Photogrammetry, Remote Sensing and Spatial Information Sciences, Volume XLI-B3, pp.43-47

[26] Levenberg, K (1944). A Method for the Solution of Certain Non-Linear Problems in Least Squares. Quarterly of Applied Mathematics. 2: 164–168.

[27] Lhuillier, M., (2008), Automatic scene structure and camera motion using a catadioptric system, Computer Vision and Image Understanding 109(2), pp.186-203.

[28] Lowe, D.G. (2004). Distinctive image features from scale-invariant keypoints, International Journal of Computer Vision, 60, 2, pp. 91-110

[29] Mabius, D. and Tang, J. (2008). Omnidirectional Imaging. Boston University URL: http://www.bu.edu/vip/files/pubs/reports/DMJT07-07buece.pdf (last date accessed 22 May 2016)

[30] Marquardt, D (1963). An Algorithm for Least-Squares Estimation of Nonlinear Parameters. SIAM Journal on Applied Mathematics. 11 (2): 431–441.

[31] Mei, C. and Rives, P. (2007). Single View Point Omnidirectional Camera Calibration from Planar Grids. Proceedings 2007 IEEE International Conference on Robotics and Automation, pp. 3945 - 3950.

[32] Micusık, B. and Pajdla, T. (2004). Autocalibration and 3D Reconstruction with Non-central Catadioptric Cameras. Computer Vision and Pattern Recognition, 2004. Vol.1 pp. I-58 - I-65

[33] Nikon FC-E9 + UR-E21 Fisheye lens (2011). Retrieved from https://commons.wikimedia.org/wiki/File:Nikon_1_V1_%2B_Fisheye_FC-E9_(3).jpg (last date accessed 7 January 2015).

[34] Ohte, A., Tsuzuki, O. and Mori, K. (2005). Practical Spherical Mirror Omnidirectional Camera. Proceedings of the 2005 IEEE International Workshop on Robotic Sensors: Robotic and Sensor Environments, pp. 8-13.

[35] Pedersen, S. M., Fountas, . and Blackmore, S. (2008) Agricultural Robots – Applications and Economic Perspectives, Serv. Robot Appl., book edited by Yoshihiko Takahashi, ISBN 978-953-7619-00-8, pp. 369-382.

[36] Puig, L. Bastanlar, Y. Sturm, P. (2001). Calibration of Central Catadioptric Cameras Using a DLT-Like Approach. International Journal of Computer Vision, 93, 101-114.

[37] Robot Shop, Retrieved from http://www.robotshop.com/en/hokuyo-urg-04lx-ug01-scanning-laser-rangefinder.html (last accessed 28 February 2016).

[38] Scaramuzza, D., Martinelli, A., Siegwart, R. (2006). A flexible technique for accurate omnidirectional camera calibration and structure from motion. Fourth IEEE International Conference on Computer Vision Systems (ICVS'06), pp. 45-55.

[39] Scaramuzza, D., Criblez, N., Martinelli, A. and Siegwart, R. (2007) Robust feature extraction and matching for omnidirectional images. Proceedings of the 6th International Conference on Field and Service Robotics (FSR 2007), Chamonix, France, July 2007 pp 71-81

[40] Scaramuzza, D., (2014), Omnidirectional Camera, Computer Vision: A Reference Guide, Editors: Katsushi Ikeuchi, ISBN: 978-0-387-30771-8 , pp 552-560.

[41] Seedahmed, G. H. and Habib, A. F., (2002). Linear recovery of the exterior orientation parameters in a planar object space. International Archives of the Photogrammetry, Remote Sensing and Spatial Information Sciences, 34(3B): 245–248.

[42] Singh, A., Gupta, A., Bhosale, A. and Poddar, S., (2015) Agribot: - An Agriculture Robot, IJARCCE, 4(1), pp. 317–319.

[43] Stereo Vision Camera (2011). Retrieved from http://www.visionhardwarepartner.nl/products/camera-%252aslash%252a-imaging/camera/oem-stereovision-camera.html (last date accessed 7 January 2015).

[44] Super Droid Robots (2013). Retrieved from http://www.sdrobots.com/4wd-tactical-scissor-lift-robot-ptz-camera/ (last date accessed 8 December 2014).

[45] Svoboda, T., Pajdla, T. and Hlavac, V. (1998). Epipolar Geometry for Panoramic Cameras. Proc. European Conf. Computer Vision, pp. 218-232.

[46] Swaminathan, R., Grossberg, M.D. & Nayar, S.K. (2006), Non-Single Viewpoint Catadioptric Cameras: Geometry and Analysis, Int J Comput Vision , pp 66-211.

[47] Tahri, O. and Araujo, H., (2012). Non-Central Catadioptric Cameras Visual Servoing for Mobile Robots using a Radial Camera Model, 2012 IEEE/RSJ International Conference on Intelligent Robots and Systems, Vilamoura, 2012, pp. 1683-1688.

[48] Thibault, S. (2008), Panoramic lens applications revisited, Published in SPIE Proceedings Vol. 7000: Optical and Digital Image Processing, pp. 1-8.

[49] Wang, Y.K., Huo, J. and Wang, X.S. (2014), A real-time robotic indoor 3d mapping system using duel 2d laser range finders. In Proceedings of the Chinese Control Conference (CCC), Nanjing, China, 28–30 July 2014; pp. 8542–8546.

[50] Wikipedia (2012). Distortion (optics): Radial lens distortion. Retrieved from http://en.wikipedia.org/wiki/Distortion %28optics%29#Radial distortion (last accessed 29 September 2015).

[51] Wolf, P.R., Dewitt, B.A. ,Wilkinson, B.E.. (2014). Elements of Photogrammetry with Applications in GIS, Fourth Edition, Figure 11-.1, pp. 268

[52] Wolf, P.R., Dewitt, B.A. ,Wilkinson, B.E.. (2014). Elements of Photogrammetry with Applications in GIS, Fourth Edition, pp. 268-273.

[53] Xiang, Z., Sun, B and Dai, X. (2012). The Camera Itself as a Calibration Pattern: A Novel Self-Calibration Method for Non-Central Catadioptric Cameras. Sensors (Basel). 2012; 12(6): 7299–7317.

[54] Zhang, Zhengyou (1998). A Flexible New Technique for Camera Calibration (PDF) (Technical report). Microsoft Research. MSR-TR-98-71.